
Article:
Apostolopoulou, A.A. orcid.org/0000-0002-8174-4372 and Lin, A.C. orcid.org/0000-0001-6310-9765 (2020) Mechanisms underlying homeostatic plasticity in the Drosophila mushroom body in vivo. Proceedings of the National Academy of Sciences, 117 (28). pp. 16606-16615. ISSN 0027-8424

https://doi.org/10.1073/pnas.1921294117

Mechanisms underlying homeostatic plasticity in the *Drosophila* mushroom body *in vivo*

Anthi A. Apostolopoulou[1,2], Andrew C. Lin[1,2]*

[1] Department of Biomedical Science, University of Sheffield, Sheffield S10 2TN, UK
[2] Neuroscience Institute, University of Sheffield, Sheffield S10 2TN, UK

*For correspondence: andrew.lin@sheffield.ac.uk, +44 114 222 3643

Classification: Biological Sciences: Neuroscience

Abstract

Neural network function requires an appropriate balance of excitation and inhibition to be maintained by homeostatic plasticity. However, little is known about homeostatic mechanisms in the intact central brain *in vivo*. Here, we study homeostatic plasticity in the *Drosophila* mushroom body, where Kenyon cells receive feedforward excitation from olfactory projection neurons and feedback inhibition from the APL neuron. We show that prolonged (4 d) artificial activation of the inhibitory APL causes increased Kenyon cell odor responses after the artificial inhibition is removed, suggesting that the mushroom body compensates for excess inhibition. In contrast, there is little compensation for lack of inhibition (blockade of APL). The compensation occurs through a combination of increased excitation of Kenyon cells and decreased activation of APL, with differing relative contributions for different Kenyon cell subtypes. Our findings establish the fly mushroom body as a model for homeostatic plasticity *in vivo*.

Keywords: *Drosophila*, olfaction, homeostatic plasticity, mushroom body

Significance statement: When a neuron fires, it excites or inhibits other neurons. These two opposing forces – excitation and inhibition – need to be carefully balanced in the brain for neural networks to function properly. Maintaining this balance requires homeostatic plasticity to compensate for perturbations in neural activity levels. Relatively little is known about how such homeostatic compensation works in the intact central brain *in vivo*. To address this problem, we developed a model for studying homeostatic plasticity *in vivo*: the *Drosophila* mushroom body (the fly's olfactory memory center). We found that this brain structure compensates for prolonged excess inhibition through a combination of increased excitation and decreased inhibition, with these two mechanisms contributing differently for different types of neurons.

Introduction

Effective information coding in neural networks requires neuronal firing rates to stay within a certain dynamic range. At the extremes, networks carry no useful

information if neurons are completely silent or constantly fire at their highest possible rate. More subtle differences in activity levels can also affect information coding; for example, sparse coding of sensory stimuli helps to maximize associative memory capacity and to separate population representations of different stimuli, thereby enhancing learned discrimination (1, 2). Yet how do neural networks achieve such "Goldilocks" activity levels, and how do they maintain them in the face of external perturbations (e.g., temperature changes) or neural plasticity caused by development or learning (e.g., Hebbian plasticity, which risks destabilizing activity levels by strengthening active synapses and weakening inactive synapses)? Theoretical studies show that this problem can be solved by homeostatic plasticity, which compensates for changes in activity levels to restore neurons to a "set point" of activity (3, 4). Such homeostatic plasticity can occur through multiple mechanisms, including changes in intrinsic excitability, strength or number of excitatory or inhibitory synaptic inputs, or changes in the threshold between synaptic potentiation vs. depression (5, 6).

These findings have mostly come from dissociated neurons *in vitro* or *ex vivo* preparations like brain slices, sometimes following *in vivo* sensory deprivation like eyelid suture (e.g., (7-13)). Yet brain slices differ in important ways from the intact brain *in vivo*: compared to the intact brain, brain slices can have less spontaneous activity (14) and more synapses (15). Even *in vivo*, neural activity differs significantly between awake and anesthetized animals (16). Homeostatic compensation has been studied *in vivo* in the spinal cord (17, 18) and more recently in the brain (19-24), but the circuit mechanisms underlying homeostatic plasticity in the intact central brain *in vivo* remain relatively unknown.

This problem can be addressed in *Drosophila*, whose genetic toolkit and numerically simple brain allows greater specificity in manipulating and measuring neural activity *in vivo* than in mammals. These tools have revealed many examples at cellular resolution of plasticity underlying associative learning (25), non-associative learning (26-28), activity-dependent remodeling (29, 30) and developmental circuit refinement (31). However, relatively little is known about homeostatic regulation of activity levels (but see, e.g., (32)). In most examples of homeostatic compensation studied in *Drosophila*, the variable being controlled is not activity levels but synaptic strength. In

particular, in the most well-understood homeostatically controlled system, the neuromuscular junction (NMJ), the goal is to maintain constant synaptic strength so that the muscle can faithfully execute the motor neuron's commands, not to maintain constant average activity levels in the muscle (33) (see also (34) in the antennal lobe). It remains unclear whether or how the adult fly brain uses homeostatic plasticity to maintain activity levels in the correct range.

We address this question in the fly mushroom body, whose principal neurons, called Kenyon cells (KCs), receive both feedforward excitation from second-order olfactory neurons called projection neurons (PNs) and feedback inhibition from a single neuron called "APL" (anterior paired lateral; **Fig. 1A**) (1, 35-37). This balance of excitation and inhibition regulates the level of activity in KCs to enforce sparse coding, in which only a small fraction of KCs responds to each odor (38). This sparse coding reduces overlap between KC odor representations and enhances learned odor discrimination (1). However, it remains unclear how KCs set the relative strength of their excitatory and inhibitory inputs. We hypothesized that this balance might be set in an activity-dependent manner, in which case the mushroom body should homeostatically adapt to perturbations in activity levels.

Here we test the homeostatic capacity of the fly mushroom body *in vivo* and dissect the underlying circuit mechanisms. We find that the mushroom body compensates for excess inhibition from APL, but shows little compensation for lack of inhibition. Compensation for excess inhibition from APL requires multiple days and occurs by both weakening odor-evoked activity of APL and increasing odor-evoked excitation of KCs, with differing relative contributions of these two mechanisms in different subtypes of KCs. These findings establish the fly mushroom body as a model for studying homeostatic plasticity *in vivo*.

Results

KCs show little compensation for loss of inhibition from APL

We first tested whether the mushroom body circuitry adapts to lack of inhibition from APL. Previously we showed that blocking synaptic output from APL by acutely

expressing tetanus toxin (TNT) in APL dramatically increases odor-evoked Ca^{2+} influx in KCs (1, 39). We now compared the effects of blocking inhibition from APL acutely (16-24 h) vs. constitutively (throughout development; **Fig. 1B**). As before, we expressed TNT in APL by intersecting the expression domains of NP2631-GAL4 and GH146-FLP, suppressing GAL4 activity in GH146-negative cells by including tubP-FRT-GAL80-FRT. The GAL80 is excised in GH146-positive cells by FLP recombinase approximately 50-70% of the time (1). This method drives expression of UAS-transgenes in APL and not in PNs or KCs ((1) and **Fig. S1A,B**). To express TNT acutely, we included tubP-$GAL80^{ts}$ to suppress GAL4 activity when flies were kept at 18 ºC, and induced expression of TNT by heating the flies to 31 ºC for 16–24 h before the experiment. To express TNT in APL constitutively, we left out the tubP-$GAL80^{ts}$ but exposed the flies to the same temperatures as the "acute" flies (**Fig. 1B**).

To confirm that tubP-$GAL80^{ts}$ effectively suppressed GAL4 activity in APL in "acute" flies, we drove CD8::GFP and mCherry in APL (see **Table S1** for full genotypes). These flies showed GFP expression in APL in 12/18 hemispheres when raised at 18 ºC and heated to 31 ºC for 16–24 h before dissection (consistent with previous studies (1)), but in 0/15 hemispheres when kept at 18 ºC. Given that both conditions have the same probability of GAL80 excision (excision occurs in development (40) so would be unaffected by heating during adulthood), it is extremely unlikely that GAL80 would be excised in APL in 12/18 hemispheres in one condition but 0/15 in the other ($p < 0.0001$, Fisher's exact test). Thus, the most plausible explanation is that GAL80 was excised in APL even in the flies kept at 18 ºC, but GAL4 activity was effectively suppressed by tubP-$GAL80^{ts}$.

To measure KC odor responses, we expressed GCaMP6f in KCs under the control of MB247-LexA (41), and TNT in APL using the above-described intersectional strategy. MB247-LexA does not drive expression in APL ((1) and **Fig. S1C,D**). To test KC responses for different strengths of excitatory input, we recorded Ca^{2+} influx in KCs evoked by the "strong" odor isoamyl acetate and the "weak" odor δ-decalactone (the former elicits more total activity in olfactor receptor neurons (42) and KCs (1)). We separately analyzed KC odor responses in the different lobes of the mushroom body, i.e., the α′ and β′ lobes (made up of axons from α′β′ KCs), the α

and β lobes (axons from αβ KCs), and the γ lobe (axons from γ KCs; see diagrams in **Fig. 1C**), because the three main KC subtypes (α′β′, αβ, and γ) have different functional properties (43-46).

We used two negative controls in which APL did not express TNT. First, we measured KC odor responses in brain hemispheres in which GAL80 was not excised in APL (i.e., identical genotype and treatment but no TNT in APL: "APL unlabeled", black in **Fig. 1C,D**). We identified which hemispheres had GAL4 activity in APL by including UAS-mCherry or immunostaining brains for TNT after the experiment. (We pooled the APL-unlabeled hemispheres from flies with and without tubP-GAL80^{ts} because their odor responses did not differ: **Fig. S2A**; conclusions from statistical analysis are unchanged if the two groups are separated: **Table S2**).

Second, to further confirm that tubP-GAL80^{ts} suppressed TNT expression in APL to functionally insignificant levels, we measured KC odor responses in flies with tubP-GAL80^{ts} that were kept at 18 ºC throughout life (diagram in **Fig. 1B**, right; data labeled "18 ºC", green in **Fig. 1C,D**). These flies showed similar responses as the "APL unlabeled" controls. Although we could not confirm whether GAL80 had been excised from tubP-FRT-GAL80-FRT in APL in these flies (due to the continued activity of GAL80^{ts}), it is unlikely that all "18 ºC" flies would have had APL unlabeled by chance, given that 28/40 hemispheres had APL labeled in the corresponding experimental flies that were heated to 31 ºC (0/10 at 18 ºC vs. 28/40 at 31 ºC, $p < 0.0001$, Fisher's exact test), by the same logic as the GFP expression experiment above. This second negative control confirms that our "acute" expression of TNT was genuinely acute, with functionally no leaky expression of TNT during development.

Compared to both of these control groups, both acute and constitutive expression of TNT in APL dramatically increased odor-evoked Ca^{2+} influx in KCs (**Fig. 1C,D**), with little evidence of homeostatic compensation. We did not observe any consistent differences in KC response amplitudes between acute vs. constitutive APL>TNT flies. In some cases, constitutive responses were lower than acute responses and in others, they were higher (KC responses imaged with GCaMP6f in **Fig. 1**, GCaMP3 in **Fig. S2B**). Other subtle differences occasionally appeared, e.g., smaller normalized

difference between responses to isoamyl acetate and δ-decalactone in constitutive APL>TNT flies, potentially suggesting compensation to restore APL's gain control function, or reduced post-odor GCaMP signal in constitutive APL>TNT flies, potentially suggesting altered calcium export (**Fig. S3**). However, again, these differences were subtle and inconsistent, and thus do not provide clear evidence of functionally significant adaptation. Thus, taken together, our data indicate that Kenyon cells show little, if any, homeostatic compensation for prolonged lack of inhibition from APL.

KC odor responses are higher following prolonged excess inhibition from APL

We next tested the reverse manipulation: rather than blocking APL, we activated APL with the temperature-sensitive cation channel dTRPA1 (47). Acutely activating APL with dTRPA1 suppresses odor responses in KCs (1) and activation with dTRPA1 throughout development induces homeostatic plasticity in larval motor neurons (29). Given that mammalian cortical plasticity induced by sensory deprivation can take several days to appear (24, 48), we initially activated APL for 4 d. We expressed GCaMP6f in KCs, and dTRPA1 and mCherry in APL, using the same drivers as in **Fig. 1**. We raised flies at 22 ºC, collected them 0–1 d after eclosion, and either left them at 22 ºC or heated them to 31 ºC for 4 d (88–96 h) before recording KC odor responses at 22 ºC (**Fig. 2A**).

If this prolonged artificial activation of APL induces homeostatic compensation, KC activity should rebound to abnormally high levels when the artificial activation is stopped. Indeed, KC odor responses recorded at 22 ºC were significantly higher in hemispheres where APL expressed dTRPA1 when the flies had been pre-heated to 31 ºC for 4 d, compared to hemispheres where APL was unlabeled or to flies that had not been pre-heated. This effect occurred in all lobes, with both the "strong" odor isoamyl acetate and the "weak" odor δ-decalactone (**Fig. 2B,C**). Similar effects were seen when measuring odor responses with GCaMP3 instead of GCaMP6f (**Fig. S4**), although the effect in α′β′ KCs was less consistent here and in later experiments (see below). Note that "APL unlabeled" and "APL>dTRPA1" hemispheres had the same genotype and in many cases were in the same fly, providing an ideal genetic control.

Increased responses in KC axonal lobes could reflect individual KCs responding more and/or more KCs responding. To test the latter possibility, we recorded KC somatic odor responses in pre-heated flies and measured the population sparseness of the resulting activity maps. Odor responses were less sparse (broader) in APL>dTRPA1 hemispheres compared to APL unlabeled hemispheres (**Fig. 2D,E, S5A**). We next asked if this broadening would also make KC odor responses more similar. Although inter-odor correlations between activity maps were somewhat higher in APL>dTRPA1 hemispheres, the effect was not statistically significant (**Fig. S5B,C**). We may lack statistical power to detect a modest effect, but our sample size provided 96% power to detect an effect as large as the increase in inter-odor correlations previously observed in APL>TNT flies (1). This difference could be explained by the fact that adaptation to APL activation causes a much smaller increase in KC odor responses than APL>TNT does (**Fig. S5D**).

The smaller effect of adaptation to APL>dTRPA1 (vs. blocking APL with TNT) also implies that the adaptation effect cannot be explained trivially as APL simply being killed or damaged by over-activation by dTRPA1 for 4 d. This trivial explanation is further excluded by the fact that even after we pre-activated APL with dTRPA1, heating flies to 31 ºC during the imaging experiment to acutely activate APL still efficiently suppressed KC odor responses (**Fig. S6,S7**, see also **Fig. 5** below). Moreover, adaptation to APL>dTRPA1 caused no obvious changes in the gross morphology of KCs or APL (**Fig. S8**). Together, these results suggest that 4 d APL>dTRPA1 activation induces homeostatic compensation to counteract the excess activity in APL or insufficient activity in Kenyon cells.

Adaptation to excess inhibition from APL is most prominent after 4 days and is temporary

To further confirm these results, we repeated the APL>dTRPA1 adaptation experiments using a different APL driver, VT43924-GAL4, to express dTRPA1 in APL (49) (see **Fig. S1** for expression pattern). Kenyon cells' odor responses recorded after 4 d pre-activation of APL were significantly higher (except in the α′ lobe) in flies where APL expressed dTRPA1, compared to flies with UAS-dTRPA1

alone (**Fig. 3A**, blue squares; **S9**), thereby reproducing the results obtained with the intersectional strategy for labeling APL.

Other model systems show homeostatic compensation in as little as 1 d (9, 19, 23, 50-52). To test whether the mushroom body might similarly compensate within 1 d, we tested flies after 1 d of pre-activating APL instead of 4 d, while still imaging them 4-5 d after eclosion (**Fig. 3**, blue squares; **S9**). Unlike with 4 d pre-heating, with 1 d pre-heating, APL>dTRPA1 flies did not have signficantly higher KC odor responses than flies with UAS-dTRPA1 alone (although in some case there was a non-significant trend toward an increase).

This difference might arise not from the length of pre-heating but rather from the timing during the fly's life: perhaps there is a critical period for homeostatic plasticity in the first day after eclosion. To test this, we pre-heated newly eclosed flies for 1 d. These flies also showed no significant difference between APL>dTRPA1 flies and UAS-dTRPA1 controls (**Fig. S10**), suggesting that the difference between 1 d and 4 d pre-heating is not due to a critical period (although there may still be a critical period such that, e.g., 10 d old flies would not show homeostatic plasticity).

To further probe when compensation occurs, we tested flies at multiple time points: 1, 2, 3 and 4 d of heating (keeping the age of the fly at imaging constant). To reproduce our timescale results with a different driver, we returned to the NP2631/GH146-FLP intersectional driver (**Fig. 3,** black circles). Consistent with the results with VT43294-GAL4, only at 4 d did we consistently observe significantly higher KC odor responses in APL>dTRPA1 hemispheres compared to control 'APL unlabeled' hemispheres (although at 1-3 d there was a trend toward an increase that was sometimes significant at 2-3 d; **Fig. 3A, S11**). Here and in **Fig. S9**, we do not exclude the possibility that some small adaptation occurs before 4 d that couldn't be detected with our statistical power, but these results suggest that the effect is more prominent after 4 d.

We next tested how long homeostatic compensation lasts, by taking flies where APL had been activated for 4 d and leaving them at 22 ºC for 1, 2, or 3 d to 'forget' the adaptation. The difference between APL>dTRPA1 and control hemispheres was no

longer statistically significant by 1-2 d (**Fig. 3B, S12**), suggesting that adaptation does not last more than 1-2 d after excess inhibition from APL stops.

APL odor responses are reduced following adaptation

We next asked what cellular or circuit mechanisms underlie the adaptation observed above, i.e., increased odor responses in KCs following excess inhibition from APL. We postulated five broad, non-mutually-exclusive categories of mechanisms: (1) increased synaptic excitation from PNs to KCs, (2) increased intrinsic excitability of KCs, (3) decreased synaptic excitation from KCs to APL, (4) decreased intrinsic excitability of APL, and (5) decreased synaptic inhibition from APL to KCs (**Fig. 4A**). Mechanisms 1, 2 and 5 center on KC activity while mechanisms 3 and 4 center on APL activity. To test these two broad groupings of hypotheses, we recorded odor responses in APL after adaptation (**Fig. 4B**). If adaptation only involves changes centered on KC activity (mechanisms 1, 2, 5), then the relation between KC activity and APL activity would be unchanged; therefore, because APL's odor input comes from KCs (1), APL should continue to copy whatever KCs do. Thus, APL odor responses should increase after adaptation just as KC odor responses do. Contrary to this prediction, after 4 d at 31 ºC, APL>dTRPA,GCaMP6f flies showed *decreased* APL odor responses compared to APL>GCaMP6f (no dTRPA1) flies (**Fig. 4C**), particularly in the peak response (compare to steady-state responses in **Fig. S13**). These results suggest that increased KC odor responses after adaptation can be explained at least in part by decreased activity in the inhibitory APL neuron (mechanism 3 and/or 4).

Different KCs show different effects of APL activation after adaptation

These results do not rule out the possibility that, in addition to changes in APL activity, adaptation also involves changes centered on KC activity (mechanisms 1, 2 and 5 above: increased intrinsic excitability, increased synaptic excitation from PNs, decreased sensitivity to inhibition from APL). To test this possibility, we re-examined data from **Fig. S6** to focus on KC odor responses during acute activation of APL (caused by heating APL>dTRPA1 flies to 31 ºC during imaging) (**Fig. 5C,D**). Artificially activating APL overrules the reduced odor-evoked activity in APL, making

APL activity equal in adapted and non-adapted flies, both before and during odor pulses (**Fig. 5A,B, S14**). Therefore, if adaptation was due only to reduced APL odor-evoked activity, then the difference in KC odor response between adapted and non-adapted flies should go away when we artificially activate APL.

We observed different results in different KCs. In αβ KCs, odor responses in adapted flies were generally still higher than in non-adapted flies even at 31 ºC (**Fig. 5E**). In contrast, in γ KCs, although odor responses were higher in adapted than non-adapted flies when recorded at 22 ºC, the odor responses declined approximately to the same level when recorded at 31 ºC (**Fig. 5E**). (Note that **Fig. 5** shows mean ΔF/F rather than maximum ΔF/F because in some cases activating APL with dTRPA1 changed the dynamics of the KC odor responses; see **Fig. S15** for maximum ΔF/F, which gives similar results.) A power analysis indicates our sample sizes would detect an effect as strong as that observed in the β lobe with power >0.95. (Odor responses in α′β′ KCs are more difficult to interpret as they did not consistently decrease when APL was activated by dTRPA1; see **Fig. S6, S7, S15**.) These results indicate that while adaptation in γ KCs can be explained by decreased APL odor responses, adaptation in αβ KCs requires an additional mechanism.

Adaptation in αβ KCs occurs at least partly through non-inhibitory plasticity

This additional mechanism in αβ KCs could be mechanism 1, 2 and/or 5: increased intrinsic excitability, increased synaptic excitation from PNs, and/or decreased sensitivity to inhibition from APL. To distinguish between these possibilities (**Fig. 6A**), we sought to block inhibition from APL in adapted flies (**Fig. 6B**). If adaptation occurred solely through weakening inhibition, whether through reducing APL activity (mechanisms 3 and 4) or reducing KC sensitivity to inhibition (mechanism 5), then blocking inhibition should remove the difference between adapted and non-adapted flies. To acutely block inhibition from APL in pre-heated APL>dTRPA1 flies, we expressed the histamine-gated Cl^- channel Ort (53) in APL, and bath-applied histamine. Ectopically expressing Ort in olfactory neurons allows histamine to potently inhibit them for at least several minutes (54). We again used the intersectional driver for APL to express dTRPA1 and Ort in APL, and mb247-LexA to express GCaMP6f in KCs. In hemispheres where APL was unlabeled, 2 mM

histamine did not affect KC odor responses (**Fig. 6C, Fig. S16**); this result is consistent with the relative absence of histamine and histamine receptors in the mushroom body (54-60), and argues against non-specific effects of histamine.

In **Fig. 2-3**, the adapted vs. non-adapted conditions were hemispheres in APL>dTRPA1 flies where APL was labeled or unlabeled, respectively. However, in this experiment, we could not use APL-unlabeled hemispheres as controls, because here we sought to compare adapted vs. non-adapted flies when APL was blocked by Ort, which is not expressed if APL is unlabeled. In theory, the non-adapted controls could be either APL>dTRPA1,Ort flies kept at 22 ºC or APL>Ort flies (without dTRPA1) kept at 31 ºC. However, in preliminary experiments, we found that in APL>dTRPA1,Ort flies kept at 22 ºC for 4 d, histamine increased KC odor responses modestly, but not as strongly as in APL>dTRPA1,Ort or APL>Ort flies kept at 31 ºC for 4 d (**Fig. S16**). This temperature dependence suggests that Ort expression was stronger at 31 ºC than 22 ºC because Gal4 activity is stronger at higher temperatures (61). Therefore, APL>dTRPA1,Ort flies kept at 22 ºC were not a suitable control. Instead, we compared only flies kept at 31 ºC for 4 d: APL>dTRPA1,Ort (adapted) and APL>Ort (non-adapted).

These genotypes replicated the adaptation effect: before adding histamine, responses in APL>dTRPA1,Ort hemispheres were higher than responses in APL>Ort (no dTRPA1) hemispheres. (In the α′ and β′ lobes, this difference was not statistically significant (**Fig. S17**); it may be that any adaptation effect in α′β′ KCs is less robust than in αβ and γ KCs, as in **Fig. S4,S9,S11,S12**). After adding histamine, KC responses in both genotypes were dramatically increased, to a similar degree as that caused by tetanus toxin expression in APL (**Fig. S18**), suggesting that in flies kept at 31 ºC, stimulating Ort in APL with 2 mM histamine suffices to block APL inhibition onto KCs.

In the α and β lobes, after adding histamine, responses to isoamyl acetate in APL>dTRPA1,Ort hemispheres were still significantly higher than in APL>Ort hemispheres (**Fig. 6C,D**). That is, even without inhibition from APL, we still observed the adaptation effect, suggesting that the adaptation from excess APL inhibition occurs at least in part through non-inhibitory plasticity, i.e., increased synaptic

388 excitation or intrinsic excitability (mechanism 1 or 2), rather than entirely through
389 decreased sensitivity to inhibition or decreased activity in APL (mechanisms 3-5). In
390 contrast, in the γ lobe, although APL>dTRPA1,Ort responses were slightly higher
391 than APL>Ort responses after adding histamine, this difference was not statistically
392 different. This result suggests that in γ KCs, adaptation from excess APL inhibition
393 mostly relies on reduced inhibition (mechanisms 3-5). Note that we do not exclude
394 the possibility that APL>dTRPA1,Ort and APL>Ort γ lobe responses were actually
395 different and we lacked the statistical power to detect a significant effect due to
396 experimental variability. Still, this difference between αβ and γ KCs is consistent with
397 the conclusion from APL activation during imaging (**Fig. 5**) that adaptation in γ KCs
398 can be explained mostly by decreased APL activity (mechanisms 3 and 4) while
399 adaptation in αβ KCs requires something extra.
400
401 **Discussion**
402
403 We have delineated the homeostatic capacity of the *Drosophila* mushroom body *in*
404 *vivo* and revealed circuit mechanisms underlying homeostatic plasticity. We found
405 that the mushroom body compensates for excess inhibition from APL, but not lack of
406 inhibition. This compensation requires multiple days and occurs by two mechanisms
407 — suppressed odor-evoked APL activity and increased odor-evoked excitation of
408 KCs — which contribute differentially to adaptation in different subtypes of KCs.
409
410 We did not observe clear evidence of compensation for lack of inhibition in APL>TNT
411 flies. Could this be because our “acute” manipulation (16-24 h TNT expression in
412 APL) was already long enough to induce adaptation? Two lines of evidence argue
413 against this possibility. First, the effect of blocking APL with 16-24 h of TNT
414 expression is at least as strong as the effect of blocking APL with shibire^{ts}, which
415 occurs over only ~15 min (1). Second, we saw similar size effects for 16-24 h
416 APL>TNT expression and APL>Ort + 5 min histamine bath application (**Fig. S18**).
417 Because 16-24 h APL>TNT expression produces a similar effect on KCs as two
418 separate acute blockades of APL, we consider it unlikely that a shorter TNT
419 blockade would produce larger KC odor responses.
420

Why do KCs show little compensation for lack of inhibition in APL>TNT flies? For example, KCs could in theory increase expression of potassium channels to reduce their excitability (45), yet apparently they do not. It may be that the mushroom body normally tries to compensate for increased KC activity by increasing inhibition from APL (i.e., mechanisms 3-5 in the scheme in **Fig. 4A**, but in the opposite direction), but this strategy fails in APL>TNT flies because synaptic output from APL is permanently blocked. (Indeed, we observed anecdotally that prolonged APL>TNT expression appeared to make APL's neurites degenerate: **Fig. S19**.) This explanation would be consistent with findings in mammals that hyperexcitability is compensated for by increased synaptic inhibition (62-64). Such mechanisms would successfully adapt for variable APL activity; their only failure mode (complete inactivation of APL) might be rare enough not to be worth evolving compensation for. The lack of compensation for blockade of APL may not be surprising in light of other findings that even strong homeostatic compensation can be imperfect (65).

We imposed excess inhibition on KCs by activating APL with dTRPA1 for 4 d. Although it was not technically feasible to verify by *in vivo* recordings that APL was continuously activated throughout the 4 d, **Fig. 5A,S14** show that (1) dTRPA1 activation drives Ca^{2+} influx in APL to a plateau lasting as long as a ~3-4 min heat stimulus and (2) APL activation during imaging is not affected by APL pre-activation for 4 d. APL is unlikely to enter depolarization block as it does not fire action potentials (66). Similarly, activating APL with dTRPA1 still suppresses KC odor responses after 4 d pre-activation (**Fig. 4,S6-7**). These results suggest that APL most likely was depolarized throughout the 4 d pre-activation.

What mechanisms underlie the observed compensation for excess inhibition from APL? We initially postulated five non-mutually-exclusive categories of mechanisms: (1) increased synaptic excitation from PNs to KCs, (2) increased intrinsic excitability of KCs, (3) decreased synaptic excitation from KCs to APL, (4) decreased intrinsic excitability of APL, and (5) decreased synaptic inhibition from APL to KCs (**Fig. 4A**). Our finding that APL shows decreased odor responses after adaptation (**Fig. 4**) implicates decreased synaptic excitation and/or intrinsic excitability of APL (mechanisms 3 and 4). The equal activation of APL by dTRPA1 in control vs. adapted flies (**Fig. 5A**) might argue against decreased intrinsic excitability of APL.

However, dTRPA1 activation might be so strong as to cause a ceiling effect, or GAL4-driven dTRPA1 expression in APL might be higher in pre-heated flies (61), cancelling out any decreased intrinsic excitability.

Our finding of decreased APL activity after APL over-activation is consistent with previous studies showing the converse result: that mammalian interneurons increase their excitability when their activity is blocked (67-69). Yet other studies found opposite effects: decreasing network activity *decreases* excitability of interneurons while increasing activity *increases* it (10, 21, 23, 51). These differences likely arise from whether the system's homeostatic set point focuses on single neurons (i.e., inhibitory interneurons try to maintain their desired activity) or the network as a whole (i.e., if total network activity is decreased, even including decreased interneuron activity, interneurons should still decrease their excitability to disinhibit the network) (70). In our case, both scenarios point in the same direction, as our manipulation activates an inhibitory interneuron (APL) that then inhibits the principal excitatory neurons (KCs); both the primary and secondary effect demand decreased APL excitability as the correct homeostatic response.

We further found that αβ (but not γ) KCs continue to show the adaptation effect when APL is artificially activated (**Fig. 5**) or blocked **(Fig. 6**), implicating increased synaptic excitation or intrinsic excitability of KC (mechanisms 1 and/or 2 in αβ KCs). These findings are consistent with other studies showing increased excitation/excitability of excitatory neurons in response to decreased activity (7, 12, 19, 52, 71, 72). Note that we do not exclude the possibility of decreased synaptic inhibition from APL to KCs (mechanism 5); such weakening of inhibition onto excitatory neurons commonly occurs in response to neuronal inactivity (7, 8, 11, 73). Finally, in contrasting αβ KCs and γ KCs, we do not claim that γ KCs show absolutely no changes in excitation, merely that we did not find evidence of such changes.

What molecular mechanisms may be involved? Neurons in the circuit might sense their abnormally high (APL) or low (KC) activity by reactive oxygen species via the redox sensor DJ-1β (29) or by Ca^{2+} levels via CaM kinase (9, 72). Our finding that adaptation takes more than 1 d suggests that the effector arm of the homeostatic mechanism may involve altered transcription or translation. Increased (KCs) or

decreased (APL) synaptic excitation (mechanisms 1 and 3 above) might occur through altered synapse size/number (30) or altered surface expression of post-synaptic nicotinic acetylcholine receptors, as occurs with AMPA receptors in plasticity of glutamatergic synapses (74, 75). Such changes could also occur by altered pre-synaptic release from PNs or KCs, respectively. However, we consider pre-synaptic plasticity in PNs less likely, as this would be expected to affect all KCs equally rather than only αβ KCs, whereas we only observed increased excitation/excitability in αβ KCs, not γ KCs. Increased (KCs) or decreased (APL) intrinsic excitability (mechanisms 2 and 4 above) might occur through altered ion channel expression, as observed in *Drosophila* larval motor neurons (32), or (for KCs) through moving the axon initial segment (76, 77).

We do not exclude the possibility that other neurons in the mushroom body could be involved in the observed homeostatic compensation. For example, DPM ('dorsal paired medial') also forms reciprocal synapses with KCs (78) and contains GABA (79), so it may be that DPM reduces inhibition of KCs to compensate for excess inhibition from APL. However, unlike APL, DPM shows little or no expression of GABAergic markers (56). Moreover, there is no published physiological evidence that DPM directly inhibits KCs; DPM and APL are connected by gap junctions (80) so findings that activating DPM increases chloride concentrations in KCs (79) could be explained by DPM activating APL. If increased KC activity arises in part from decreased DPM activity causing decreased APL activity via DPM-APL gap junctions, this could be considered a special case of decreased synaptic excitation from KCs to APL.

Our findings that adaptation occurs over multiple days (**Fig. 3, S9-S11**) fit in with diverse adaptation timescales in other *in vivo* studies. Following sensory deprivation in mammals, recovery of cortical activity levels from their nadir can take ~1-3 d (21, 48, 81), even up to 7 d (24). In other cases, adaptation occurs within 24 h (19, 23, 50, 51). It may be that the incomplete suppression of KC odor responses by APL>dTRPA1 activation (**Fig. 5, S6-7**) is a less drastic effect than, e.g., the effect of eyelid suture on visually evoked cortical activity. Intuitively, it is reasonable that homeostatic mechanisms may take longer to sense and respond to a less drastic activity perturbation. Alternatively, it may simply be that the mushroom body is less

efficient at compensating for activity perturbations than mammalian cortex, whether due to differences between species or types of brain structures. Future studies may address these and other questions about the timescale of adaptation, such as whether adaptation occurs in older flies, or whether different underlying mechanisms kick in at different times during the multi-day unfolding of homeostatic adaptation.

Finally, what is the behavioral significance of homeostatic adaptation in Kenyon cells? In the example studied here, increased KC activity following excess inhibition makes odor responses less sparse (**Fig. 2D**), which could impair learned odor discrimination (1). However, it is unclear if the relatively modest decrease in sparseness would measurably impair odor discrimination, especially as we did not detect a significant increase in inter-odor correlations. Indeed, the adaptation might even improve associative olfactory learning, given that improved learning is seen when KC activity is modestly increased by downregulating GABA synthesis in APL (vs. blocking APL output completely) (1, 36, 37). Future work may address which (if any) of these potential behavioral outcomes occurs. Conversely, given that homeostatic compensation following APL>dTRPA1 pre-activation allows αβ (but not γ) KC odor responses to approach normal amplitudes during acute APL>dTRPA1 activation despite the excess inhibition (**Fig. 5**), it will be interesting to test whether pre-activating APL analogously allows flies to resist whatever learning impairment (if any) might normally result from acutely inhibiting KCs with APL>dTRPA1. If so, homeostatic adaptation might help flies avoid detection failures in the case of hyper-inhibition. Indeed, a greater need to avoid detection failures than discrimination failures could explain why the mushroom body compensates for KC hypo-activity but not hyper-activity. More generally, homeostatic plasticity may reflect broader activity-dependent parameter setting in KCs that helps achieve reliably distributed sparse odor coding (82).

Methods

See **SI Appendix, Supplementary Methods** for details.

Fly strains

Flies were raised on standard cornmeal agar at the temperatures described. Details of fly strains are given in **Supplementary Methods**.

Imaging

Brains were imaged by two-photon microscopy on a Movable Objective Microscope (Sutter) using ScanImage software (Vidrio), as described (1, 43). Volume imaging was performed in sawtooth mode (typically 10-16 z slices, volume rate ~3 Hz). Movies were motion-corrected in X-Y using the moco ImageJ plugin (83), and motion-corrected in Z by maximizing the pixel-by-pixel correlation between each volume and the average volume across time points (43). ΔF/F traces were calculated in ImageJ using manually-drawn ROIs for the background and brain structure of interest, and smoothed with a 0.2 s boxcar filter and interpolated to common frame times for averaging traces in Igor Pro 7 (WaveMetrics). ΔR/R in **Fig. 5, Fig. S14** was calculated by dividing GCaMP6f signal by dsRed signal, to remove motion artifacts caused by heating. Sparseness and correlation were analyzed as in (1). Histamine (2 mM, Sigma H7250) was added 5 min before imaging in APL>Ort experiments.

Data availability statement

All data necessary to reproduce our findings and figures is included in the SI Dataset. Analysis code is available at https://github.com/aclinlab/calcium-imaging.

Acknowledgements

We thank members of the Lin and Juusola labs for discussions, Moshe Parnas, Mikko Juusola, and Anton Nikolaev for comments on the manuscript, Lily Bolsover, Chloe Donahue, Kath Whitley, Josh Marston, Rachael Thomas, and Rachid Achour for technical assistance, and Chi-hon Lee (Academia Sinica), the Bloomington Stock Center, and the Vienna *Drosophila* Resource Center for flies. This work was supported by the European Research Council (639489) and the Biotechnology and Biological Sciences Research Council (BB/S016031/1).

Figure legends

Fig. 1. Kenyon cells show little compensation for loss of inhibition from APL

(A) Schematic of mushroom body circuitry: Kenyon cells (KCs) receive feedforward excitation from projection neurons (PNs) and feedback inhibition from APL.

(B) Diagram of genotype (green shows GCaMP6f expression; orange X shows blockade with TNT) and experimental protocol. Flies were raised at 18 ºC, collected 0–1 d after eclosion, then kept at 18 ºC for 3 d and heated to 31 ºC for 16–24 h (middle panel) or kept at 18 ºC for 4 d (right panel) before the imaging experiment, which was always done at 22 ºC.

(C) Responses of different KC lobes to isoamyl acetate (IA, upper) or δ-decalactone (δDL, lower), imaged with GCaMP6f. Black bars, 5 s odor pulse; shading, s.e.m. Diagrams show the locations of different lobes in the mushroom body (green; medial is left, dorsal is up). See also **Fig. S2-3**.

(D) Maximum ΔF/F of data from C. Half-filled circles mean the category pools data, i.e., APL labeled and unlabeled (green), with $GAL80^{ts}$ and without (black). Mean ± 95% confidence interval. # $p < 0.05$ between acute vs. constitutive, * $p < 0.001$ between TNT expressed (acute or constitutive) vs. TNT not expressed (18 ºC or APL unlabeled), ANOVA (see **Table S2** for details). n, given as # hemispheres (# flies), left to right: α′ and α, 9 (5), 9 (7), 22 (15), 17 (10); β′, β and γ, 10 (5), 19 (14), 28 (19), 26 (15).

Fig. 2. Kenyon cell odor responses are higher following prolonged excess inhibition from APL

(A) Diagram of genotype (green shows GCaMP6f expression; magenta shows activation with dTRPA1) and experimental protocol. Flies were raised at 22 ºC, collected 0–1 d after eclosion, kept at 22 ºC (control) or 31 ºC (pre-heated) for 4 d, and returned to 22 ºC for the imaging experiment.

(B) Responses of the γ lobe to isoamyl acetate, for flies kept at 22 ºC (upper) or 31 ºC (lower), where APL was unlabeled (grey/black) or expressed dTRPA1 (pink/red). Black bars, 5 s odor pulse; shading, s.e.m. Responses of all lobes shown in **Fig. S4**.

(C) Maximum ΔF/F of odor responses in all lobes to isoamyl acetate (IA) and δ-decalactone (δDL). * $p < 0.05$, ** $p < 0.01$, *** $p < 0.001$, ANOVA (see **Table S2** for details). n, given as # hemispheres (# flies), left to right within each graph: 9 (8), 15 (11), 11 (7), 13 (8).

(D) Activity maps of responses to isoamyl acetate in KC somata. Grayscale shows baseline fluorescence of GCaMP6f; false-color overlay shows odor-responsive pixels. Scale bar 10 μm.

(E) Average sparseness to a panel of 6 odors (δ-decalactone, isoamyl acetate, ethyl butyrate, methylcyclohexanol, 3-octanol, benzaldehyde; sparseness to each odor shown separately in **Fig. S5**). Mean ± 95% confidence interval. *** $p < 0.001$, unpaired t-test.

Fig. 3. Adaptation to excess inhibition from APL is most prominent after 4 days and is temporary

(A) Adaptation after 1, 2, 3, or 4 d of APL activation. Flies were raised at 22 ºC and collected 0-1 d after eclosion, then kept at 22 ºC for 0-3 d, then kept at 31 ºC for 1-4 d, and imaged at 22 ºC at 4-5 d post-eclosion. Graphs show effect size of adaptation (maximum ΔF/F of KC response to isoamyl acetate, APL>dTRPA1 minus control), calculated using bootstrap-coupled estimation statistics (84), driving dTRPA1 expression in APL using NP2631+GH146-FLP (black circles; control is APL unlabeled) or VT43924-GAL4 (blue squares; control is UAS-dTRPA1/+). Error bars, 95% confidence intervals. In the diagram of the genotype (upper left), green shows GCaMP6f expression, magenta shows activation with dTRPA1. * $p < 0.05$ for APL>dTRPA1 vs. control, ANOVA (see **Table S2** for details). ns ($p > 0.05$) applies to both drivers at 1 d. Full data and sample sizes for all lobes in **Fig. S9-11**.

(B) As in A, except flies were all kept at 31 ºC for 4 d, then kept at 22 ºC for 0-3 d before imaging. Data for 0 d is repeated from '4 d' in panel A for comparison. Full data in **Fig. S12.**

Fig. 4. APL odor responses are reduced following adaptation

(A) Diagrams of potential mechanisms that might underlie increased KC odor responses following adaptation. This figure tests mechanisms 1, 2, 5 vs. mechanisms 3-4, and shows evidence for mechanisms 3-4 (blue box).

(B) Diagram of genotype (APL expresses dTRPA1 and GCaMP6f) and experimental protocol (all flies were raised at 22 ºC and kept at 31 ºC for 4 d before imaging).

(C) Responses of different lobes of APL (as determined by the anatomical marker mb247-dsRed) to isoamyl acetate in APL>GCaMP6f ("no dTRPA1") or APL>dTRPA1,GCaMP6f ("APL>dTRPA1") flies kept at 31 ºC for 4 d. Diagrams show the locations of different lobes (green) within APL, which innervates the whole mushroom body. Graphs show maximum ΔF/F, mean ± 95% confidence interval; shading, s.e.m. * $p < 0.05$, ** $p < 0.01$, unpaired t-test or Mann-Whitney test (see **Table S2** for details). n, left to right: α′ and α, 12 (9 flies), 12(8 flies); β′, β and γ, 12 (9 flies), 13 (8 flies).

Fig. 5. Different KCs show different effects of APL activation after adaptation

(A) APL is equally activated by dTRPA1 regardless of pre-heating. Upper traces show GCaMP6f signal of β lobe of APL (as determined by the anatomical marker mb247-dsRed), normalized to dsRed signal (hence ΔR/R, not ΔF/F), during perfusion heating of saline, in APL>TRPA,GCaMP6f flies kept at 22 ºC (black) or 31 ºC (red) for 4 d. Blue shading shows periods used for quantification in (B): After temperature reached a plateau (period 1), isoamyl acetate (period 2) and δ-decalactone (period 3) were presented. Lower traces show the saline temperature corresponding to recordings in the upper traces (same color scheme and time scale). Shading, s.e.m. Other lobes shown in **Fig. S14**.

(B) Quantification of periods from A: average ΔR/R during temperature plateau (period 1) and maximum ΔR/R during odors (periods 2, 3). Maximum ΔR/R is used for odors for consistency with **Fig. 4**. Graphs show mean ± 95% confidence interval. n.s. $p > 0.05$, unpaired t-test or Mann-Whitney test. n: 22 ºC, 10 (8 flies); 31 ºC, 8 (6 flies).

(C) This figure tests mechanisms 1, 2, 5 vs. mechanisms 3-4, and shows evidence for mechanisms 1, 2, 5 (blue box) in αβ KCs.

(D) Diagram of genotype (APL expresses dTRPA1, KCs express GCaMP6f) and experimental protocol for (E).

(E) Traces show responses of the α, β, and γ lobes to isoamyl acetate (IA, left) and δ-decalactone (δDL, right) in KC>GCaMP6f, APL>dTRPA1 flies kept at

22 ºC or 31 ºC for 4 d, recorded at 22 ºC (black) or 31 ºC (magenta). Only paired recordings are shown (same fly recorded at both temperatures). Black bars, 5 s odor pulse; shading, s.e.m. Bar graphs quantify traces using mean ΔF/F during the odor pulse (same color scheme as traces; bars show mean, thin lines show paired data recorded at 22 ºC and 31 ºC). Data for α′β′ KCs and maximum ΔF/F given in **Fig. S15**. * $p < 0.05$, ** $p < 0.01$, *** $p < 0.001$, paired t-test or Wilcoxon test (22 ºC vs. 31 ºC), unpaired t-test or Mann-Whitney test (across flies), with Holm-Bonferroni correction (see **Table S2** for details). n as in **Fig. S6, S7**.

Fig. 6. Adaptation effect remains in αβ KCs after removing inhibition from APL

(A) This figure tests mechanisms 1-2 vs. mechanisms 3-5, and shows evidence for mechanisms 1-2 (blue box) in αβ KCs.

(B) Diagram of genotype and experimental protocol. Flies were raised at 22 ºC, collected 0–1 d after eclosion, kept at 31 ºC for 4 d, and returned to 22 ºC for the imaging experiment. During the experiment, odor responses were recorded before and after bath-applying 2 mM histamine.

(C) Responses of α, β and γ lobes to isoamyl acetate before (black) and after (orange) bath-applying 2 mM histamine. Genotypes: mixture of hemispheres from APL>Ort and APL>dTRPA1,Ort flies where APL was unlabeled (left); APL>Ort, APL labeled (middle); APL>dTRPA1,Ort, APL labeled (right). Shading, s.e.m. Traces of other lobes and responses to δ-decalactone are shown in **Fig. S16,S17**.

(D) Maximum ΔF/F for traces in (C). Genotypes: APL>Ort (left), APL>dTRPA1,Ort (right). Bars show mean, thin lines show paired data (same hemisphere before and after histamine). The effect of histamine was statistically significant in all cases ($p < 0.001$, paired t-test or Wilcoxon test). * $p < 0.05$, ** $p < 0.01$, unpaired t-test or Mann-Whitney test, Holm-Bonferroni correction for multiple comparisons (see **Table S2** for details). n: no dTRPA1, 17 (11 flies); APL>dTRPA1, 16 (11 flies).

References

1. Lin AC, Bygrave AM, de Calignon A, Lee T, Miesenböck G (2014) Sparse, decorrelated odor coding in the mushroom body enhances learned odor discrimination. *Nat Neurosci* 17(4):559–568.

2. Olshausen BA, Field D (2004) Sparse coding of sensory inputs. *Curr Opin Neurobiol* 14(4):481–487.

3. Litwin-Kumar A, Doiron B (2014) Formation and maintenance of neuronal assemblies through synaptic plasticity. *Nature Communications* 5(1):1–12.

4. O'Leary T, Williams AH, Franci A, Marder E (2014) Cell Types, Network Homeostasis, and Pathological Compensation from a Biologically Plausible Ion Channel Expression Model.

5. Keck T, Hübener M, Bonhoeffer T (2017) Interactions between synaptic homeostatic mechanisms: an attempt to reconcile BCM theory, synaptic scaling, and changing excitation/inhibition balance. *Curr Opin Neurobiol* 43:87–93.

6. Turrigiano G (2011) Too many cooks? Intrinsic and synaptic homeostatic mechanisms in cortical circuit refinement. *Annu Rev Neurosci* 34:89–103.

7. Maffei A, Nelson SB, Turrigiano GG (2004) Selective reconfiguration of layer 4 visual cortical circuitry by visual deprivation. *Nat Neurosci* 7(12):1353–1359.

8. Maffei A, Turrigiano GG (2008) Multiple Modes of Network Homeostasis in Visual Cortical Layer 2/3. *J Neurosci* 28(17):4377–4384.

9. Goold CP, Nicoll RA (2010) Single-cell optogenetic excitation drives homeostatic synaptic depression. *Neuron* 68(3):512–528.

10. Chang MC, et al. (2010) Narp regulates homeostatic scaling of excitatory synapses on parvalbumin-expressing interneurons. *Nat Neurosci* 13(9):1090–1097.

11. Lau CG, Murthy VN (2012) Activity-Dependent Regulation of Inhibition via GAD67. *J Neurosci* 32(25):8521–8531.

12. Desai NS, Cudmore RH, Nelson SB, Turrigiano GG (2002) Critical periods for experience-dependent synaptic scaling in visual cortex. *Nat Neurosci* 5(8):783–789.

13. Wenner P (2014) Homeostatic synaptic plasticity in developing spinal networks driven by excitatory GABAergic currents. *Neuropharmacology* 78:55–62.

14. Destexhe A, Rudolph M, Paré D (2003) The high-conductance state of neocortical neurons in vivo. *Nat Rev Neurosci* 4(9):739–751.

15. Kirov SA, Sorra KE, Harris KM (1999) Slices have more synapses than perfusion-fixed hippocampus from both young and mature rats. *J Neurosci*

19(8):2876–2886.

16. Cazakoff BN, Lau BYB, Crump KL, Demmer HS, Shea SD (2014) Broadly tuned and respiration-independent inhibition in the olfactory bulb of awake mice. *Nat Neurosci* 17(4):569–576.

17. Knogler LD, Liao M, Drapeau P (2010) Synaptic scaling and the development of a motor network. *J Neurosci* 30(26):8871–8881.

18. Mongeon R, et al. (2008) Synaptic Homeostasis in a Zebrafish Glial Glycine Transporter Mutant. *J Neurophysiol* 100(4):1716–1723.

19. Keck T, et al. (2013) Synaptic scaling and homeostatic plasticity in the mouse visual cortex in vivo. *Neuron* 80(2):327–334.

20. Barnes SJ, et al. (2015) Subnetwork-Specific Homeostatic Plasticity in Mouse Visual Cortex In Vivo. *Neuron* 86(5):1290–1303.

21. Hengen KB, Lambo ME, Van Hooser SD, Katz DB, Turrigiano GG (2013) Firing rate homeostasis in visual cortex of freely behaving rodents. *Neuron* 80(2):335–342.

22. Hengen KB, Torrado Pacheco A, McGregor JN, Van Hooser SD, Turrigiano GG (2016) Neuronal Firing Rate Homeostasis Is Inhibited by Sleep and Promoted by Wake. *Cell* 165(1):180–191.

23. Kuhlman SJ, et al. (2013) A disinhibitory microcircuit initiates critical-period plasticity in the visual cortex. *Nature* 501(7468):543–546.

24. Greenhill SD, Ranson A, Fox K (2015) Hebbian and Homeostatic Plasticity Mechanisms in Regular Spiking and Intrinsic Bursting Cells of Cortical Layer 5. *Neuron* 88(3):539–552.

25. Amin H, Lin AC (2019) Neuronal mechanisms underlying innate and learned olfactory processing in Drosophila. *Current Opinion in Insect Science* 36:9–17.

26. Devaud JM, Acebes A, Ferrus A (2001) Odor exposure causes central adaptation and morphological changes in selected olfactory glomeruli in Drosophila. *J Neurosci* 21(16):6274–6282.

27. Sachse S, et al. (2007) Activity-dependent plasticity in an olfactory circuit. *Neuron* 56(5):838–850.

28. Das S, et al. (2011) Plasticity of local GABAergic interneurons drives olfactory habituation. *Proc Natl Acad Sci USA* 108(36):E646–E654.

29. Oswald MC, et al. (2018) Reactive oxygen species regulate activity-dependent neuronal plasticity in Drosophila. *Elife* 7:1321.

30. Kremer MC, et al. (2010) Structural long-term changes at mushroom body input synapses. 20(21):1938–1944.

795 31. Doll CA, Vita DJ, Broadie K (2017) Fragile X Mental Retardation Protein
796 Requirements in Activity-Dependent Critical Period Neural Circuit Refinement.
797 27(15):2318–2330.e3.

798 32. Mee CJ, Pym ECG, Moffat KG, Baines RA (2004) Regulation of neuronal
799 excitability through pumilio-dependent control of a sodium channel gene. *J*
800 *Neurosci* 24(40):8695–8703.

801 33. Davis GW (2013) Homeostatic signaling and the stabilization of neural
802 function. *Neuron* 80(3):718–728.

803 34. Kazama H, Wilson RI (2008) Homeostatic matching and nonlinear
804 amplification at identified central synapses. *Neuron* 58(3):401–413.

805 35. Gruntman E, Turner GC (2013) Integration of the olfactory code across
806 dendritic claws of single mushroom body neurons. *Nat Neurosci* 16(12):1821–
807 1829.

808 36. Liu X, Davis RL (2008) The GABAergic anterior paired lateral neuron
809 suppresses and is suppressed by olfactory learning. *Nat Neurosci* 12(1):53–
810 59.

811 37. Lei Z, Chen K, Li H, Liu H, Guo A (2013) The GABA system regulates the
812 sparse coding of odors in the mushroom bodies of Drosophila. *Biochem*
813 *Biophys Res Commun* 436(1):35–40.

814 38. Honegger KS, Campbell RAA, Turner GC (2011) Cellular-resolution population
815 imaging reveals robust sparse coding in the Drosophila mushroom body. *J*
816 *Neurosci* 31(33):11772–11785.

817 39. Mittal AM, Gupta D, Singh A, Lin AC, Gupta N (2020) Multiple network
818 properties overcome random connectivity to enable stereotypic sensory
819 responses. *Nature Communications* 11(1):1–15.

820 40. Mayseless O, et al. (2018) Developmental Coordination during Olfactory
821 Circuit Remodeling in Drosophila. *Neuron* 99(6):1204–1215.e5.

822 41. Pitman JL, et al. (2011) A pair of inhibitory neurons are required to sustain
823 labile memory in the Drosophila mushroom body. *Current Biology* 21(10):855–
824 861.

825 42. Hallem EA, Carlson JR (2006) Coding of Odors by a Receptor Repertoire. *Cell*
826 125(1):143–160.

827 43. Bielopolski N, et al. (2019) Inhibitory muscarinic acetylcholine receptors
828 enhance aversive olfactory learning in adult Drosophila. *Elife* 8:463.

829 44. Turner GC, Bazhenov M, Laurent G (2008) Olfactory representations by
830 Drosophila mushroom body neurons. *J Neurophysiol* 99(2):734–746.

831 45. Groschner LN, Chan Wah Hak L, Bogacz R, DasGupta S, Miesenböck G
832 (2018) Dendritic Integration of Sensory Evidence in Perceptual Decision-

Making. *Cell* 173(4):894–905.e13.

46. Inada K, Tsuchimoto Y, Kazama H (2017) Origins of Cell-Type-Specific Olfactory Processing in the Drosophila Mushroom Body Circuit. *Neuron* 95(2):357–367.e4.

47. Hamada FN, et al. (2008) An internal thermal sensor controlling temperature preference in Drosophila. *Nature* 454(7201):217–220.

48. Frenkel MY, Bear MF (2004) How Monocular Deprivation Shifts Ocular Dominance in Visual Cortex of Young Mice. *Neuron* 44(6):917–923.

49. Wu C-L, Shih M-FM, Lee P-T, Chiang A-S (2013) An octopamine-mushroom body circuit modulates the formation of anesthesia-resistant memory in Drosophila. *Current Biology* 23(23):2346–2354.

50. Barnes SJ, et al. (2017) Deprivation-Induced Homeostatic Spine Scaling In Vivo Is Localized to Dendritic Branches that Have Undergone Recent Spine Loss. *Neuron* 96(4):871–882.e5.

51. Gainey MA, Aman JW, Feldman DE (2018) Rapid Disinhibition by Adjustment of PV Intrinsic Excitability during Whisker Map Plasticity in Mouse S1. *J Neurosci* 38(20):4749–4761.

52. Turrigiano GG, Leslie KR, Desai NS, Rutherford LC, Nelson SB (1998) Activity-dependent scaling of quantal amplitude in neocortical neurons. *Nature* 391(6670):892–896.

53. Pantazis A, et al. (2008) Distinct roles for two histamine receptors (hclA and hclB) at the Drosophila photoreceptor synapse. *J Neurosci* 28(29):7250–7259.

54. Liu WW, Wilson RI (2013) Transient and specific inactivation of Drosophila neurons in vivo using a native ligand-gated ion channel. 23(13):1202–1208.

55. Pollack I, Hofbauer A (1991) Histamine-like immunoreactivity in the visual system and brain of Drosophila melanogaster. *Cell Tissue Res* 266(2):391–398.

56. Aso Y, et al. (2019) Nitric oxide acts as a cotransmitter in a subset of dopaminergic neurons to diversify memory dynamics. *Elife* 8:e49257.

57. Croset V, Treiber CD, Waddell S (2018) Cellular diversity in the Drosophila midbrain revealed by single-cell transcriptomics. *Elife* 7:e34550.

58. Davie K, et al. (2018) A Single-Cell Transcriptome Atlas of the Aging Drosophila Brain. *Cell* 174(4):982–998.e20.

59. Shih M-FM, Davis FP, Henry GL, Dubnau J (2019) Nuclear Transcriptomes of the Seven Neuronal Cell Types That Constitute the Drosophila Mushroom Bodies. *G3 (Bethesda)* 9(1):81–94.

60. Crocker A, Guan X-J, Murphy CT, Murthy M (2016) Cell-Type-Specific

Transcriptome Analysis in the Drosophila Mushroom Body Reveals Memory-Related Changes in Gene Expression. *Cell Rep* 15(7):1580–1596.

61. Duffy JB (2002) GAL4 system in Drosophila: a fly geneticist's Swiss army knife. *genesis* 34(1-2):1–15.

62. Sim S, et al. (2013) Increased cell-intrinsic excitability induces synaptic changes in new neurons in the adult dentate gyrus that require Npas4. *J Neurosci* 33(18):7928–7940.

63. Peng Y-R, et al. (2010) Postsynaptic spiking homeostatically induces cell-autonomous regulation of inhibitory inputs via retrograde signaling. *J Neurosci* 30(48):16220–16231.

64. Xue M, Atallah BV, Scanziani M (2014) Equalizing excitation-inhibition ratios across visual cortical neurons. *Nature* 511(7511):596–600.

65. Howard MA, Rubenstein JLR, Baraban SC (2014) Bidirectional homeostatic plasticity induced by interneuron cell death and transplantation in vivo. *Proc Natl Acad Sci USA* 111(1):492–497.

66. Papadopoulou M, Cassenaer S, Nowotny T, Laurent G (2011) Normalization for sparse encoding of odors by a wide-field interneuron. *Science* 332(6030):721–725.

67. Bartley AF, Huang ZJ, Huber KM, Gibson JR (2008) Differential Activity-Dependent, Homeostatic Plasticity of Two Neocortical Inhibitory Circuits. *J Neurophysiol* 100(4):1983–1994.

68. Rutherford LC, Nelson SB, Turrigiano GG (1998) BDNF Has Opposite Effects on the Quantal Amplitude of Pyramidal Neuron and Interneuron Excitatory Synapses. *Neuron* 21(3):521–530.

69. Desai NS, Rutherford LC, Turrigiano GG (1999) BDNF regulates the intrinsic excitability of cortical neurons. *Learn Mem* 6(3):284–291.

70. Wenner P (2011) Mechanisms of GABAergic Homeostatic Plasticity. *Neural Plast* 2011(5161):1–6.

71. Burrone J, O'Byrne M, Murthy VN (2002) Multiple forms of synaptic plasticity triggered by selective suppression of activity in individual neurons. *Nature* 420(6914):414–418.

72. Ibata K, Sun Q, Turrigiano GG (2008) Rapid synaptic scaling induced by changes in postsynaptic firing. *Neuron* 57(6):819–826.

73. Hartman KN, Pal SK, Burrone J, Murthy VN (2006) Activity-dependent regulation of inhibitory synaptic transmission in hippocampal neurons. *Nat Neurosci* 9(5):642–649.

74. Anggono V, Huganir RL (2012) Regulation of AMPA receptor trafficking and synaptic plasticity. *Curr Opin Neurobiol* 22(3):461–469.

908 75. Wierenga CJ, Ibata K, Turrigiano GG (2005) Postsynaptic expression of
909 homeostatic plasticity at neocortical synapses. *J Neurosci* 25(11):2895–2905.

910 76. Grubb MS, Burrone J (2010) Activity-dependent relocation of the axon initial
911 segment fine-tunes neuronal excitability. *Nature* 465(7301):1070–1074.

912 77. Trunova S, Baek B, Giniger E (2011) Cdk5 regulates the size of an axon initial
913 segment-like compartment in mushroom body neurons of the Drosophila
914 central brain. *J Neurosci* 31(29):10451–10462.

915 78. Takemura S-Y, et al. (2017) A connectome of a learning and memory center in
916 the adult Drosophila brain. *Elife* 6:5643.

917 79. Haynes PR, Christmann BL, Griffith LC (2015) A single pair of neurons links
918 sleep to memory consolidation in Drosophila melanogaster. *Elife* 4.
919 doi:10.7554/eLife.03868.

920 80. Wu C-L, et al. (2011) Heterotypic gap junctions between two neurons in the
921 drosophila brain are critical for memory. 21(10):848–854.

922 81. Kaneko M, Stellwagen D, Malenka RC, Stryker MP (2008) Tumor Necrosis
923 Factor-α Mediates One Component of Competitive, Experience-Dependent
924 Plasticity in Developing Visual Cortex. *Neuron* 58(5):673–680.

925 82. Luo SX, Axel R, Abbott LF (2010) Generating sparse and selective third-order
926 responses in the olfactory system of the fly. *Proc Natl Acad Sci USA*
927 107(23):10713–10718.

928 83. Dubbs A, Guevara J, Yuste R (2016) moco: Fast Motion Correction for
929 Calcium Imaging. *Front Neuroinform* 10:6.

930 84. Ho J, Tumkaya T, Aryal S, Choi H, Claridge-Chang A (2019) Moving beyond P
931 values: data analysis with estimation graphics. *Nat Methods* 16(7):565–566.

932

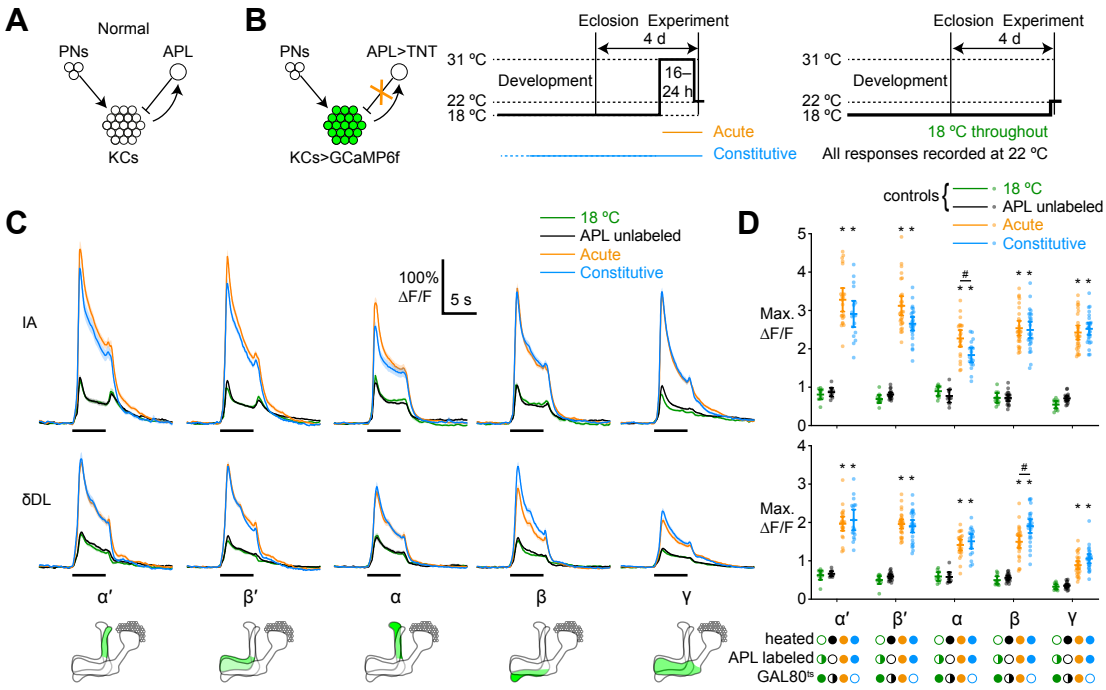
A
Normal
PNs
APL
KCs
B
PNs
APL>TNT
KCs>GCaMP6f
Eclosion
Experiment
4 d
31 ºC
Development
16–
24 h
22 ºC
18 ºC
Acute
Constitutive
18 ºC throughout
All responses recorded at 22 ºC
C
18 ºC
APL unlabeled
Acute
Constitutive
100%
ΔF/F
5 s
lA
δDL
α′
β′
α
β
γ
D
controls
Max.
ΔF/F
heated
APL labeled
GAL80ts

Figure 1

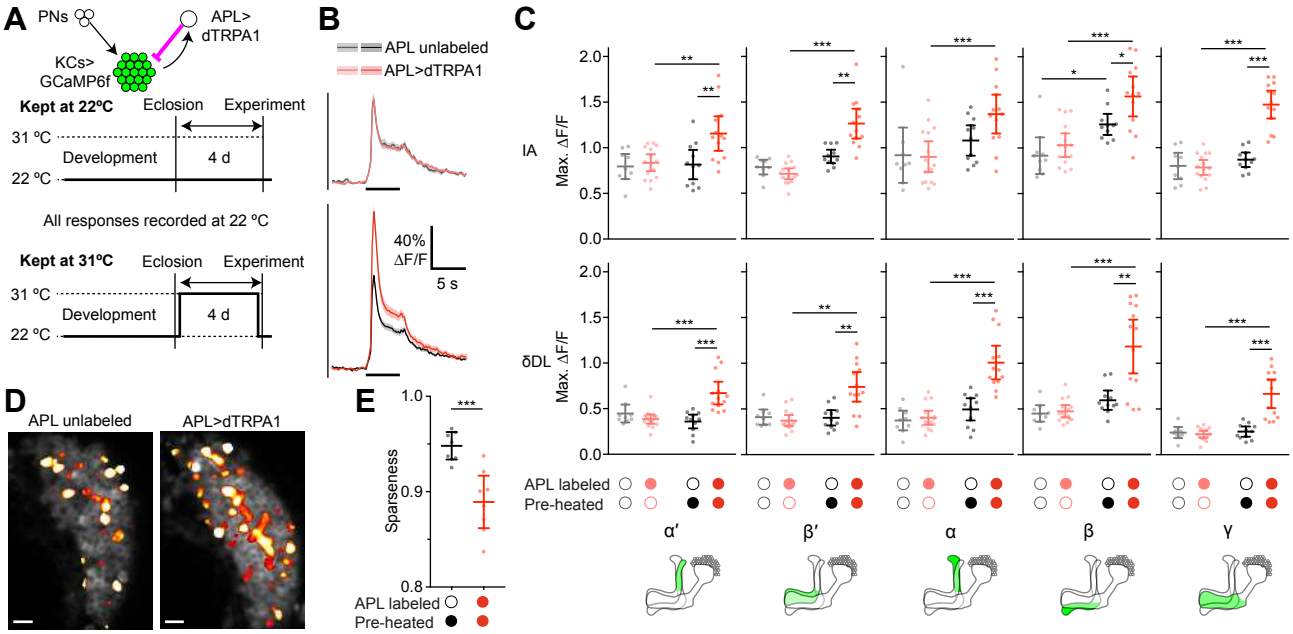
A
PNs
APL>
dTRPA1
KCs>
GCaMP6f
Kept at 22ºC
Eclosion
Experiment
31 ºC
Development
4 d
22 ºC
All responses recorded at 22 ºC
Kept at 31ºC
Eclosion
Experiment
31 ºC
Development
4 d
22 ºC
B
APL unlabeled
APL>dTRPA1
40%
ΔF/F
5 s
C
IA
Max. ΔF/F
δDL
Max. ΔF/F
APL labeled
Pre-heated
α′
β′
α
β
γ
D
APL unlabeled
APL>dTRPA1
E
Sparseness
APL labeled
Pre-heated

Figure 2

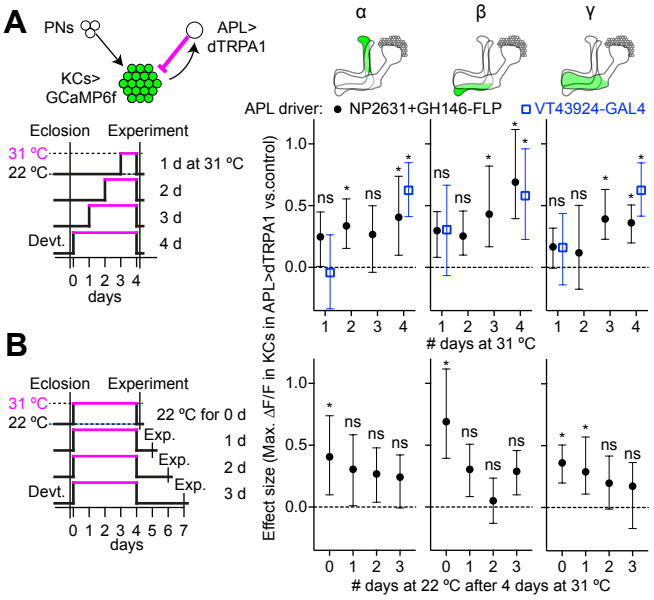
A
PNs
APL>
dTRPA1
KCs>
GCaMP6f
Eclosion
Experiment
31 ºC
22 ºC
Devt.
1 d at 31 ºC
2 d
3 d
4 d
0 1 2 3 4
days
B
Eclosion
Experiment
31 ºC
22 ºC
22 ºC for 0 d
Exp.
1 d
Exp.
2 d
Exp.
3 d
Devt.
0 1 2 3 4 5 6 7
days
α
β
γ
APL driver: NP2631+GH146-FLP
VT43924-GAL4
Effect size (Max. ΔF/F in KCs in APL>dTRPA1 vs.control)
days at 31 ºC
days at 22 ºC after 4 days at 31 ºC
ns
*

Figure 3

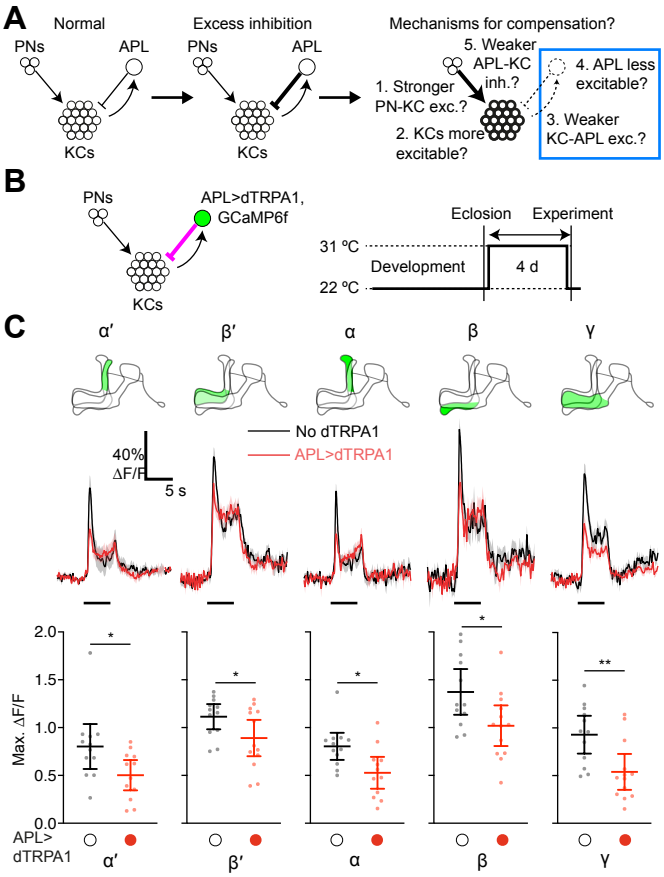
A
Normal
PNs
APL
KCs
Excess inhibition
PNs
APL
KCs
Mechanisms for compensation?
1. Stronger PN-KC exc.?
2. KCs more excitable?
5. Weaker APL-KC inh.?
4. APL less excitable?
3. Weaker KC-APL exc.?
B
PNs
APL>dTRPA1, GCaMP6f
KCs
Eclosion
Experiment
31 ºC
Development
4 d
22 ºC
C
α′
β′
α
β
γ
No dTRPA1
APL>dTRPA1
40% ΔF/F
5 s
Max. ΔF/F
2.0
1.5
1.0
0.5
0.0
APL> dTRPA1
α′
β′
α
β
γ

Figure 4

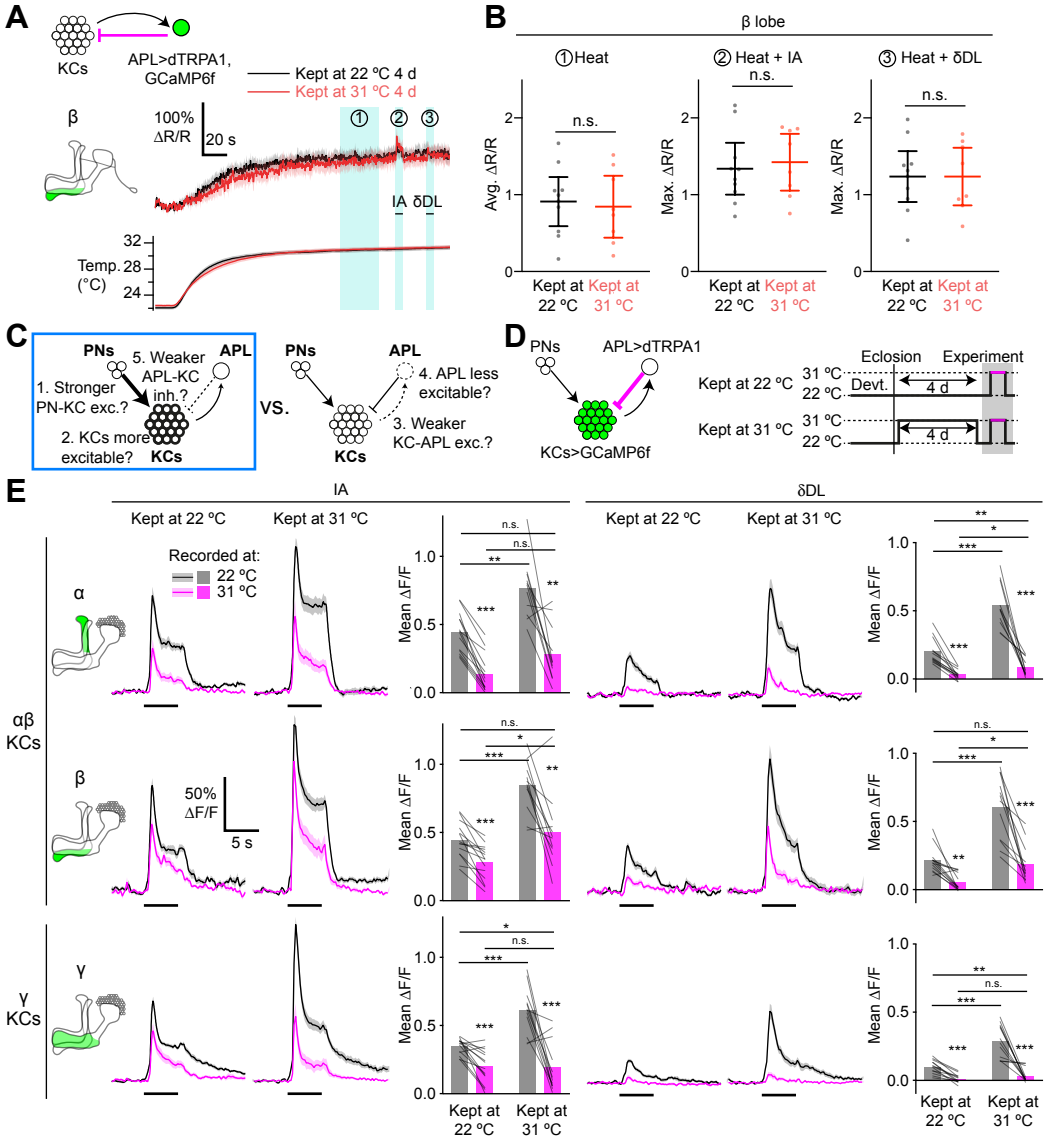
A
KCs
APL>dTRPA1, GCaMP6f
Kept at 22 °C 4 d
Kept at 31 °C 4 d
β
100% ΔR/R
20 s
① ② ③
IA δDL
Temp. (°C)
32
28
24
B
β lobe
①Heat
② Heat + IA
③ Heat + δDL
n.s.
Avg. ΔR/R
Max. ΔR/R
Kept at 22 °C
Kept at 31 °C
C
PNs
APL
KCs
1. Stronger PN-KC exc.?
2. KCs more excitable?
5. Weaker APL-KC inh.?
VS.
4. APL less excitable?
3. Weaker KC-APL exc.?
D
PNs
APL>dTRPA1
KCs>GCaMP6f
Eclosion
Experiment
Devt.
4 d
Kept at 22 °C
Kept at 31 °C
31 °C
22 °C
E
IA
δDL
Recorded at:
22 °C
31 °C
α
β
γ
αβ KCs
γ KCs
50% ΔF/F
5 s
Mean ΔF/F
n.s.
*
**
***

Figure 5

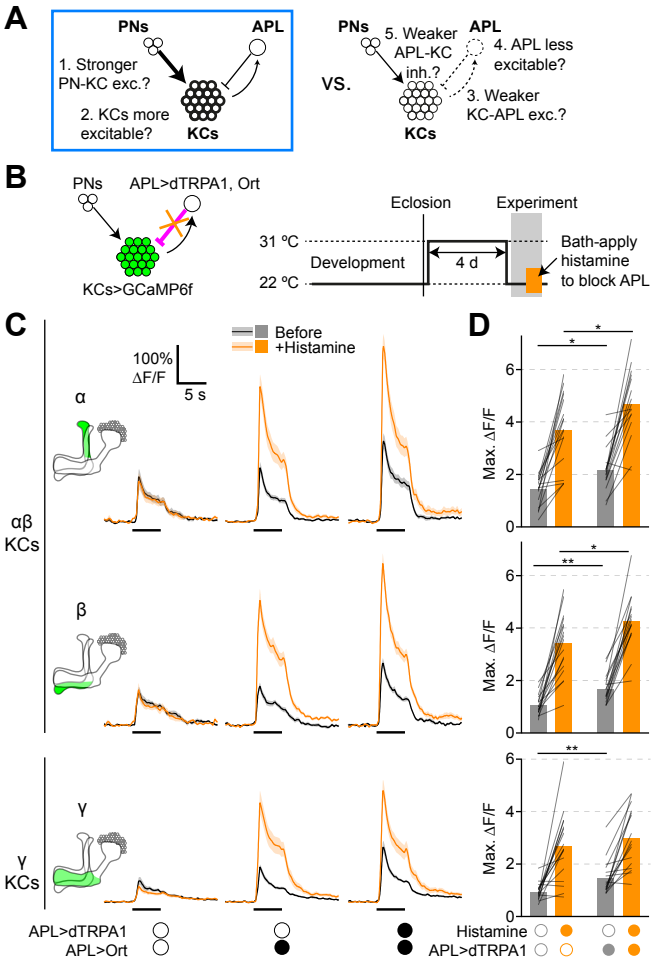
A
PNs
APL
1. Stronger PN-KC exc.?
2. KCs more excitable?
KCs
VS.
5. Weaker APL-KC inh.?
4. APL less excitable?
3. Weaker KC-APL exc.?
B
PNs
APL>dTRPA1, Ort
KCs>GCaMP6f
Eclosion
Experiment
31 °C
22 °C
Development
4 d
Bath-apply histamine to block APL
C
Before
+Histamine
100% ΔF/F
5 s
α
αβ KCs
β
γ
γ KCs
APL>dTRPA1
APL>Ort
D
Max. ΔF/F
Histamine
APL>dTRPA1

Figure 6

PNAS
www.pnas.org

Supplementary Information for

Mechanisms underlying homeostatic plasticity in the *Drosophila* mushroom body *in vivo*

Anthi A. Apostolopoulou, Andrew C. Lin
Department of Biomedical Science, University of Sheffield, Sheffield S10 2TN, UK
Neuroscience Institute, University of Sheffield, Sheffield S10 2TN, UK

For correspondence: Andrew C. Lin
Email: andrew.lin@sheffield.ac.uk

This PDF file includes:

Supplementary Information Text

Supplementary Methods

Fly strains

Fly strains (see below) were raised on standard cornmeal agar (80 g medium cornmeal, 18 g dried yeast, 10 g soya flour, 80 g malt extract, 40 g molasses, 8 g agar, 25 ml 10% nipagin in ethanol, 4 ml propionic acid per 1 L water), at 25 ºC for preparatory fly crosses, and at 18 ºC ($GAL80^{ts}$ flies) or 22 ºC (dTRPA1 flies) as described, and in some cases heated to 31 ºC after eclosion as described. Flies were imaged at the ages specified in the Results section.

The following transgenic strains were used: NP2631-GAL4 (1), GH146-FLP (2), tubP-FRT-GAL80-FRT (for dTRPA1, on chromosome 2: (3); for TNT, on chromosome 2 or 3: (4)), UAS-TNT (5), tubP-$GAL80^{ts}$ (6), UAS-CD8::GFP (7), UAS-mCherry-CAAX (8), MB247-LexA::VP16 (9), lexAop-GCaMP6f (10), lexAop-GCaMP3 (11), UAS-dTRPA1 (12), VT43924-GAL4 (13) (note that we did not include UAS-GAL4), UAS-Ort (14) (gift from Chi-hon Lee).

Functional imaging

Calcium imaging was performed as described (11, 15). Cuticle and trachea in a window overlying the mushroom body were removed, and the exposed brain was superfused (perfusion pump Watson-Marlow 120S DM2, ~2.7 ml/min) with carbogenated (95% O_2, 5% CO_2) solution containing 103 mM NaCl, 3 mM KCl, 5 mM trehalose, 10 mM glucose, 26 mM $NaHCO_3$, 1 mM NaH_2PO_4, 3 mM $CaCl_2$, 4 mM $MgCl_2$, 5 mM N-Tris (TES), pH 7.3. Odors (10^{-2} for isoamyl acetate, δ-decalactone; 10^{-1} for ethyl butyrate, benzaldehyde, 4-methylcyclohexanol, 3-octanol) were delivered by switching mass-flow controlled carrier and stimulus streams (Sensirion) via software controlled solenoid valves (The Lee Company). The flow rate at the fly was ~0.5 L/min. Flies were heated during imaging using a perfusion heater (Scientifica, SM-4600). Histamine (2 mM, Sigma H7250) was added 5 min before imaging in APL>Ort experiments. Although histamine was reported to effectively suppress activity in Ort-expressing neurons at 100 µM (14), in preliminary experiments we found that 100 µM histamine did not increase KC odor responses in APL>Ort flies but 2 mM histamine did (Fig. 6), possibly because a mere reduction in APL activity (as opposed to a total blockade) would be canceled out by increased KC activity due to the KC-APL negative feedback loop.

Brains were imaged by two-photon microscopy (16, 17). Fluorescence was excited by 75-80 fs pulses (pulse width measured by APE Carpe autocorrelator) of 910 nm light at 80 MHz from a Ti:Sapphire laser (Spectra-Physics eHP DS), attenuated by a Pockels cell (Conoptics, Model 350-80LA) and coupled to a galvo-resonant scanner on a Movable Objective Microscope (Sutter Instruments). Excitation light was focused by a 20X, 1.0 NA objective (Olympus XLUMPLFLN20XW), and emitted photons were passed through a 750 nm short pass filter (to exclude excitation light) and bandpass filters (green: 525/50; red: 605/70), and detected by GaAsP photomultiplier tubes (Hamamatsu Photonics, H10770PA-40SEL), whose currents were amplified (Thorlabs, TIA60) and transferred to the imaging computer running ScanImage 5 (Vidrio Technologies). Volume imaging was performed using a piezo objective stage (nPFocus400, nPoint) using ScanImage's FastZ control in sawtooth mode (typically 10-16 z slices, volume rate ~3 Hz).

Movies were motion-corrected in X-Y using the moco ImageJ plugin (18), with pre-processing to collapse volume movies in Z and to smooth the image with a Gaussian filter (standard deviation = 4 pixels; the displacements generated from the smoothed movie were then applied to the original, unsmoothed movie), and motion-corrected in Z by maximizing the pixel-by-pixel correlation between each volume and the average volume across time points (15). $\Delta F/F$ traces were calculated in ImageJ using manually-drawn ROIs for the background and brain structure of interest, and smoothed with a 0.2 s boxcar filter in Igor Pro 7 (WaveMetrics). $\Delta R/R$ in Fig. 5, Fig. S14 was calculated by dividing GCaMP6f signal by dsRed signal, to remove motion artifacts caused by heating. Where traces with different frame times needed to be averaged, traces were linearly interpolated to a frame time of 0.018 s, except for Fig. 5a, Fig. S14c, where they were interpolated to 0.2878 s due to software limitations. Flies were excluded if the neurons of interest did not respond to odor, the GCaMP6f signal was too low/noisy, or the brain moved too much to correct for motion artifacts.

Activity maps were generated as in (11, 15). Briefly, movies were smoothed with a 5-pixel-square Gaussian filter (standard deviation 2). Baseline fluorescence was taken as the average fluorescence during the pre-stimulus period. Frames with sudden, large axial movements were discarded by correlating each frame to the baseline image and discarding it if the correlation fell below a threshold value, which was manually selected for each brain by noting the constant high correlation value when the brain was stationary and sudden drops in correlation when the brain moved. ΔF/F was calculated for each pixel as the difference between mean fluorescence during the stimulus period vs. the baseline fluorescence (ΔF), divided by the baseline fluorescence. For pixels where ΔF did not exceed 2 times the standard deviation over time of that pixel's intensity during the pre-stimulus period, the pixel was considered non-responsive. We excluded non-responsive flies and flies whose motion could not be corrected.

Inter-odor correlations were calculated by first aligning the activity maps of each odor response by maximizing the inter-odor correlations of baseline fluorescence, and then converting image matrices of the activity maps of each odor response into linear vectors and calculating the Pearson correlation coefficients between each "odor vector". Where a pair of volume movies did not fully align in z, a subset of z-slices was chosen that did align. A threshold for baseline fluorescence was applied as a mask to the activity map to exclude pixels with no baseline GCaMP6f signal. Areas with non-GCaMP6f fluorescence (e.g., cuticle) or non-KC-soma areas (e.g., calyx) were manually excluded. Population sparseness was calculated for activity maps using the following equation (19, 20):

$$S_P = \frac{1}{1-\frac{1}{N}}\left(1-\frac{\left(\sum_{i=1}^{N}\frac{r_i}{N}\right)^2}{\sum_{i=1}^{N}\frac{{r_i}^2}{N}}\right)$$

where N is the number of pixels and r_i is the response of each pixel. Analysis code is available at https://github.com/aclinlab/calcium-imaging.

Structural imaging

To visualize tetanus toxin expression in APL>TNT flies, we either included UAS-mCherry in the genotype as in (15) or immunostained with anti-TNT antibody (Abcam, ab53829, formerly known as POL 016 from Statens Serum Institut). mCherry expression in APL was distinguished from 3XP3-driven dsRed from the GH146-FLP transgene by using separate filter cubes for dsRed (49004, Chroma: 545/25 excitation; 565 dichroic; 605/70 emission) and mCherry (LED-mCherry-A-000, Semrock: 578/21 excitation; 596 dichroic; 641/75 emission). Immunostaining was carried out as described in (11, 21). Dissected brains were fixed in 4% (wt/vol) paraformaldehyde in PBT (100 mM Na_2PO_4, 0.3% Triton-X-100, pH 7.2), washed in PBT (2 quick washes, then 3 20 min washes), blocked with 5% goat serum (Sigma, G6767) in PBT, incubated in primary antibody (1:100 in blocking solution) at 4 ºC over 2-3 nights, washed in PBT (2 quick washes, then 3 20 min washes), incubated in secondary antibody (goat anti-rabbit Alexa 546, 1:500, ThermoFisher A11071), washed in PBT (2 quick washes, then 3 20 min washes), and mounted in Vectashield (Vector Laboratories, H-1000). mCherry expression or anti-TNT staining was scored using epifluorescence.

Statistics

Statistical analyses were performed in Prism 8 (GraphPad) and MATLAB. Bootstrap-coupled estimation statistics (22) were analysed using the DABEST package (https://github.com/ACCLAB/DABEST-python). Parametric (t-test, ANOVA) or non-parametric tests (Mann-Whitney, Friedman, Kruskal-Wallis) were used depending on whether raw data (for pairwise comparisons) or residuals (for ANOVAs) passed the D'Agostino-Pearson normality test. For ANOVAs and unpaired t-tests, Welch or Greenhouse-Geisser corrections were applied when variances were significantly different between groups. Random assignment to experimental groups was not used as all manipulations were genetic. In general, no statistical tests were done to pre-determine sample size, but where a conclusion relied on the absence of a significant effect, a power analysis was performed to confirm if the sample size was sufficient to detect an effect of the expected size; if not, the lack of statistical power was explicitly noted. The experimenter was blind to which APL neurons were labeled before post-experimental dissection (Fig. 1-3,5-6) and for some acute vs. constitutive experiments in Fig. S2c, but not otherwise.

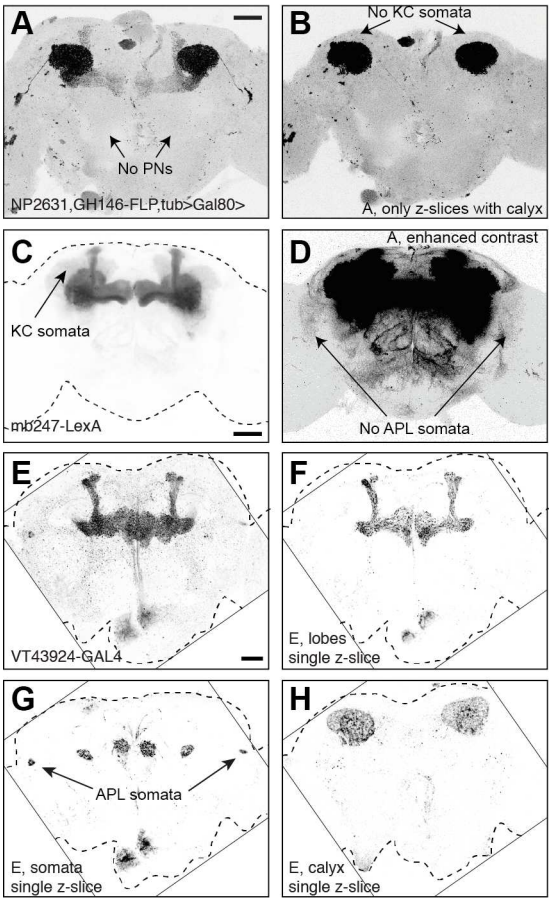

Fig. S1 (related to all figures). Expression pattern of APL and KC drivers

(A) Expression pattern of the intersection of NP2631-GAL4 and GH146-FLP where both APL neurons are labeled (data from ref. 11, Fig. 4c). Projection neurons (PNs) are not labeled.
(B) Image in A with maximum intensity projection through only the z-slices containing the calyx. No KC somata are labelled (should appear dorsally and laterally to the calyx, as visible in panel C, but even stronger here as this brain was imaged posterior side up).
(C) Expression pattern of MB247-LexA (data from ref. 11, Fig. 1e).
(D) Image in C with enhanced contrast, to show that APL is not labelled by MB247-LexA.
(E) Expression pattern of VT43924-GAL4 driving UAS-CD8::GFP. Maximum intensity projection of z-stack of unfixed brain captured on a two-photon microscope. The non-APL expression along the midline and in the periesophageal neuropils can also be seen in Fig. 1C of (13). Note the lack of expression in the antennal lobes.
(F) Single z-slice of (E) 30 µm deep revealing the typical neurite structure of APL in the mushroom body lobes, indicating that other mushroom body neurons are not labeled. Contrast in (F-H) differs from (E) and from each other to compensate for decreased signal deep in uncleared tissue.
(G) Single z-slice of (E) 48 µm deep showing the APL cell bodies.
(H) Single z-slice of (E) 134 µm deep showing APL in the calyces.

Scale bars 50 µm. Dashed outlines outline the brain. Thin diagonal lines outline the boundaries of the rotated field of view.

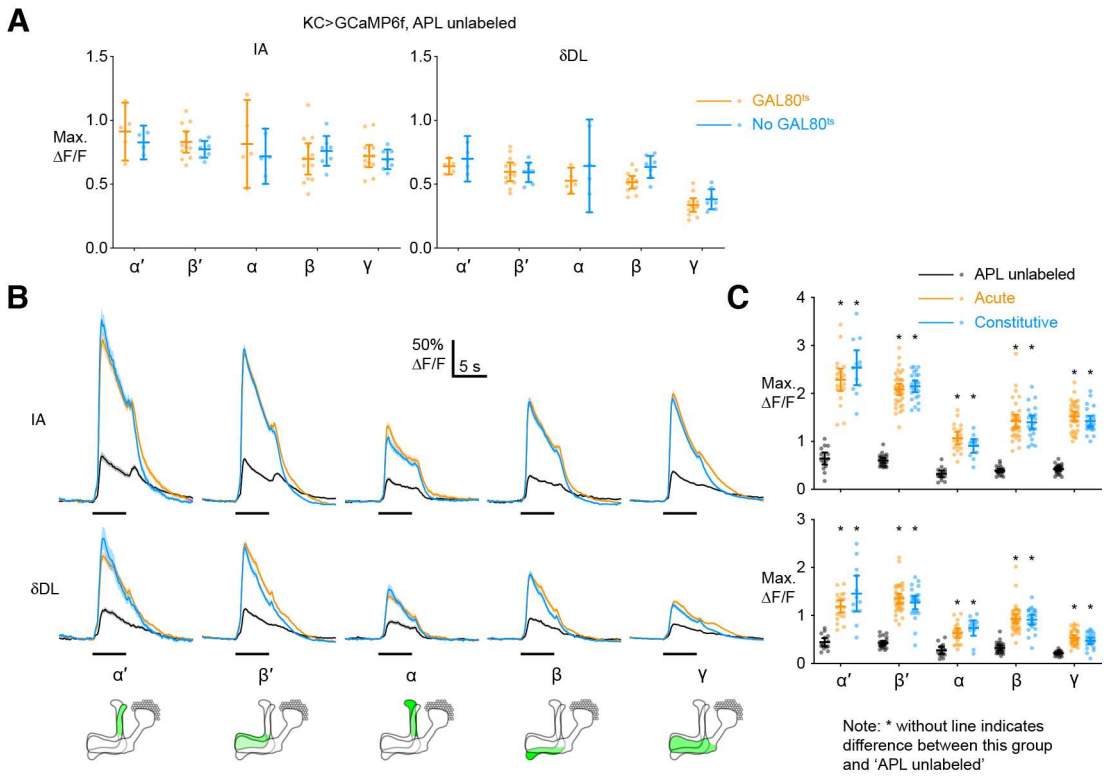

Fig. S2 (related to Fig. 1). Additional data for APL>TNT

(A) KC>GCaMP6f odor responses in APL-unlabeled control hemispheres are the same in flies with (orange) and without (blue) GAL80^{ts}. Graph shows maximum ΔF/F (data taken from **Fig. 1C**, "APL unlabeled"), mean ± 95% confidence interval. n, given as # hemispheres (# flies): GAL80^{ts}, α′ and α, 5 (4), β′, β and γ, 7 (5); no GAL80^{ts}, α′ and α, 4 (3), β′, β and γ, 12 (9). Mixed-effects model (matching across lobes) finds no significant effect of genotype (GAL80^{ts} vs. no GAL80^{ts}) ($p > 0.05$).

(B) Responses of different Kenyon cell lobes to isoamyl acetate (IA, upper) or δ-decalactone (δDL, lower), imaged with GCaMP3 instead of GCaMP6f. Horizontal bar shows time of odor presentation. Error shading shows s.e.m. Data for 'acute' and 'APL unlabeled' (with GAL80^{ts}) flies from ref. 23.

(C) Maximum ΔF/F of data from panel B. Mean ± 95% confidence interval. # $p < 0.05$ between acute vs. constitutive, * $p < 0.001$, Welch ANOVA with Dunnett's T3 multiple comparisons test, or Kruskal-Wallis ANOVA with Dunn's multiple comparisons test. n, given as # hemispheres (# flies), left to right within each graph: α′ and α, 11 (10), 20 (14), 12 (9); β′, β and γ, 18 (15), 36 (24), 24 (16).

In all panels, * without line indicates different from APL unlabeled. Detailed statistical analysis given in **Table S2**.

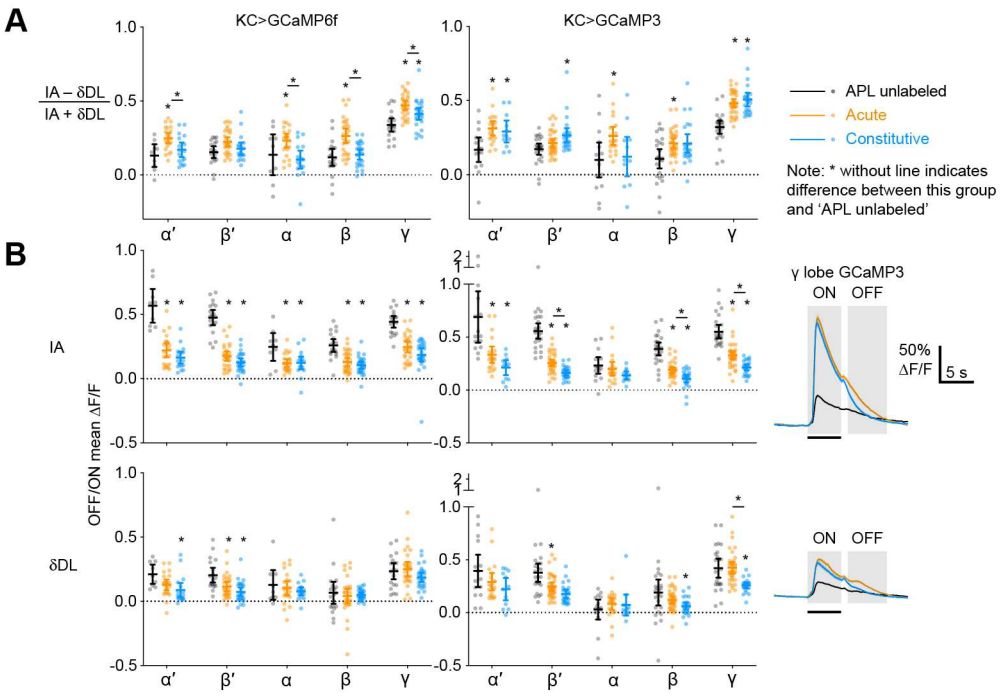

Fig. S3 (related to Fig. 1). Dynamics of KC odor responses with APL>TNT

(A) Normalized difference between maximum ΔF/F response to IA vs. δDL, taken as (IA-δDL)/(IA+δDL), for data from **Fig. 1C** (KC>GCaMP6f, left) and **Fig. S2C** (KC>GCaMP3, right). n as in those panels. For GCaMP6f, but not GCaMP3, the normalized difference is higher with acute APL>TNT than both APL unlabeled controls and constitutive APL>TNT. * $p < 0.05$, mixed-effects model (matching across lobes) with Geisser-Greenhouse correction and Holm-Sidak multiple comparisons test (GCaMP6f), Welch's 1-way ANOVA with Holm-Sidak multiple comparisons or Kruskal-Wallis ANOVA with Dunn's multiple comparisons test (GCaMP3).

(B) Post-odor GCaMP signal (KC>GCaMP6f, left; KC>GCaMP3, right), for IA (top) and δDL (bottom), analysed as mean ΔF/F 1-6 s after the end of the odor pulse divided by mean ΔF/F during the 5 s odor pulse (ON and OFF periods shown in right panel as shading superimposed on γ lobe responses). Data from **Fig. 1C** and **Fig. S2B** (n as in those panels). * $p < 0.05$, ordinary 1-way ANOVA with Holm-Sidak multiple comparisons test or Kruskal-Wallis ANOVA with Dunn's multiple comparisons test.

In all panels, * without line indicates different from APL unlabeled. Detailed statistical analysis given in **Table S2**.

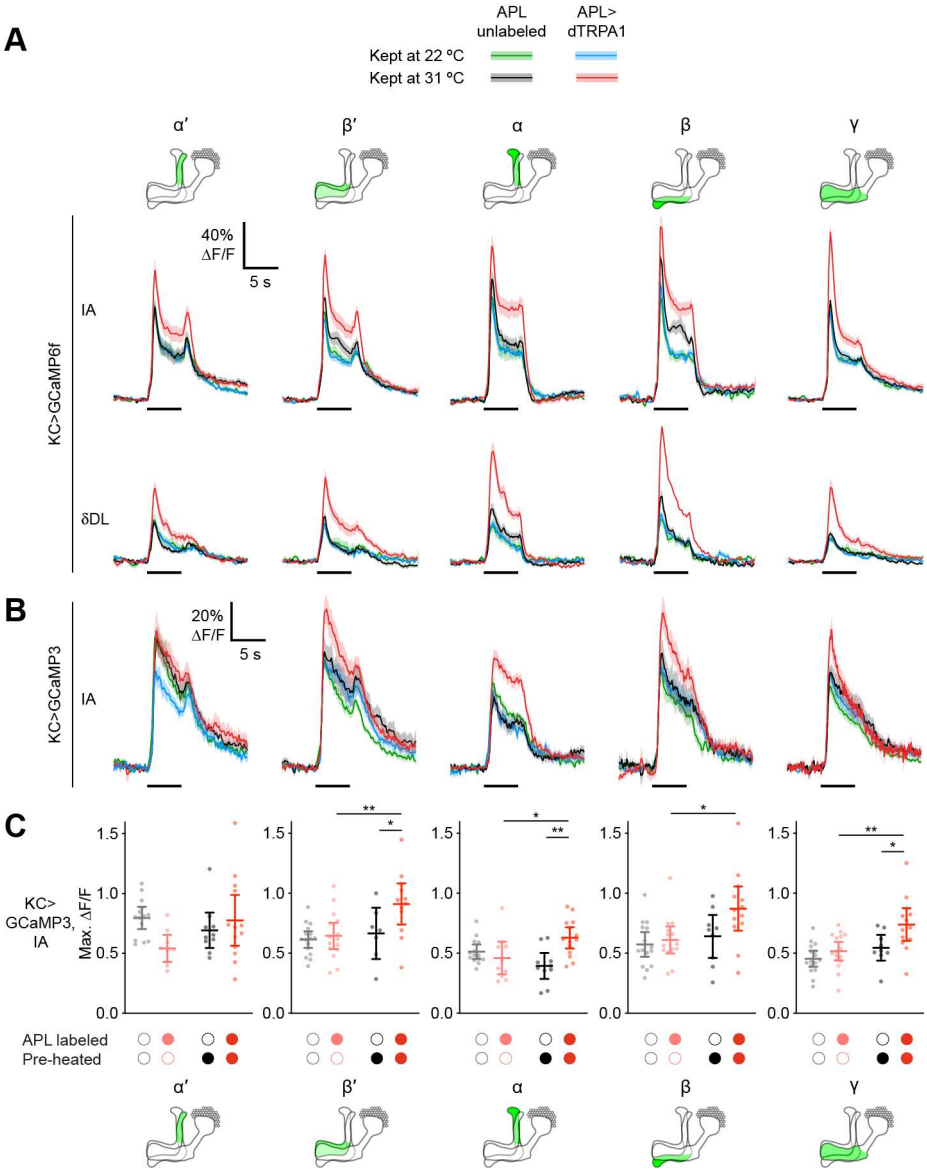

Fig. S4 (related to Fig. 2). Odor response traces and GCaMP3 data for Fig. 2 (Kenyon cell odor responses are increased following excess activation of the inhibitory APL neuron)

(A) Responses of all lobes to isoamyl acetate (IA) and δ-decalactone (δDL) for KC>GCaMP6f, APL>dTRPA1 flies kept at 22 ºC or 31 ºC, where APL was unlabeled or expressed dTRPA1, recorded at 22 ºC. Legend shows 2x2 grid: APL unlabeled, kept at 22 ºC (green), APL>dTRPA1, kept at 22 ºC (blue), APL unlabeled, kept at 31 ºC (black), APL>dTRPA1, kept at 31 ºC (red). Horizontal bars show time of odor presentation. Error shading shows s.e.m. Diagrams of the mushroom body show the α′, β′, α, β and γ lobes. n as in **Fig. 2**.

(B) Same as (A) except measured with KC>GCaMP3 instead of KC>GCaMP6f.

(C) Maximum ΔF/F response from panel B. Mean ± 95% confidence interval.* $p < 0.05$, ** $p < 0.01$, ordinary 1-way ANOVA with Holm-Sidak multiple comparisons test or Kruskal-Wallis test with Dunn's multiple comparisons test, comparing only conditions where a single variable changed (see **Table S2** for details). n, given as # hemispheres (# flies), left to right within each graph: α′, 14 (9), 9 (7), 10 (9), 13 (11); β′, 16 (11), 15 (11), 7 (6), 12 (10); α, 14 (9), 10 (7), 10 (9), 14 (11); β, 15 (10), 14 (11), 9 (8), 13 (11); γ, 16 (11), 16 (12), 9 (8), 13 (11).

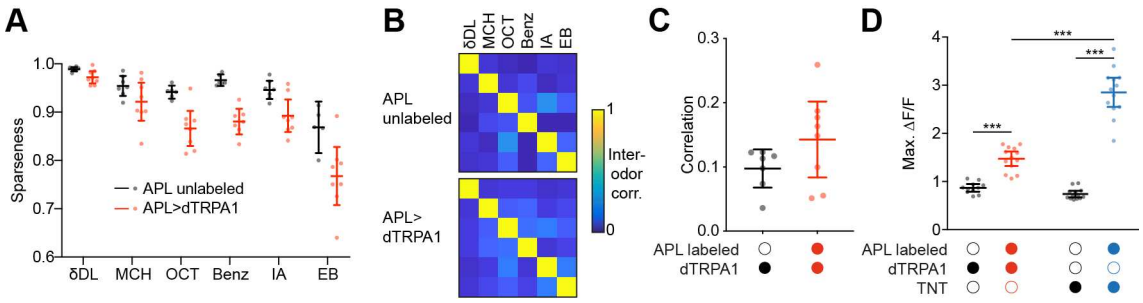

Fig. S5 (related to Fig. 2). Sparseness and inter-odor correlation of KC odor responses after adaptation to APL>dTRPA1 adaptation

(A) Population sparseness of activity maps of KC somatic responses to a panel of 6 odors: δ-decalactone, 4-methylcyclohexanol, 3-octanol, benzaldehyde, isoamyl acetate, ethyl butyrate. δ-decalactone and isoamyl acetate were at 10^{-2} dilution for consistency with the rest of the study; the others were at 10^{-1} to ease detection of broader odor responses. All flies were kept at 31 ºC for 4 d before imaging at 22 ºC as in **Fig. 2**. APL unlabeled, n = 7 (6 flies); APL>dTRPA1, n = 8 (6 flies). p = 0.0004, significant main effect of genotype in mixed-effects model.

(B) Pairwise correlations between activity maps of KC somatic responses to the odors in A.

(C) Mean inter-odor correlation (mean of all non-diagonal squares in B) does not significantly differ between APL unlabeled and APL>dTRPA1 hemispheres. n as in (A). p = 0.15, unpaired t-test. p = 0.18, main effect of genotype in mixed-effects model when considering each odor pair separately. p < 0.0001, main effect of odor-pair identity, indicating that our data reliably report that some odor pairs are more similar than others (see grids in B).

(D) Maximum ΔF/F of γ lobe responses to isoamyl acetate, duplicated from **Fig. 1C, 2C**. Odor responses are higher with APL blocked by TNT (blue) than after adaptation following 4 d APL activation by dTRPA1 (red), possibly explaining why adaptation to APL>dTRPA1 does not affect inter-odor correlations, whereas blocking APL with TNT does (11). *** p < 0.001, Welch ANOVA with Holm-Sidak multiple comparisons test (see **Table S2** for details).

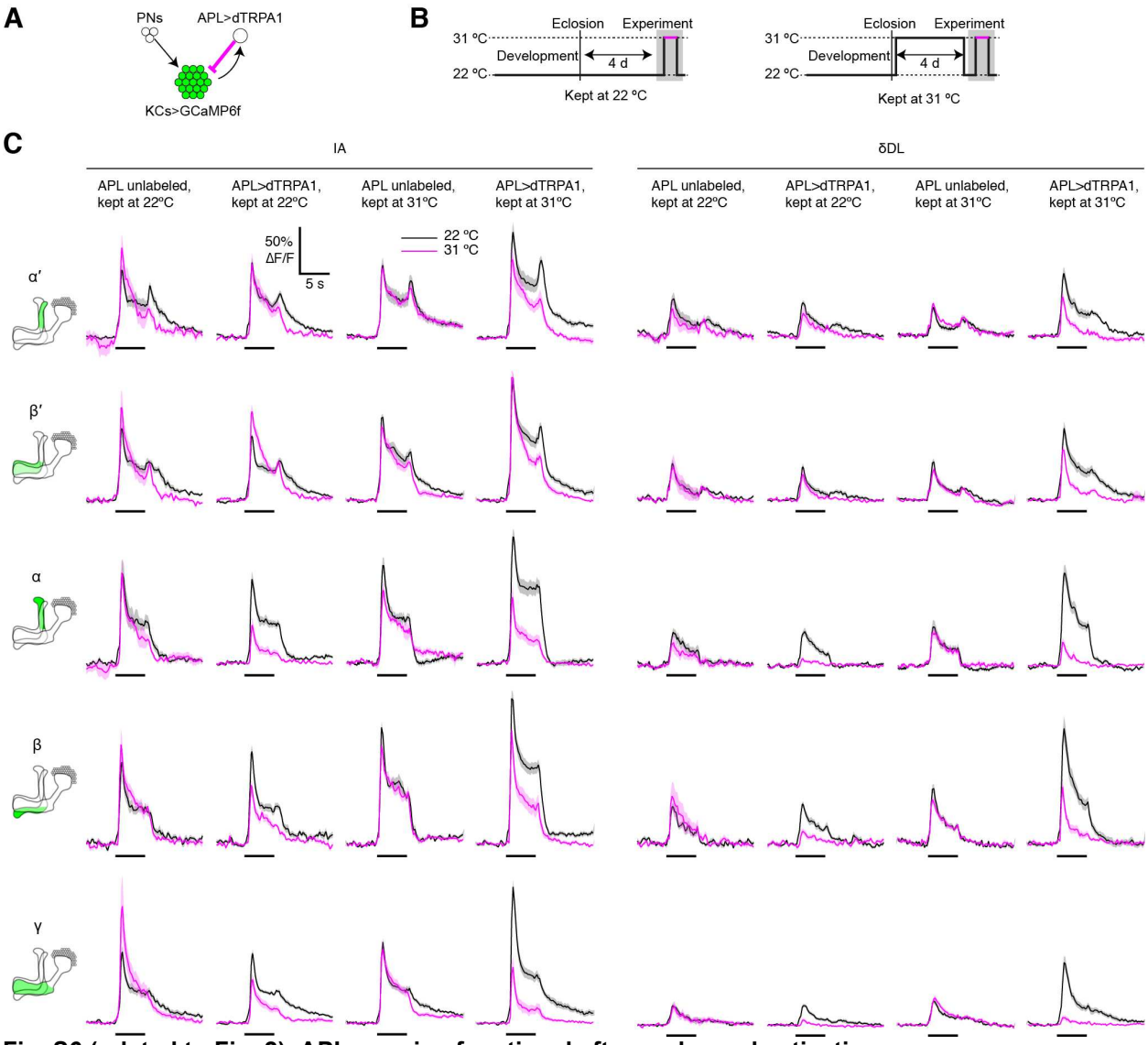

Fig. S6 (related to Fig. 2). APL remains functional after prolonged activation

(A) Diagram of genotype (green shows GCaMP6f expression; magenta shows activation with dTRPA1).

(B) Diagrams show experimental protocol: Flies were raised at 22 ºC, collected 0–1 d after eclosion, kept at 22 ºC (control) or 31 ºC (pre-heated) for 4 d, and returned to 22 ºC before the imaging experiment.

(C) Responses of all lobes to isoamyl acetate (IA) and δ-decalactone (δDL) for KC>GCaMP6f, APL>dTRPA1 flies kept at 22 ºC or 31 ºC, where APL was unlabeled or expressed dTRPA1, recorded at 22 ºC (black) or 31 ºC (magenta). Horizontal bars show time of odor presentation. Error shading shows s.e.m. Diagrams of the mushroom body show the α′, β′, α, β and γ lobes.

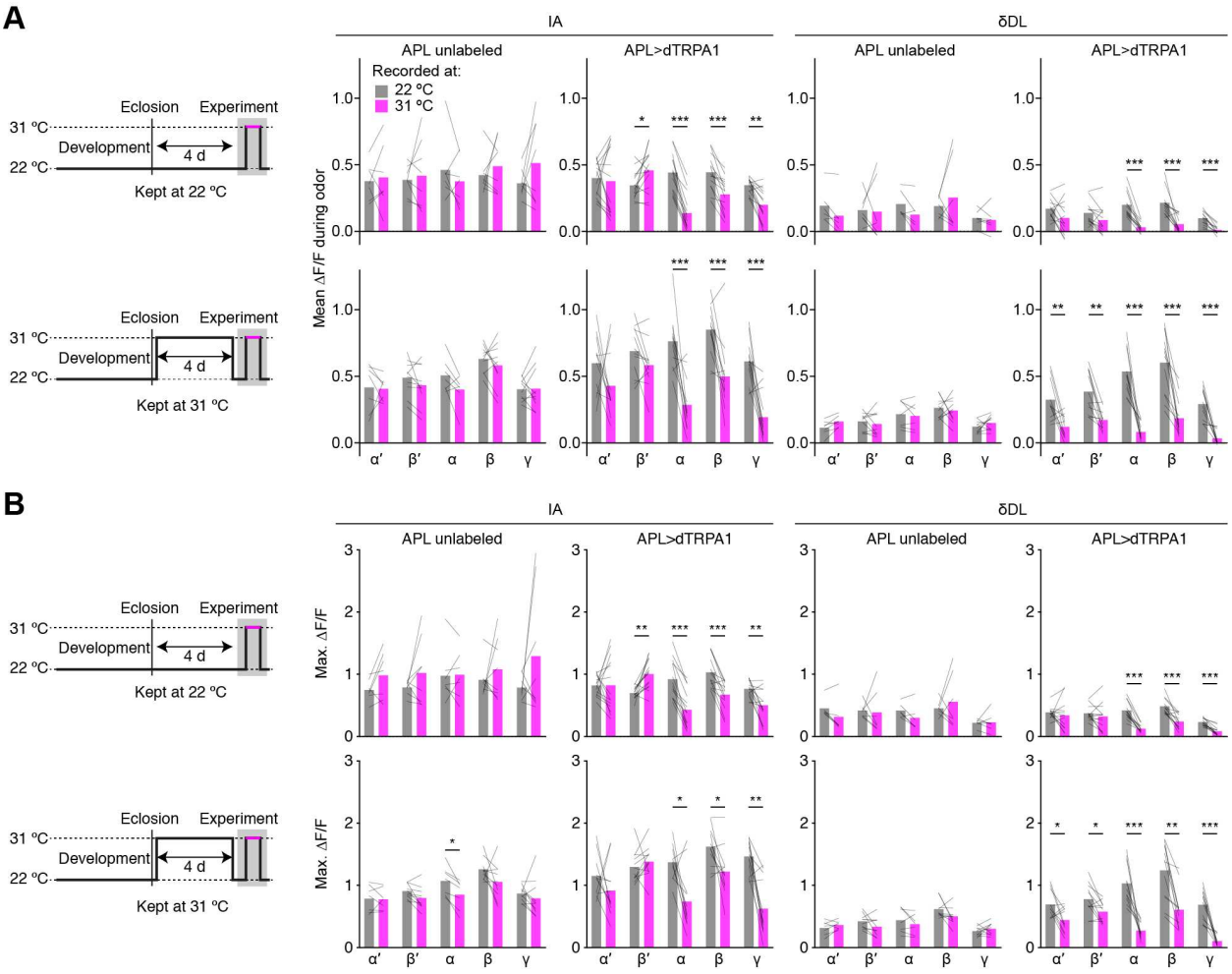

Fig. S7 (related to Fig. 2). APL remains functional after prolonged activation, quantification

(A) Mean ΔF/F during odor recorded at 22 ºC (grey) vs. recorded at 31 ºC (magenta), for APL unlabeled or APL>dTRPA1 hemispheres, kept at 22 ºC or kept at 31 ºC, for odors isoamyl acetate or δ-decalactone. Here we quantified odor responses using mean ΔF/F rather than maximum ΔF/F because in some cases activating APL with dTRPA1 changed the dynamics of the KC odor responses, such that the decrease in mean ΔF/F was more obvious than the decrease in maximum ΔF/F. Bars show mean, thin lines show paired data (recorded at 22 ºC and 31 ºC). * $p < 0.05$, ** $p < 0.01$, *** $p < 0.001$, 2-way repeated measures ANOVA or mixed-effects model with Geisser-Greenhouse correction with Holm-Sidak multiple comparisons test (see **Table S2** for details). n, given as # hemispheres (# flies) in the order APL unlabeled, kept at 22 ºC; APL>dTRPA1, kept at 22 ºC; APL unlabeled, kept at 31 ºC; APL>dTRPA1, kept at 31 ºC (n for IA and δDL equal except where noted): α′ and α, 7 (7) [6 (6) for δDL], 14 (10) [13 (9) for δDL], 7 (4), 11 (6); β′, β and γ, 8 (7) [7 (6) for δDL], 14 (10) [13 (9) for δDL], 10 (6), 12 (7). Responses recorded at 22 ºC are the same as in **Fig. 2** except excluding flies without a response at 31 ºC (fly died, motion artifacts, etc.).

(B) Same as panel A except with maximum ΔF/F instead of mean ΔF/F.

Note: The lesser effect of activating APL with dTRPA1 on α′β′ odor responses, compared to αβ and γ responses, is consistent with our previous data (11) and with findings that α′β′ KCs are more excitable (24, 25) and have higher spontaneous activity than αβ and γ KCs (spontaneous activity ~0.3 Hz in α′β′ KCs vs. 0 Hz in αβ and γ KCs; (26)). Although all three types of KCs respond equally to optogenetic activation of APL (25), it may be that APL activation suppresses spontaneous activity in α′β′ KCs, which would make the inhibitory effect on the odor-evoked ΔF/F less apparent due to the lower baseline GCaMP6f fluorescence.

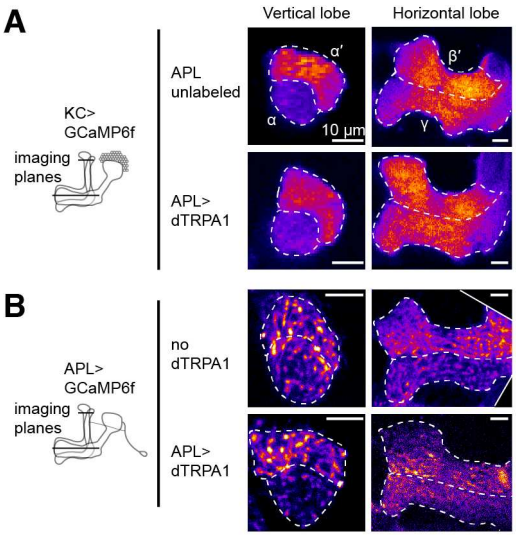

Fig. S8 (related to Fig. 2). Gross morphology of APL and KCs is unaffected by APL>dTRPA1 adaptation

(A) Example single optical sections of KCs expressing GCaMP6f in the vertical (left) and horizontal (right) lobes, in control APL-unlabeled hemispheres (upper) and APL>dTRPA1 hemispheres (lower), kept at 31 ºC for 4 d.

(B) Example single optical sections of APL expressing GCaMP6f in the vertical (left) and horizontal (right) lobes, in APL>GCaMP6f only (no dTRPA1) flies (upper) and APL>GCaMP6f,dTRPA1 flies (lower), kept at 31 ºC for 4 d. Diagonal lines indicate the edge of the rotated field of view. Note typical APL neurite morphology, parallel to KC axons (hence perpendicular to the imaging plane in the vertical, and running left and right in the horizontal lobe).

Diagrams illustrate approximate z-depth of imaging planes of each optical section. Scale bars 10 µm.

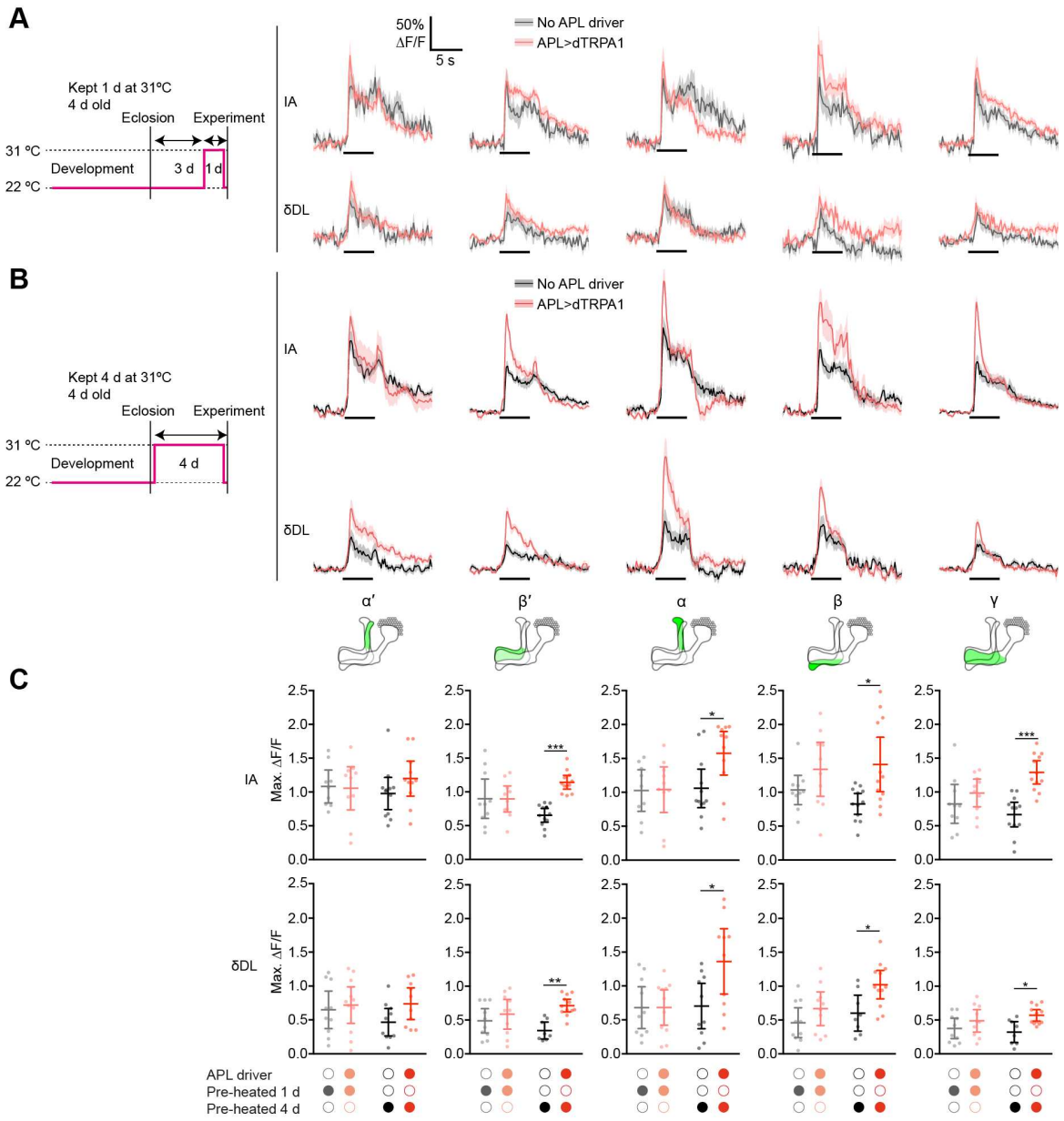

Fig. S9 (related to Fig. 3). Stronger adaptation to APL activation after 4 days than 1 day (using VT43924-GAL4)

(A) Responses of different lobes of the mushroom body to isoamyl acetate (IA) and δ-decalactone (δDL) for 1 d adapted (4 d old) flies, where APL did not express (grey) or expressed dTRPA1 (pink) driven by VT43924-GAL4. Horizontal bar shows time of odor presentation. Error shading shows s.e.m. Diagram at left shows experimental protocol: Flies were raised at 22 ºC and collected 0–1 d after eclosion, then kept at 22 ºC for 3 days and moved to 31 ºC for 1 d (4 d old). All flies were imaged at 22 ºC.

(B) As A, except flies kept at 31 ºC for 4 d after eclosion.

(C) Maximum ΔF/F of traces in (B-C). * $p < 0.05$, ** $p < 0.01$, *** $p < 0.001$, 1-way ANOVA with Holm-Sidak multiple comparisons test or Kruskal-Wallis test with Dunn's multiple comparisons test, comparing only conditions where a single variable changed. 2-way ANOVAs revealed interactions between genotype and length of pre-heating in the β′ and γ lobes (see **Table S2** for details). n, given as # hemispheres (# flies), left to right within each graph: IA, α and α′, 9 (5), 10 (5), 12 (6), 11 (6); β, β′ and γ, 10 (5), 10 (5), 12 (6), 12 (6); δDL, α and α′, 10 (5), 11 (6), 10 (5), 10 (5); β, β′ and γ, 10 (5), 10 (5), 8 (4), 12 (6).

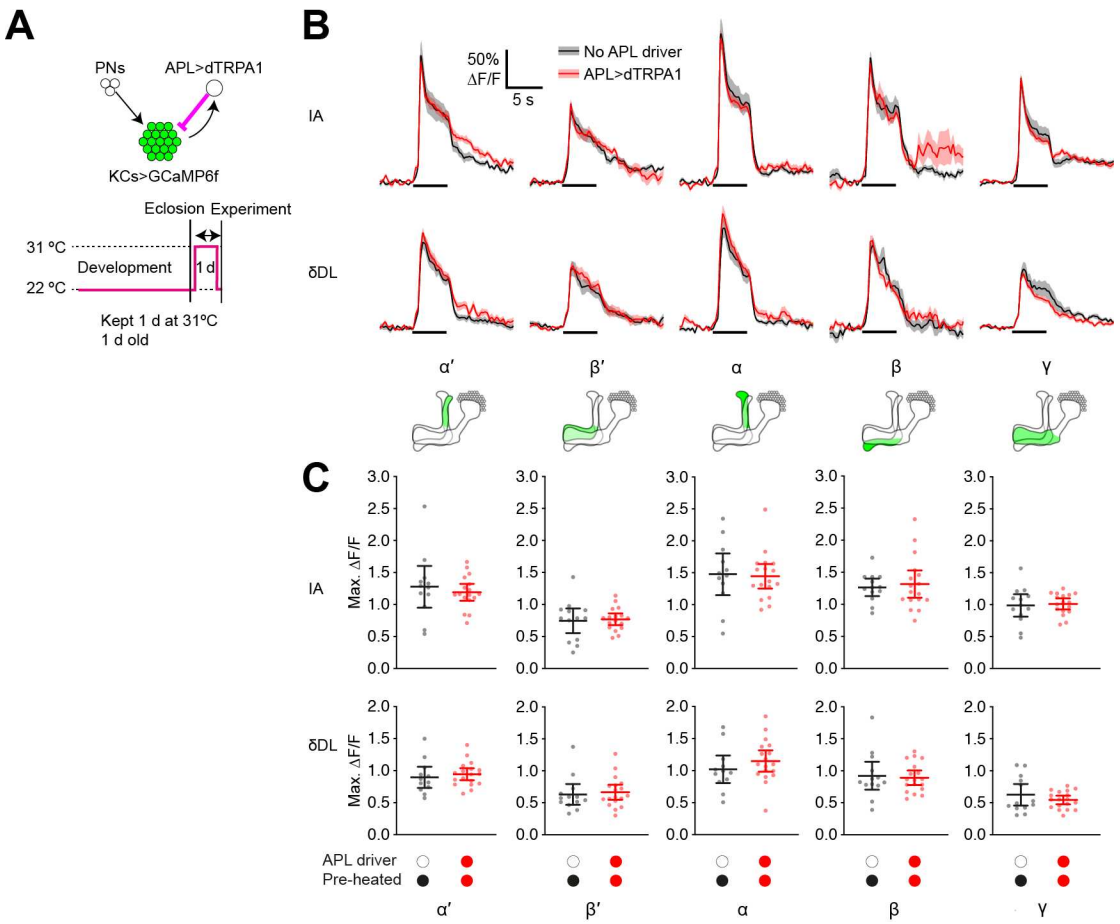

Fig. S10 (related to Fig. 3). No adaptation after 1 d APL activation in 1 d old flies (using VT43924-GAL4)

(A) Diagram of experimental protocol. Flies were raised at 22 ºC and collected 0–1 d after eclosion, then immediately moved to 31 ºC for 1 d, and then imaged at 22 ºC.

(B) Responses of different lobes of the mushroom body to isoamyl acetate and δ-decalactone in 1 d old flies kept at 31 ºC for 1 d (diagram in A), where APL did not express (grey) or expressed dTRPA1 (orange) driven by VT43924-GAL4. Horizontal bar shows time of odor presentation. Error shading shows s.e.m.

(C) Maximum ΔF/F from panel B. Mean ± 95% confidence interval. n, given as # hemispheres (# flies) in the order UAS-TRPA alone; APL>dTRPA1: IA, α′ and α, 12(7), 17(10); β′, β and γ, 13(7), 17(10); δDL, α′ and α, 12(7), 18(10); β′, β and γ, 13(7), 18(10). $p > 0.05$ for all comparisons, unpaired t-test or Mann-Whitney test (see **Table S2** for details).

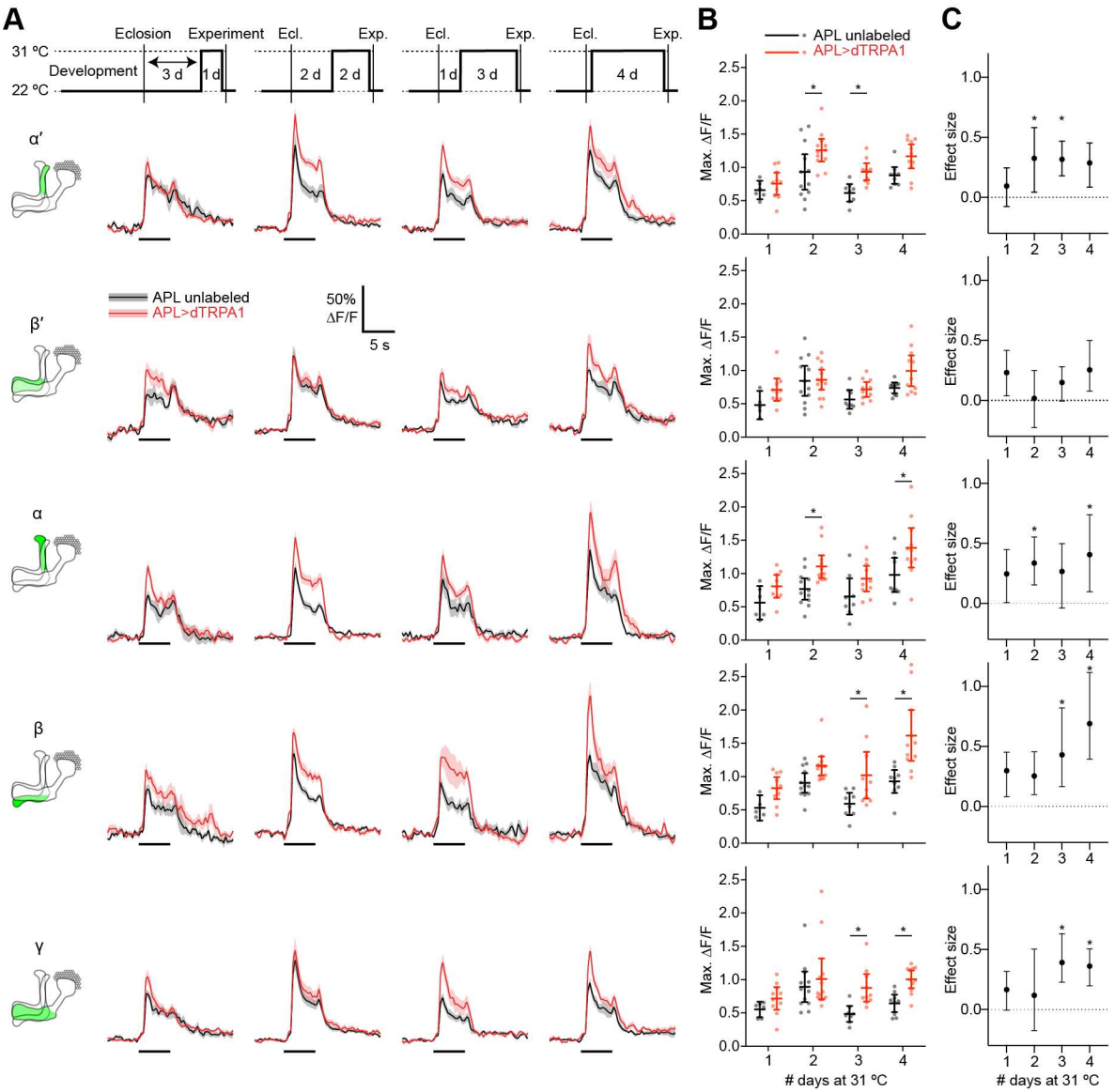

Fig. S11 (related to Fig. 3). Adaptation after 1, 2, 3, and 4 d pre-activation of APL

(A) Responses of all lobes to isoamyl acetate for KC>GCaMP6f, APL>dTRPA1 flies kept at 31 ºC for 1, 2, 3 or 4 d (as shown on diagrams at top), where APL was unlabeled (black) or expressed dTRPA1 (red). Horizontal bars show time of odor presentation. Error shading shows s.e.m. Diagrams of the mushroom body show the α′, β′, α, β and γ lobes.

(B) Maximum ΔF/F response from panel A. Mean ± 95% confidence interval. * $p < 0.05$, 2-way ANOVA with Sidak's multiple comparisons test. n, given as # hemispheres (# flies), left to right within each graph: 1 d: 6 (5) [5 (4) for β and β′], 10 [9 for α] (7); 2 d: 12 (9), 12 (8); 3 d: 8 (6), 10 (7); 4 d: 9 (7), 11 (8).

(C) Effect size of adaptation (KC response with APL>dTRPA1 minus KC response with APL unlabeled), calculated using bootstrap-coupled estimation statistics (22). Error bars, 95% confidence intervals.

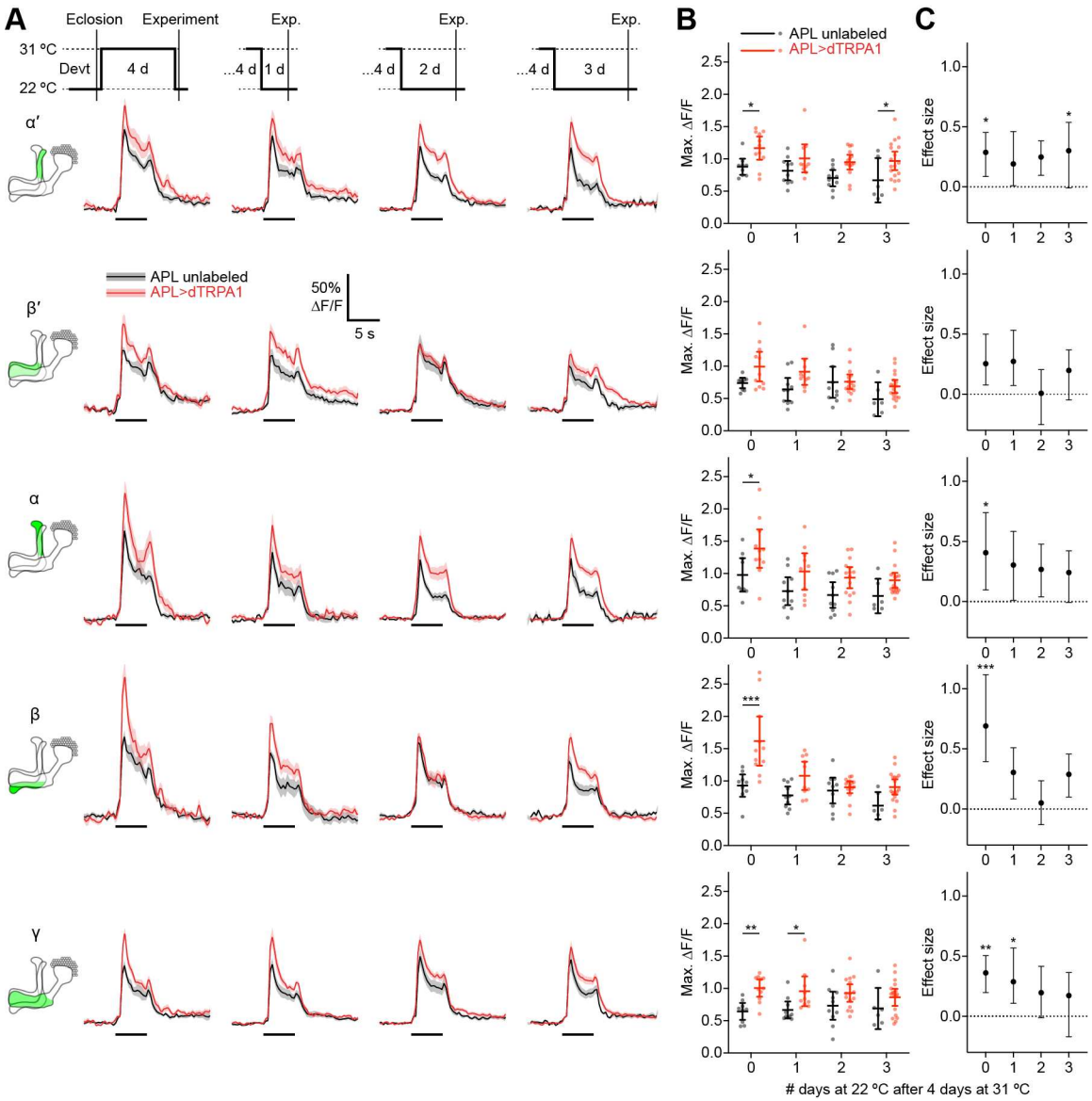

Fig. S12 (related to Fig. 3). Loss of adaptation 0, 1, 2, and 3 d after the end of pre-activation of APL

(A) Responses of all lobes to isoamyl acetate for KC>GCaMP6f, APL>dTRPA1 flies kept at 31 ºC for 4 d and then 22 ºC for 0, 1, 2, or 3 d (as shown on diagrams at top), where APL was unlabeled (black) or expressed dTRPA1 (red). Horizontal bars show time of odor presentation. Error shading shows s.e.m. Diagrams of the mushroom body show the α′, β′, α, β and γ lobes.

(B) Maximum ΔF/F response from panel A. Mean ± 95% confidence interval. * $p < 0.05$, 2-way ANOVA with Sidak's multiple comparisons test. n, given as # hemispheres (# flies), left to right within each graph: 0 d: 9 (7), 11 (8); 1 d: 10 (9), 10 (9); 2 d: 10 (9), 15 (11); 3 d: 6 (4), 18 (10). $p < 0.01$ for the β lobe, interaction between genotype (APL unlabeled vs. APL>dTRPA1) and time (# days at 22 ºC) (see **Table S2**).

(C) Effect size of adaptation (KC response with APL>dTRPA1 minus KC response with APL unlabeled), calculated using bootstrap-coupled estimation statistics (22). Error bars, 95% confidence intervals.

Data for 0 d repeated from condition '4 d' in **Fig. S11** for comparison.

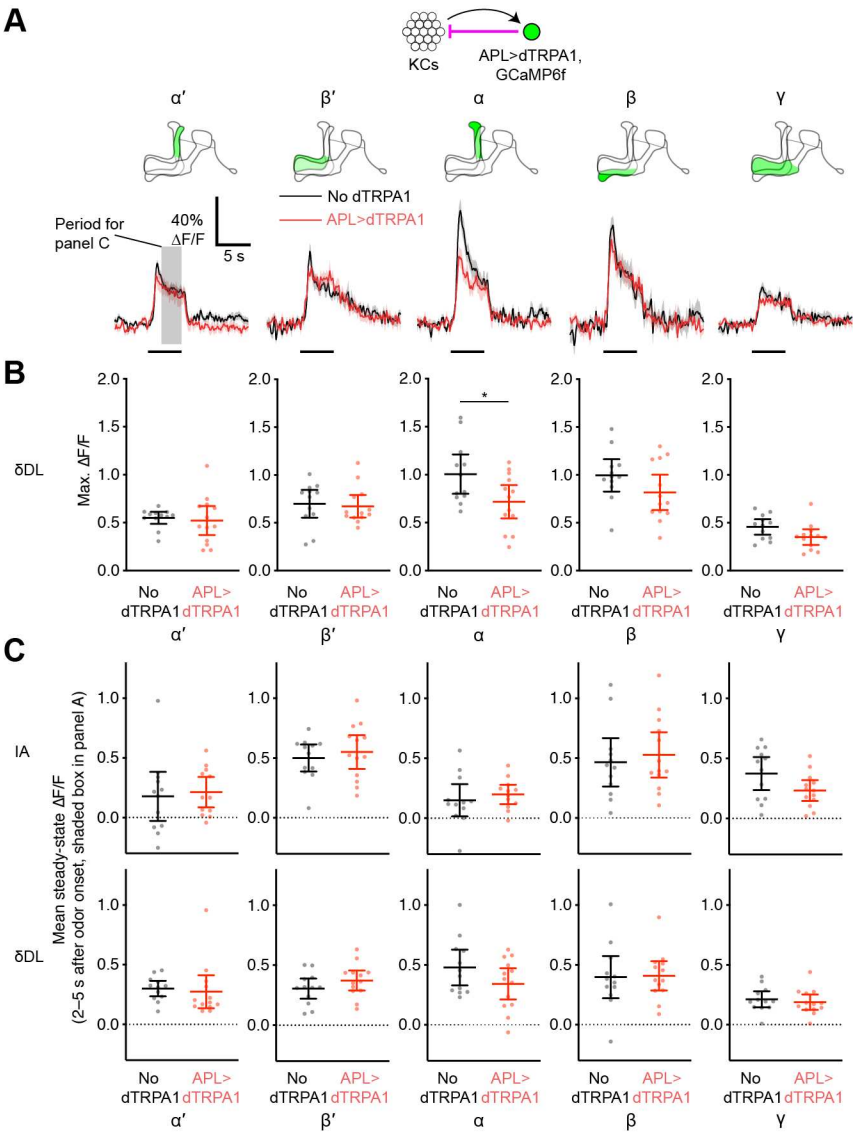

Fig. S13 (related to Fig. 4). APL responses to δ-decalactone, and quantification of APL steady-state responses, following adaptation.

(A) Traces show responses of different lobes of APL (as determined by the anatomical marker MB247-dsRed) to δ-decalactone in APL>GCaMP6f ("no dTRPA1") or APL>dTRPA1,GCaMP6f ("APL>dTRPA1") flies kept at 31 ºC for 4 d. Shading shows s.e.m. Grey rectangle shows "steady-state" period for (C).

(B) Maximum ΔF/F of traces from (A). Mean ± 95% confidence interval. * $p < 0.05$, unpaired t-test. n, given as # hemispheres (# flies): no dTRPA1, 12 (9); APL>dTRPA1, 13 (8). Most lobes show decreased responses in adapted APL>dTRPA1 flies, but unlike responses to isoamyl acetate (**Fig. 4**), in most cases this is not statistically significant, possibly due to the lower amplitude responses (to δ-decalactone compared to isoamyl acetate) combined with the overall noisy GCaMP6f signal (due to recording from only the single APL neuron).

(C) Mean steady-state ΔF/F of traces from (A) and **Fig. 4,** during 2 – 5 s after odor onset (grey rectangle in (A)). Mean ± 95% confidence interval. n as in those panels. $p > 0.05$ for all comparisons, unpaired t-test or Mann-Whitney test (see **Table S2** for details).

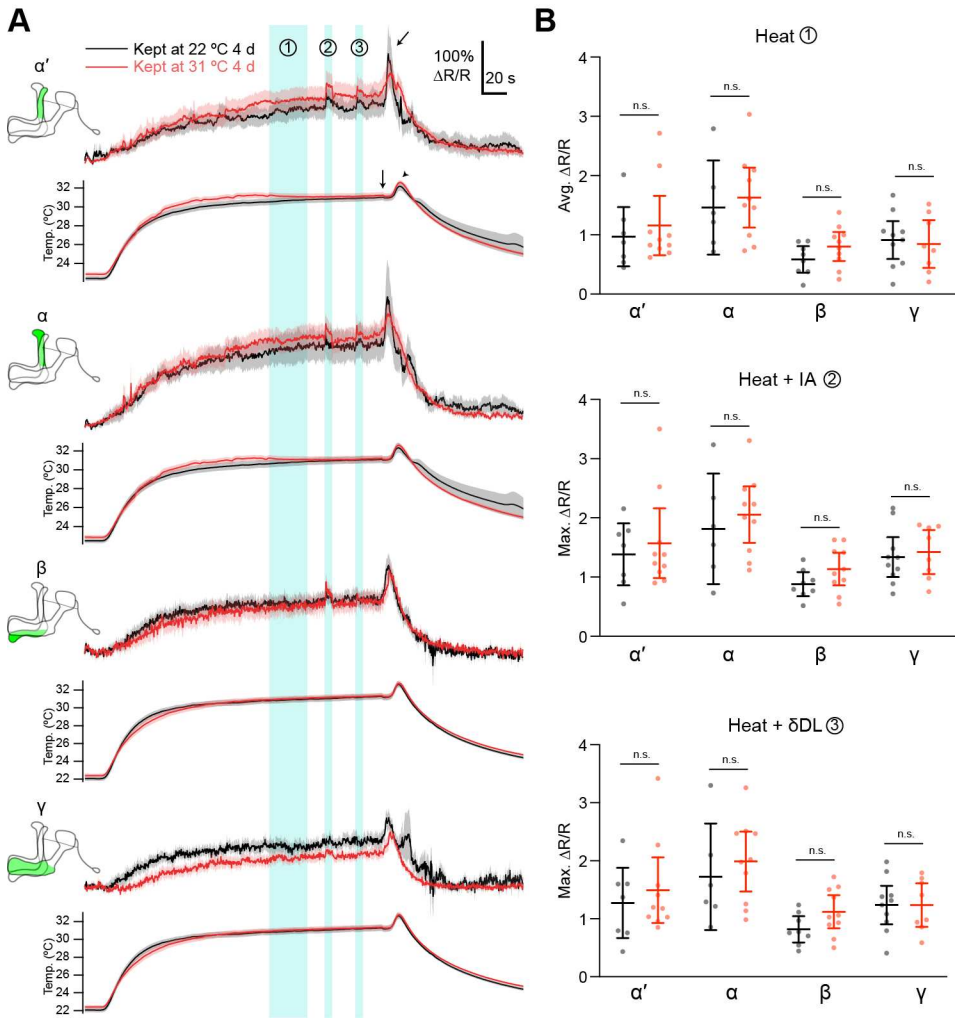

Fig. S14 (related to Fig. 5). Additional data for activation of APL following adaptation

(A) Data as in **Fig. 5A,B** but including α′, α and γ APL lobes. n, given as # hemispheres (# flies), left to right within each graph: α′, 7(5), 10(6); α, 4(5), 9(6); β, 10(8), 8(6); γ, 10(8), 8(6). We omitted the β′ lobe because due to technical limitations in this experiment we could only image one focal plane at a time, and whereas the α′ and α lobes can be captured in one plane, as can the β and γ lobes, the β′ lobe requires another movie, which we deemed non-essential given that **Fig. 5** does not address the β′ lobe. The peak after δ-decalactone presentation (diagonal arrow) is most likely an artifact of our perfusion protocol. To accelerate cooling, upon turning off the heater, we sped up the perfusion from ~2.7 ml/min to ~9.8 ml/min. In doing so, we inadvertently briefly increased the saline temperature (arrowhead) because heated saline from the heater had less time to cool down before reaching the fly. Note that the secondary increase in GCaMP6f signal (arrow) aligns not with the secondary rise temperature (arrowhead) but with a slight discontinuity in temperature at the vertical arrow, which reflects the change in perfusion speed. The most likely explanation is that, due to turbulence in the perfusion chamber, the fly received the brief pulse of heat before the thermometer did. Note that this artifact does not affect our interpretation, because the key result of this experiment is only the activation of APL during heating.

(B) Quantification of data from panel A, as in **Fig. 5B**.

Detailed statistical analysis given in **Table S2**.

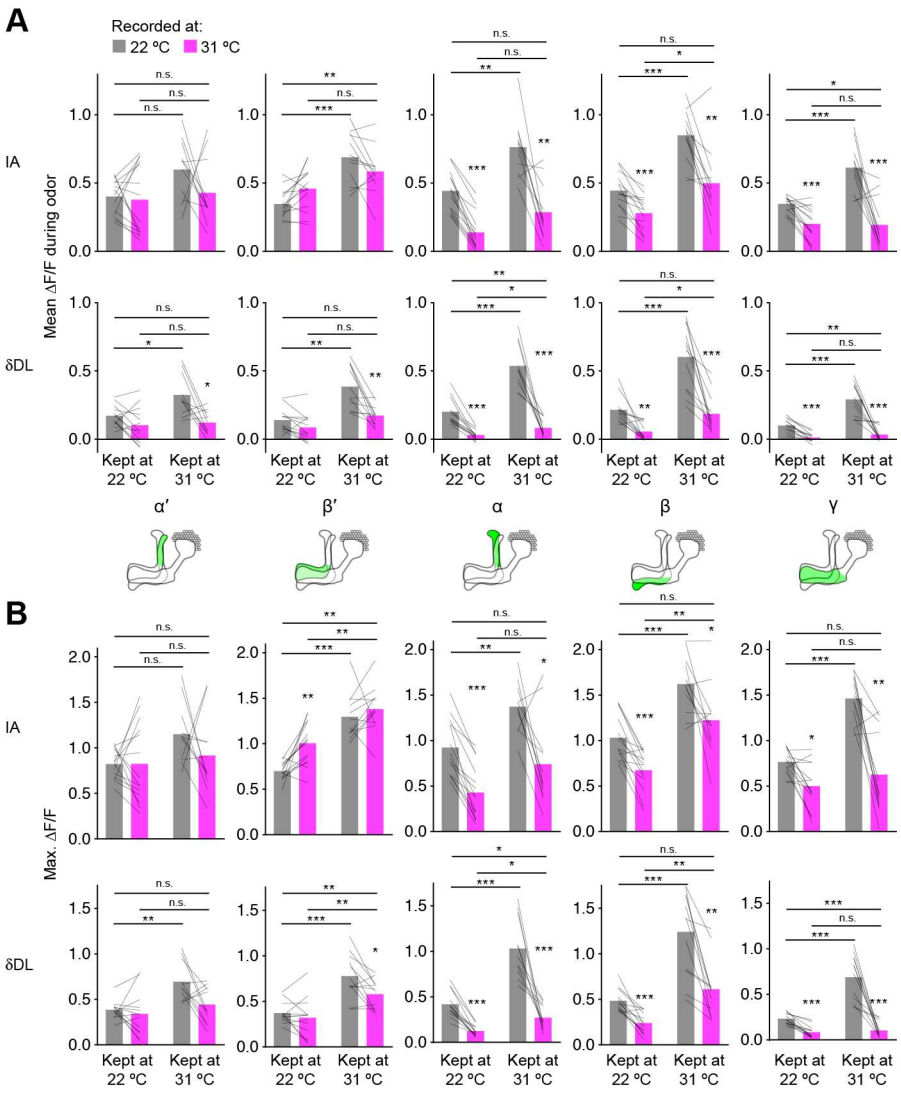

Fig. S15 (related to Fig. 5). Additional data for activation of APL following adaptation

(A) Data as in **Fig. 5E** but including α′β′ KCs

(B) Data as in panel A, but showing maximum ΔF/F during odor response instead of mean ΔF/F.

All data from traces in **Fig. S6**, n as in that figure. Detailed statistical analysis given in **Table S2**.

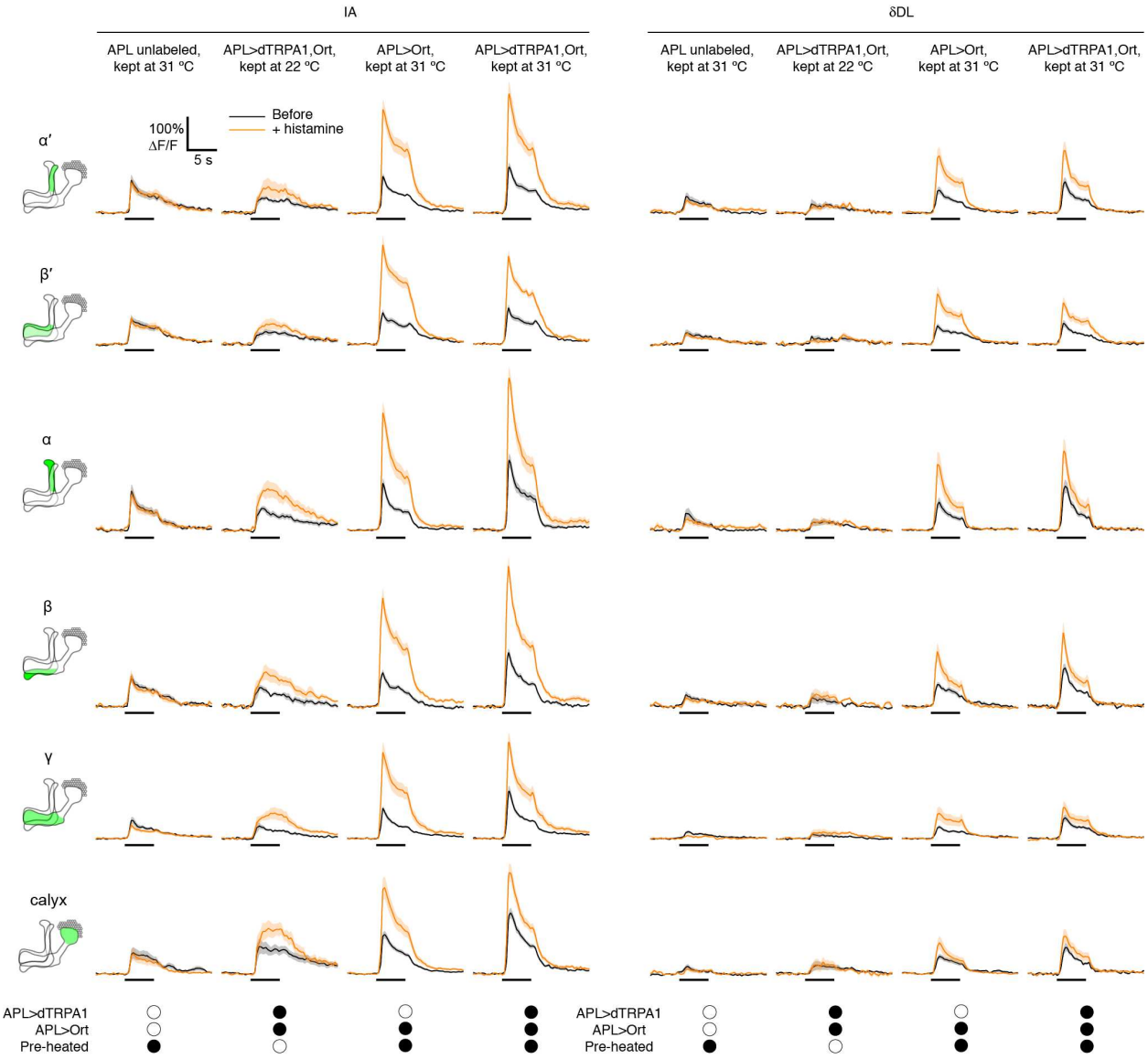

Fig. S16 (related to Fig. 6). KC odor responses with APL>Ort.
Average responses of all lobes to isoamyl acetate (IA) or δ-decalactone (δDL), before (black) and after (orange) bath-applying 2 mM histamine. Error shading shows s.e.m. Genotypes as described on the Fig. (see **Table S1** for details); "APL unlabeled" is a mixture of hemispheres from APL>Ort and APL>dTRPA1,Ort flies where APL was unlabeled. n, given as # hemispheres (# flies), left to right for each lobe: 10 (9), 6 (4), 17 (11), 16 (11) [15 (10) for δDL].

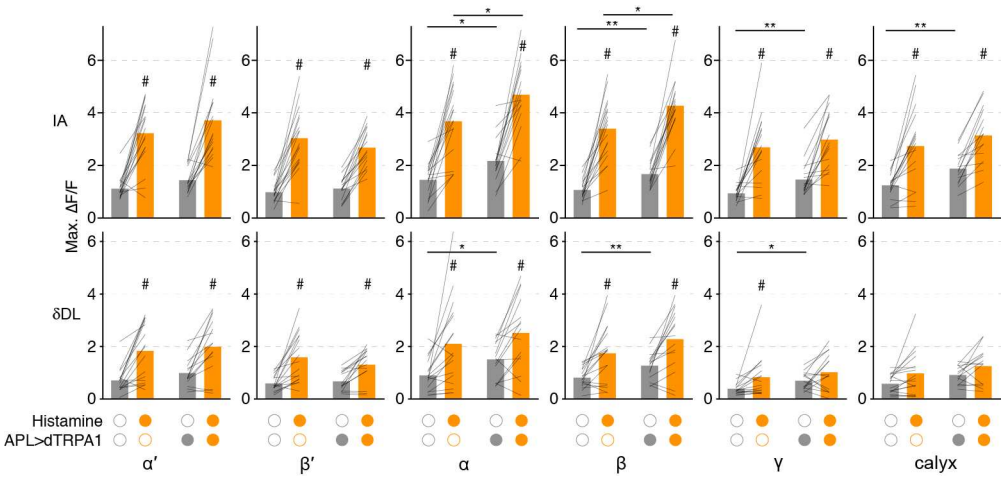

Fig. S17 (related to Fig. 6). Responses in all KC lobes with APL>Ort.
Maximum ΔF/F for odor responses in all lobes to isoamyl acetate or δ-decalactone, before (gray) and after (orange) bath-applying 2 mM histamine. Genotypes: APL>Ort (left), APL>dTRPA1,Ort (right). Bars show mean, thin lines show paired data (same hemisphere before and after histamine). # $p < 0.05$ effect of histamine, paired t-test or Wilcoxon matched-pairs signed rank test; * $p < 0.05$, ** $p < 0.01$, unpaired t-test or Mann-Whitney test, Holm-Bonferroni correction for multiple comparisons (see **Table S2** for details). n, given as # hemispheres (# flies): no dTRPA1, 17 (11); APL>dTRPA1, 16 (11) [15 (10) for δDL]. Responses from the calyx are shown for completeness but it is difficult to draw conclusions from the calyx as it combines all three types of KCs. Note that for the α and β lobes, unlike for the strong odor isoamyl acetate, for the weak odor δ-decalactone, while APL>dTRPA1,Ort responses were higher than APL>Ort responses after adding histamine, the difference was not statistically significant. This might be due to experimental variability: in some cases even the effect of histamine was not statistically significant for δ-decalactone, suggesting that our experimental manipulation was less reliable with a weaker sensory stimulus.

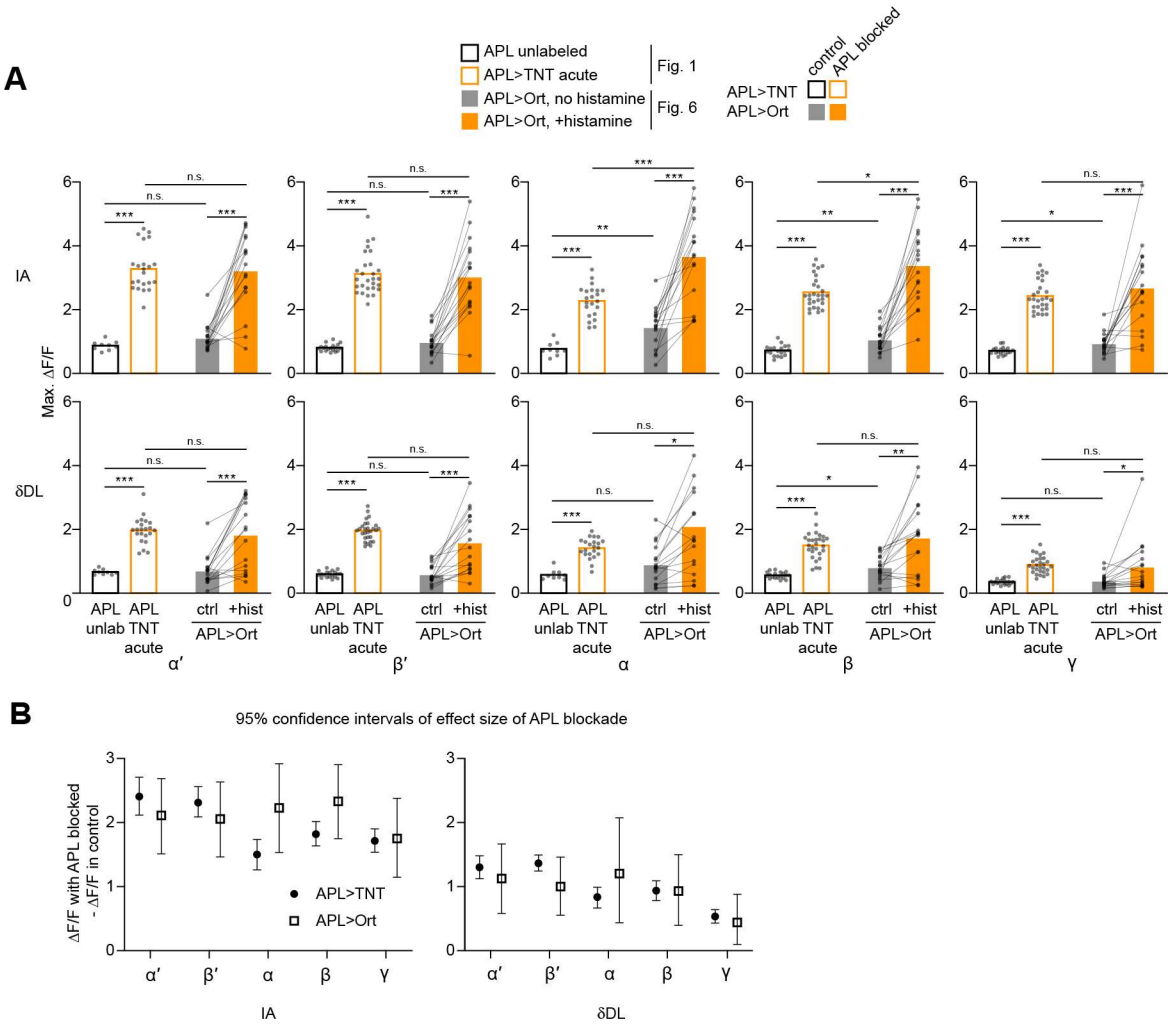

Fig. S18 (related to Fig. 6). Blocking APL with Ort or TNT causes similar increases in KC odor responses

(A) The effect of histamine on APL>Ort (no dTRPA1) flies (filled bars) has similar magnitude as the effect of acute (16-24 h) APL>TNT expression (open bars). Greater variability in APL>Ort flies compared to APL>TNT flies may reflect the more invasive dissection (the perineural sheath had to be removed in APL>Ort flies to allow histamine to penetrate) or variability in penetration of histamine into the brain. αβ KC responses were generally higher in APL>Ort flies than APL>TNT flies (independent of whether APL was blocked or not), for unknown reasons. Bars show mean, thin lines show paired data (same hemisphere before and after histamine). * $p < 0.05$, ** $p < 0.01$, unpaired t-test or Mann-Whitney test, Holm-Bonferroni correction for multiple comparisons (see **Table S2** for details). n as in **Fig. 1** and **6**.

(B) Effect sizes of blocking APL with APL>TNT or with histamine on APL>Ort flies, calculated using bootstrap-coupled estimation statistics (22). The overlapping error bars for APL>TNT and APL>Ort show the overlap between the 95% confidence intervals of the mean difference between control and APL-blocked conditions, for the two manipulations.

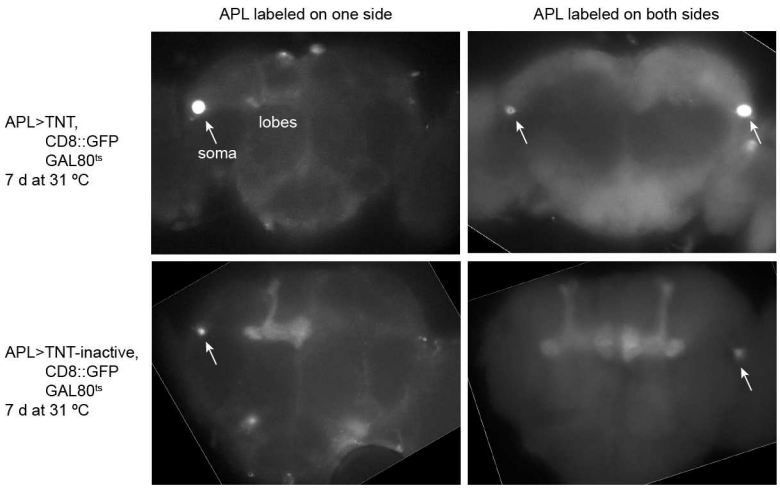

Fig. S19 (related to Fig. 6). Prolonged expression of tetanus toxin in APL may damage its morphology. The panels show epifluorescence images of live dissected brains from flies expressing TNT (upper panels) or TNT-inactive (lower panels) and CD8::GFP in APL driven by NP2631-GAL4, GH146-FLP, with tubP-GAL80^{ts}, kept at 31 ºC for 7 d. Arrows indicate the APL cell bodies. APL neurons expressing TNT show extremely bright cell bodies and dim or no fluorescence in the mushroom body lobes, suggesting that the neurites in the lobes may have degenerated, consistent with previous reports from photoreceptors (27). Scale bars not available.

Table S1. List of genotypes used

Figure	Shorthand name / Purpose	Full genotype
(text)	APL>TNT, GFP, GAL80^{ts}	NP2631-GAL4, GH146-FLP/tub-FRT-GAL80-FRT, UAS-TNT, tubP-GAL80^{ts}; UAS-CD8::GFP/UAS-mCherry
1, S3	APL>TNT, GAL80^{ts}	NP2631-GAL4, GH146-FLP/tub-FRT-GAL80-FRT, UAS-TNT, tubP-GAL80^{ts}; MB247-LexA, lexAop-GCaMP6f/UAS-mCherry or NP2631-GAL4, GH146-FLP/UAS-TNT, tubP-GAL80^{ts}; MB247-LexA, lexAop-GCaMP6f/tub-FRT-GAL80-FRT
1, S3	APL>TNT	NP2631-GAL4, GH146-FLP/tub-FRT-GAL80-FRT, UAS-TNT, UAS-mCherry; MB247-LexA, lexAop-GCaMP6f/+
S1	VT43924>GFP	UAS-CD8::GFP/CyO; VT43924-GAL4
S2, S3	APL>TNT, GAL80^{ts}, KC>GCaMP3	NP2631-GAL4, GH146-FLP/tub-FRT-GAL80-FRT, UAS-TNT, tubP-GAL80^{ts}; MB247-LexA, lexAop-GCaMP3/UAS-mCherry or NP2631-GAL4, GH146-FLP/UAS-TNT, tubP-GAL80^{ts}; MB247-LexA, lexAop-GCaMP3/tub-FRT-GAL80-FRT
S2, S3	APL>TNT, KC>GCaMP3	NP2631-GAL4, GH146-FLP/UAS-TNT; MB247-LexA, lexAop-GCaMP3,tub-FRT-GAL80-FRT/UAS-mCherry
2, 3, 5, S4-8, S11-12, S15	APL>dTRPA1	NP2631-GAL4, GH146-FLP/tubP-FRT-GAL80-FRT, UAS-dTRPA1, UAS-mCherry; MB247-LexA, lexAop-GCaMP6f/+
S4	APL>dTRPA1, KC>GCaMP3	NP2631-GAL4, GH146-FLP/tubP-FRT-GAL80-FRT, UAS-dTRPA1, UAS-mCherry; MB247-LexA, lexAop-GCaMP3/+
3, S9, S10	APL>dTRPA1	UAS-dTRPA1/+; MB247-LexA, lexAop-GCaMP6f/VT43924-GAL4(attP2)
3, S9, S10	UAS-dTRPA1/+	UAS-dTRPA1/+; MB247-LexA, lexAop-GCaMP6f/+
4, 5, S8, S14	APL>dTRPA1, GCaMP6f	NP2631-GAL4, GH146-FLP, MB247-dsRed/tubP-FRT-GAL80-FRT, UAS-dTRPA1; UAS-GCaMP6f/+
4, S8	APL>GCaMP6f	NP2631-GAL4, GH146-FLP, MB247-dsRed/tubP-FRT-GAL80-FRT; UAS-GCaMP6f/+
6, S16, S17	APL>dTRPA1, Ort	NP2631-GAL4, GH146-FLP/tubP-FRT-GAL80-FRT, UAS-dTRPA1, UAS-Ort; MB247-LexA, lexAop-GCaMP6f/UAS-mCherry
6, S16-18	APL>Ort	NP2631-GAL4, GH146-FLP/tubP-FRT-GAL80-FRT, UAS-Ort; MB247-LexA, lexAop-GCaMP6f/UAS-mCherry
S19	APL>TNT(-inactive),GFP, Gal80^{ts}	NP2631, GH146-FLP/UAS-TNT(-inactive), tubP-GAL80^{ts}; UAS-CD8:GFP/tub-FRT-GAL80-FRT

Table S2. Details of statistical analyses: Appended after references

SI References

1. Tanaka NK, Tanimoto H, Ito K (2008) Neuronal assemblies of the Drosophila mushroom body. *J Comp Neurol* 508(5):711–755.

2. Hong W, et al. (2009) Leucine-rich repeat transmembrane proteins instruct discrete dendrite targeting in an olfactory map. *Nat Neurosci* 12(12):1542–1550.

3. Gao S, et al. (2008) The neural substrate of spectral preference in Drosophila. 60(2):328–342.

4. Gordon MD, Scott K (2009) Motor control in a Drosophila taste circuit. *Neuron* 61(3):373–384.

5. Sweeney ST, Broadie K, Keane J, Niemann H, O'Kane CJ (1995) Targeted expression of tetanus toxin light chain in Drosophila specifically eliminates synaptic transmission and causes behavioral defects. *Neuron* 14(2):341–351.

6. Mao Z, Roman G, Zong L, Davis RL (2004) Pharmacogenetic rescue in time and space of the rutabaga memory impairment by using Gene-Switch. *Proc Natl Acad Sci USA* 101(1):198–203.

7. Lee T, Lee A, Luo L (1999) Development of the Drosophila mushroom bodies: sequential generation of three distinct types of neurons from a neuroblast. *Development* 126(18):4065–4076.

8. Kakihara K, Shinmyozu K, Kato K, Wada H, Hayashi S (2008) Conversion of plasma membrane topology during epithelial tube connection requires Arf-like 3 small GTPase in Drosophila. *Mechanisms of Development* 125(3-4):325–336.

9. Pitman JL, et al. (2011) A pair of inhibitory neurons are required to sustain labile memory in the Drosophila mushroom body. *Current Biology* 21(10):855–861.

10. Barnstedt O, et al. (2016) Memory-Relevant Mushroom Body Output Synapses Are Cholinergic. *Neuron* 89(6):1237–1247.

11. Lin AC, Bygrave AM, de Calignon A, Lee T, Miesenböck G (2014) Sparse, decorrelated odor coding in the mushroom body enhances learned odor discrimination. *Nat Neurosci* 17(4):559–568.

12. Hamada FN, et al. (2008) An internal thermal sensor controlling temperature preference in Drosophila. *Nature* 454(7201):217–220.

13. Wu C-L, Shih M-FM, Lee P-T, Chiang A-S (2013) An octopamine-mushroom body circuit modulates the formation of anesthesia-resistant memory in Drosophila. *Current Biology* 23(23):2346–2354.

14. Liu WW, Wilson RI (2013) Transient and specific inactivation of Drosophila neurons in vivo using a native ligand-gated ion channel. 23(13):1202–1208.

15. Bielopolski N, et al. (2019) Inhibitory muscarinic acetylcholine receptors enhance aversive olfactory learning in adult Drosophila. *Elife* 8:463.

16. Ng MM, et al. (2002) Transmission of olfactory information between three populations of neurons in the antennal lobe of the fly. *Neuron* 36(3):463–474.

17. Wang JW, Wong AM, Flores J, Vosshall LB, Axel R (2003) Two-photon calcium imaging reveals an odor-evoked map of activity in the fly brain. *Cell* 112(2):271–282.

18. Dubbs A, Guevara J, Yuste R (2016) moco: Fast Motion Correction for Calcium Imaging. *Front*

Neuroinform 10:6.

19. Vinje WE, Gallant JL (2000) Sparse coding and decorrelation in primary visual cortex during natural vision. *Science* 287(5456):1273–1276.

20. Willmore B, Tolhurst DJ (2001) Characterizing the sparseness of neural codes. *Network* 12(3):255–270.

21. Wu JS, Luo L (2006) A protocol for dissecting Drosophila melanogaster brains for live imaging or immunostaining. *Nat Protoc* 1(4):2110–2115.

22. Ho J, Tumkaya T, Aryal S, Choi H, Claridge-Chang A (2019) Moving beyond P values: data analysis with estimation graphics. *Nat Methods* 16(7):565–566.

23. Mittal AM, Gupta D, Singh A, Lin AC, Gupta N (2020) Multiple network properties overcome random connectivity to enable stereotypic sensory responses. *Nature Communications* 11(1):1–15.

24. Groschner LN, Chan Wah Hak L, Bogacz R, DasGupta S, Miesenböck G (2018) Dendritic Integration of Sensory Evidence in Perceptual Decision-Making. *Cell* 173(4):894–905.e13.

25. Inada K, Tsuchimoto Y, Kazama H (2017) Origins of Cell-Type-Specific Olfactory Processing in the Drosophila Mushroom Body Circuit. *Neuron* 95(2):357–367.e4.

26. Turner GC, Bazhenov M, Laurent G (2008) Olfactory representations by Drosophila mushroom body neurons. *J Neurophysiol* 99(2):734–746.

27. Haberman A, et al. (2012) The synaptic vesicle SNARE neuronal Synaptobrevin promotes endolysosomal degradation and prevents neurodegeneration. - PubMed - NCBI. *J Cell Biol* 196(2):261–276.

Table S2: Details of statistics

Figure	Data	Statistical test	Comparison	P-value	Significance
1C: APL>TNT, IA	alpha', IA	Welch's ANOVA		<0.0001	****
		Dunnett's T3 multiple comparisons test	18 ºC vs. APL unlabeled	0.9372	ns
			18 ºC vs. acute	<0.0001	****
			18 ºC vs. constitutive	<0.0001	****
			APL unlabeled vs. acute	<0.0001	****
			APL unlabeled vs. constitutive	<0.0001	****
			acute vs. constitutive	0.4529	ns
	alpha', IA, separating APL unlabeled, Gal80ts vs. no Gal80ts	Dunnett's T3 multiple comparisons test	18 ºC vs. APL unlabeled, Gal80ts	0.9209	ns
			18 ºC vs. acute	<0.0001	****
			18 ºC vs. APL unlabeled, no Gal80ts	>0.9999	ns
			18 ºC vs. constitutive	<0.0001	****
			APL unlabeled, Gal80ts vs. acute	<0.0001	****
			APL unlabeled, Gal80ts vs. APL unlabeled, no Gal80ts	0.9477	ns
			APL unlabeled, no Gal80ts vs. constitutive	<0.0001	****
			acute vs. constitutive	0.5461	ns
	beta', IA	Kruskal-Wallis test		<0.0001	****
		Dunn's multiple comparisons test	18 ºC vs. APL unlabeled	>0.9999	ns
			18 ºC vs. acute	<0.0001	****
			18 ºC vs. constitutive	<0.0001	****
			APL unlabeled vs. acute	<0.0001	****
			APL unlabeled vs. constitutive	<0.0001	****
			acute vs. constitutive	0.4911	ns
	beta', IA, separating APL unlabeled, Gal80ts vs. no Gal80ts	Dunn's multiple comparisons test	18 ºC vs. APL unlabeled, Gal80ts	>0.9999	ns
			18 ºC vs. acute	<0.0001	****
			18 ºC vs. APL unlabeled, no Gal80ts	>0.9999	ns
			18 ºC vs. constitutive	<0.0001	****
			APL unlabeled, Gal80ts vs. acute	<0.0001	****
			APL unlabeled, Gal80ts vs. APL unlabeled, no Gal80ts	>0.9999	ns
			APL unlabeled, no Gal80ts vs. constitutive	0.007	**
			acute vs. constitutive	0.6548	ns
	alpha, IA	Welch's ANOVA		<0.0001	****
		Dunnett's T3 multiple comparisons test	18 ºC vs. APL unlabeled	0.6682	ns
			18 ºC vs. acute	<0.0001	****
			18 ºC vs. constitutive	<0.0001	****
			APL unlabeled vs. acute	<0.0001	****
			APL unlabeled vs. constitutive	<0.0001	****
			acute vs. constitutive	0.0204	*
	alpha, IA, separating APL unlabeled, Gal80ts vs. no Gal80ts	Dunnett's T3 multiple comparisons test	18 ºC vs. APL unlabeled, Gal80ts	0.9944	ns
			18 ºC vs. acute	<0.0001	****
			18 ºC vs. APL unlabeled, no Gal80ts	0.3794	ns
			18 ºC vs. constitutive	<0.0001	****
			APL unlabeled, Gal80ts vs. acute	<0.0001	****
			APL unlabeled, Gal80ts vs. APL unlabeled, no Gal80ts	0.9901	ns
			APL unlabeled, no Gal80ts vs. constitutive	<0.0001	****
			acute vs. constitutive	0.0269	*
	beta, IA	Welch's ANOVA		<0.0001	****
		Dunnett's T3 multiple comparisons test	18 ºC vs. APL unlabeled	>0.9999	ns
			18 ºC vs. acute	<0.0001	****
			18 ºC vs. constitutive	<0.0001	****
			APL unlabeled vs. acute	<0.0001	****
			APL unlabeled vs. constitutive	<0.0001	****
			acute vs. constitutive	0.9997	ns
	beta, IA, separating APL unlabeled, Gal80ts vs. no Gal80ts	Dunnett's T3 multiple comparisons test	18 ºC vs. APL unlabeled, Gal80ts	>0.9999	ns
			18 ºC vs. acute	<0.0001	****
			18 ºC vs. APL unlabeled, no Gal80ts	0.9993	ns
			18 ºC vs. constitutive	<0.0001	****
			APL unlabeled, Gal80ts vs. acute	<0.0001	****
			APL unlabeled, Gal80ts vs. APL unlabeled, no Gal80ts	0.9759	ns
			APL unlabeled, no Gal80ts vs. constitutive	<0.0001	****
			acute vs. constitutive	>0.9999	ns
	gamma, IA	Welch's ANOVA		<0.0001	****
		Dunnett's T3 multiple comparisons test	18 ºC vs. APL unlabeled	0.0285	*
			18 ºC vs. acute	<0.0001	****
			18 ºC vs. constitutive	<0.0001	****
			APL unlabeled vs. acute	<0.0001	****
			APL unlabeled vs. constitutive	<0.0001	****
			acute vs. constitutive	0.9578	ns
			18 ºC vs. APL unlabeled, Gal80ts	0.0569	ns
			18 ºC vs. acute	<0.0001	****

Table S2: Details of statistics

Figure	Data	Statistical test	Comparison	P-value	Significance
	gamma, IA, separating APL unlabeled, Gal80ts vs. no Gal80ts	Dunnett's T3 multiple comparisons test	18 ºC vs. APL unlabeled, no Gal80ts	0.0931	ns
			18 ºC vs. constitutive	<0.0001	****
			APL unlabeled, Gal80ts vs. acute	<0.0001	****
			APL unlabeled, Gal80ts vs. APL unlabeled, no Gal80ts	0.9993	ns
			APL unlabeled, no Gal80ts vs. constitutive	<0.0001	****
			acute vs. constitutive	0.9846	ns
1C: APL>TNT, d-DL	alpha', d-DL	Kruskal-Wallis test		<0.0001	****
		Dunn's multiple comparisons test	18 ºC vs. APL unlabeled	>0.9999	ns
			18 ºC vs. acute	0.0001	***
			18 ºC vs. constitutive	<0.0001	****
			APL unlabeled vs. acute	0.0002	***
			APL unlabeled vs. constitutive	0.0001	***
			acute vs. constitutive	>0.9999	ns
	alpha', dDL, separating APL unlabeled, Gal80ts vs. no Gal80ts	Dunn's multiple comparisons test	18 ºC vs. APL unlabeled, Gal80ts	>0.9999	ns
			18 ºC vs. acute	0.0001	***
			18 ºC vs. APL unlabeled, no Gal80ts	>0.9999	ns
			18 ºC vs. constitutive	0.0001	***
			APL unlabeled, Gal80ts vs. acute	0.0037	**
			APL unlabeled, Gal80ts vs. APL unlabeled, no Gal80ts	>0.9999	ns
			APL unlabeled, no Gal80ts vs. constitutive	0.0228	*
			acute vs. constitutive	>0.9999	ns
	beta', d-DL	Kruskal-Wallis test		<0.0001	****
		Dunn's multiple comparisons test	18 ºC vs. APL unlabeled	>0.9999	ns
			18 ºC vs. acute	<0.0001	****
			18 ºC vs. constitutive	<0.0001	****
			APL unlabeled vs. acute	<0.0001	****
			APL unlabeled vs. constitutive	<0.0001	****
			acute vs. constitutive	>0.9999	ns
	beta', dDL, separating APL unlabeled, Gal80ts vs. no Gal80ts	Dunn's multiple comparisons test	18 ºC vs. APL unlabeled, Gal80ts	>0.9999	ns
			18 ºC vs. acute	<0.0001	****
			18 ºC vs. APL unlabeled, no Gal80ts	>0.9999	ns
			18 ºC vs. constitutive	<0.0001	****
			APL unlabeled, Gal80ts vs. acute	<0.0001	****
			APL unlabeled, Gal80ts vs. APL unlabeled, no Gal80ts	>0.9999	ns
			APL unlabeled, no Gal80ts vs. constitutive	0.0015	**
			acute vs. constitutive	>0.9999	ns
	alpha, d-DL	Kruskal-Wallis test		<0.0001	****
		Dunn's multiple comparisons test	18 ºC vs. APL unlabeled	>0.9999	ns
			18 ºC vs. acute	0.0005	***
			18 ºC vs. constitutive	<0.0001	****
			APL unlabeled vs. acute	0.0003	***
			APL unlabeled vs. constitutive	<0.0001	****
			acute vs. constitutive	>0.9999	ns
	alpha, dDL, separating APL unlabeled, Gal80ts vs. no Gal80ts	Dunn's multiple comparisons test	18 ºC vs. APL unlabeled, Gal80ts	>0.9999	ns
			18 ºC vs. acute	0.0006	***
			18 ºC vs. APL unlabeled, no Gal80ts	>0.9999	ns
			18 ºC vs. constitutive	0.0001	***
			APL unlabeled, Gal80ts vs. acute	0.0044	**
			APL unlabeled, Gal80ts vs. APL unlabeled, no Gal80ts	>0.9999	ns
			APL unlabeled, no Gal80ts vs. constitutive	0.0167	*
			acute vs. constitutive	>0.9999	ns
	beta, d-DL	Welch's ANOVA		<0.0001	****
		Dunnett's T3 multiple comparisons test	18 ºC vs. APL unlabeled	0.759	ns
			18 ºC vs. acute	<0.0001	****
			18 ºC vs. constitutive	<0.0001	****
			APL unlabeled vs. acute	<0.0001	****
			APL unlabeled vs. constitutive	<0.0001	****
			acute vs. constitutive	0.0055	**
	beta, d-DL, separating APL unlabeled, Gal80ts vs. no Gal80ts	Dunnett's T3 multiple comparisons test	18 ºC vs. APL unlabeled, Gal80ts	>0.9999	ns
			18 ºC vs. acute	<0.0001	****
			18 ºC vs. APL unlabeled, no Gal80ts	0.1759	ns
			18 ºC vs. constitutive	<0.0001	****
			APL unlabeled, Gal80ts vs. acute	<0.0001	****
			APL unlabeled, Gal80ts vs. APL unlabeled, no Gal80ts	0.1014	ns
			APL unlabeled, no Gal80ts vs. constitutive	<0.0001	****
			acute vs. constitutive	0.0073	**
		Kruskal-Wallis test		<0.0001	****
			18 ºC vs. APL unlabeled	>0.9999	ns
			18 ºC vs. acute	<0.0001	****

Table S2: Details of statistics

Figure	Data	Statistical test	Comparison	P-value	Significance
	gamma, d-DL	Dunn's multiple comparisons test	18 ºC vs. constitutive	<0.0001	****
			APL unlabeled vs. acute	<0.0001	****
			APL unlabeled vs. constitutive	<0.0001	****
			acute vs. constitutive	0.8711	ns
	gamma, dDL, separating APL unlabeled, Gal80ts vs. no Gal80ts	Dunn's multiple comparisons test	18 ºC vs. APL unlabeled, Gal80ts	>0.9999	ns
			18 ºC vs. acute	<0.0001	****
			18 ºC vs. APL unlabeled, no Gal80ts	>0.9999	ns
			18 ºC vs. constitutive	<0.0001	****
			APL unlabeled, Gal80ts vs. acute	<0.0001	****
			APL unlabeled, Gal80ts vs. APL unlabeled, no Gal80ts	>0.9999	ns
			APL unlabeled, no Gal80ts vs. constitutive	0.0003	***
			acute vs. constitutive	>0.9999	ns
S2A: KC>GCaMP6f, APL unlabeled, with vs. without GAL80ts	IA	Mixed-effects model with Geisser-Greenhouse correction (matching across lobes)	Lobe	0.0973	ns
			Genotype	0.6698	ns
			Lobe x Genotype	0.6685	ns
	dDL	Mixed-effects model with Geisser-Greenhouse correction (matching across lobes)	Lobe	<0.0001	****
			Genotype	0.0802	ns
			Lobe x Genotype	0.2552	ns
S2C: KC>GCaMP3, APL>TNT, IA	alpha', IA	Welch's ANOVA		<0.0001	****
		Dunnett's T3 multiple comparisons test	APL unlabeled vs. acute	<0.0001	****
			APL unlabeled vs. constitutive	<0.0001	****
			acute vs. constitutive	0.5147	ns
	beta', IA	Welch's ANOVA		<0.0001	****
		Dunnett's T3 multiple comparisons test	APL unlabeled vs. acute	<0.0001	****
			APL unlabeled vs. constitutive	<0.0001	****
			acute vs. constitutive	0.8257	ns
	alpha, IA	Welch's ANOVA		<0.0001	****
		Dunnett's T3 multiple comparisons test	APL unlabeled vs. acute	<0.0001	****
			APL unlabeled vs. constitutive	<0.0001	****
			acute vs. constitutive	0.2323	ns
	beta, IA	Kruskal-Wallis test		<0.0001	****
		Dunn's multiple comparisons test	APL unlabeled vs. acute	<0.0001	****
			APL unlabeled vs. constitutive	<0.0001	****
			acute vs. constitutive	>0.9999	ns
	gamma, IA	Welch's ANOVA		<0.0001	****
		Dunnett's T3 multiple comparisons test	APL unlabeled vs. acute	<0.0001	****
			APL unlabeled vs. constitutive	<0.0001	****
			acute vs. constitutive	0.4235	ns
S2C: KC>GCaMP3, APL>TNT, d-DL	alpha', d-DL	Welch's ANOVA		<0.0001	****
		Dunnett's T3 multiple comparisons test	APL unlabeled vs. acute	<0.0001	****
			APL unlabeled vs. constitutive	0.0002	***
			acute vs. constitutive	0.3843	ns
	beta', d-DL	Kruskal-Wallis test		<0.0001	****
		Dunn's multiple comparisons test	APL unlabeled vs. acute	<0.0001	****
			APL unlabeled vs. constitutive	<0.0001	****
			acute vs. constitutive	>0.9999	ns
	alpha, d-DL	Welch's ANOVA		<0.0001	****
		Dunnett's T3 multiple comparisons test	APL unlabeled vs. acute	<0.0001	****
			APL unlabeled vs. constitutive	<0.0001	****
			acute vs. constitutive	0.5274	ns
	beta, d-DL	Kruskal-Wallis test		<0.0001	****
		Dunn's multiple comparisons test	APL unlabeled vs. acute	<0.0001	****
			APL unlabeled vs. constitutive	<0.0001	****
			acute vs. constitutive	>0.9999	ns
	gamma, d-DL	Welch's ANOVA		<0.0001	****
		Dunnett's T3 multiple comparisons test	APL unlabeled vs. acute	<0.0001	****
			APL unlabeled vs. constitutive	<0.0001	****
			acute vs. constitutive	0.3781	ns
S3A: (IA-dDL)/(IA+dDL), KC>GCaMP6f	Mixed-effects model with Geisser-Greenhouse correction (matching across lobes)		Lobe	<0.0001	****
			Genotype	<0.0001	****
			Lobe x Genotype	0.0262	*
	alpha'	Holm-Sidak multiple comparison tests	APL unlabeled vs. acute	0.024	*
			APL unlabeled vs. constitutive	0.3438	ns
			acute vs. constitutive	0.024	*
	beta'	Holm-Sidak multiple comparison tests	APL unlabeled vs. acute	0.0177	*
			APL unlabeled vs. constitutive	0.563	ns
			acute vs. constitutive	0.0319	*
	alpha	Holm-Sidak multiple comparison tests	APL unlabeled vs. acute	0.3056	ns
			APL unlabeled vs. constitutive	0.6328	ns

Table S2: Details of statistics

Figure	Data	Statistical test	Comparison	P-value	Significance
			acute vs. constitutive	0.0039	**
	beta	Holm-Sidak multiple comparison tests	APL unlabeled vs. acute	0.0005	***
			APL unlabeled vs. constitutive	0.575	ns
			acute vs. constitutive	0.0001	***
	gamma	Holm-Sidak multiple comparison tests	APL unlabeled vs. acute	<0.0001	****
			APL unlabeled vs. constitutive	0.0274	*
			acute vs. constitutive	0.0274	*
S3A: (IA-dDL)/(IA+dDL), KC>GCaMP3	2-way ANOVA		N/A: residuals not normal		
	alpha'	ordinary 1-way ANOVA		0.0034	**
		Holm-Sidak multiple comparisons test	APL unlabeled vs. acute	0.0036	**
			APL unlabeled vs. constitutive	0.0248	*
			acute vs. constitutive	0.6375	ns
	beta'	Kruskal-Wallis test		0.0127	*
		Dunn's multiple comparisons test	APL unlabeled vs. acute	0.9179	ns
			APL unlabeled vs. constitutive	0.0117	*
			acute vs. constitutive	0.1072	ns
	alpha	Kruskal-Wallis test		0.0157	*
		Dunn's multiple comparisons test	APL unlabeled vs. acute	0.0246	*
			APL unlabeled vs. constitutive	>0.9999	ns
			acute vs. constitutive	0.1044	ns
	beta	Kruskal-Wallis test		0.0236	*
		Dunn's multiple comparisons test	APL unlabeled vs. acute	0.0208	*
			APL unlabeled vs. constitutive	0.2035	ns
			acute vs. constitutive	>0.9999	ns
	gamma	Kruskal-Wallis test		<0.0001	****
		Dunn's multiple comparisons test	APL unlabeled vs. acute	<0.0001	****
			APL unlabeled vs. constitutive	<0.0001	****
			acute vs. constitutive	>0.9999	ns
S1e: OFF/ON, KC>GCaMP6f	alpha', IA	Ordinary 1-way ANOVA		<0.0001	****
		Holm-Sidak multiple comparisons test	APL unlabeled vs. acute	<0.0001	****
			APL unlabeled vs. constitutive	<0.0001	****
			acute vs. constitutive	0.1596	ns
	beta', IA	Ordinary 1-way ANOVA		<0.0001	****
		Holm-Sidak multiple comparisons test	APL unlabeled vs. acute	<0.0001	****
			APL unlabeled vs. constitutive	<0.0001	****
			acute vs. constitutive	0.0651	ns
	alpha, IA	Ordinary 1-way ANOVA		0.0039	**
		Holm-Sidak multiple comparisons test	APL unlabeled vs. acute	0.0054	**
			APL unlabeled vs. constitutive	0.0054	**
			acute vs. constitutive	0.9967	ns
	beta, IA	Ordinary 1-way ANOVA		<0.0001	****
		Holm-Sidak multiple comparisons test	APL unlabeled vs. acute	<0.0001	****
			APL unlabeled vs. constitutive	<0.0001	****
			acute vs. constitutive	0.2841	ns
	gamma, IA	Kruskal-Wallis test		<0.0001	****
		Dunn's multiple comparisons test	APL unlabeled vs. acute	<0.0001	****
			APL unlabeled vs. constitutive	<0.0001	****
			acute vs. constitutive	0.5456	ns
S3B: OFF/ON, KC>GCaMP6f	alpha', d-DL	Kruskal-Wallis test		0.0087	**
		Dunn's multiple comparisons test	APL unlabeled vs. acute	0.2945	ns
			APL unlabeled vs. constitutive	0.0074	**
			acute vs. constitutive	0.1976	ns
	beta', d-DL	Kruskal-Wallis test		0.0004	***
		Dunn's multiple comparisons test	APL unlabeled vs. acute	0.041	*
			APL unlabeled vs. constitutive	0.0002	***
			acute vs. constitutive	0.2542	ns
	alpha, d-DL	Kruskal-Wallis test		0.8892	ns
	beta, d-DL	Kruskal-Wallis test		0.8892	ns
	gamma, d-DL	Kruskal-Wallis test		0.1644	ns
S3B: OFF/ON, KC>GCaMP3	alpha', IA	Kruskal-Wallis test		<0.0001	****
		Dunn's multiple comparisons test	APL unlabeled vs. acute	0.0019	**
			APL unlabeled vs. constitutive	<0.0001	****
			acute vs. constitutive	0.2982	ns
	beta', IA	Welch's ANOVA		<0.0001	****
		Dunnett's T3 multiple comparisons test	APL unlabeled vs. acute	<0.0001	****
			APL unlabeled vs. constitutive	<0.0001	****
			acute vs. constitutive	<0.0001	****
	alpha, IA	Kruskal-Wallis test		0.0736	ns
		Kruskal-Wallis test		<0.0001	****

Table S2: Details of statistics

Figure	Data	Statistical test	Comparison	P-value	Significance
	beta, IA	Dunn's multiple comparisons test	APL unlabeled vs. acute	<0.0001	****
			APL unlabeled vs. constitutive	<0.0001	****
			acute vs. constitutive	0.017	*
	gamma, IA	Kruskal-Wallis test		<0.0001	****
		Dunn's multiple comparisons test	APL unlabeled vs. acute	<0.0001	****
			APL unlabeled vs. constitutive	<0.0001	****
			acute vs. constitutive	0.0022	**
S3B: OFF/ON, KC>GCaMP3	alpha', d-DL	Kruskal-Wallis test		0.218	ns
	beta', d-DL	Kruskal-Wallis test		<0.0001	****
		Dunnett's T3 multiple comparisons test	APL unlabeled vs. acute	0.032	*
			APL unlabeled vs. constitutive	<0.0001	****
			acute vs. constitutive	0.0599	ns
	alpha, d-DL	Kruskal-Wallis test		0.4053	ns
	beta, d-DL	Kruskal-Wallis test		0.0191	****
		Dunn's multiple comparisons test	APL unlabeled vs. acute	>0.9999	ns
			APL unlabeled vs. constitutive	0.0192	*
			acute vs. constitutive	0.1087	ns
	gamma, d-DL	Kruskal-Wallis test		<0.0001	****
		Dunn's multiple comparisons test	APL unlabeled vs. acute	>0.9999	ns
			APL unlabeled vs. constitutive	0.0015	**
			acute vs. constitutive	<0.0001	****
2C: APL>dTRPA1 adaptation, IA	alpha', IA	2-way ANOVA	interaction	0.0354	*
			kept at 22 C vs. kept at 31 C	0.0168	*
			APL unlabeled vs. APL labeled	0.008	**
		Ordinary 1-way ANOVA		0.0009	***
		Holm-Sidak's multiple comparisons test	APL unlab, kept 22ºC vs. APL>dTRPA1, kept 22ºC	0.8942	ns
			APL unlab, kept 22ºC vs. APL unlab, kept 31ºC	0.8942	ns
			APL>dTRPA1, kept 22ºC vs. APL>dTRPA1, kept 31ºC	0.0031	**
			APL unlab, kept 31ºC vs. APL>dTRPA1, kept 31ºC	0.0031	**
	beta', IA	2-way ANOVA	n/a (residuals not normal)		
		Welch's ANOVA		<0.0001	****
		Dunnett's T3 multiple comparisons test	APL unlab, kept 22ºC vs. APL>dTRPA1, kept 22ºC	0.3687	ns
			APL unlab, kept 22ºC vs. APL unlab, kept 31ºC	0.097	ns
			APL>dTRPA1, kept 22ºC vs. APL>dTRPA1, kept 31ºC	<0.0001	****
			APL unlab, kept 31ºC vs. APL>dTRPA1, kept 31ºC	0.0018	**
	alpha, IA	2-way ANOVA	interaction	0.1146	ns
			kept at 22 C vs. kept at 31 C	0.002	**
			APL unlabeled vs. APL labeled	0.1613	ns
		Kruskal-Wallis test		0.0009	***
		Dunn's multiple comparisons test	APL unlab, kept 22ºC vs. APL>dTRPA1, kept 22ºC	>0.9999	ns
			APL unlab, kept 22ºC vs. APL unlab, kept 31ºC	0.731	ns
			APL>dTRPA1, kept 22ºC vs. APL>dTRPA1, kept 31ºC	0.0039	**
			APL unlab, kept 31ºC vs. APL>dTRPA1, kept 31ºC	0.4608	ns
		Ordinary 1-way ANOVA	(NB: D'Agostino-Pearson test on residuals p=0.0501)	0.0023	**
		Holm-Sidak's multiple comparisons test	APL unlab, kept 22ºC vs. APL>dTRPA1, kept 22ºC	0.898	ns
			APL unlab, kept 22ºC vs. APL unlab, kept 31ºC	0.4796	ns
			APL>dTRPA1, kept 22ºC vs. APL>dTRPA1, kept 31ºC	0.0018	**
			APL unlab, kept 31ºC vs. APL>dTRPA1, kept 31ºC	0.101	ns
	beta, IA	2-way ANOVA	interaction	0.2336	ns
			kept at 22 C vs. kept at 31 C	<0.0001	****
			APL unlabeled vs. APL labeled	0.0109	*
		Ordinary 1-way ANOVA		<0.0001	****
		Holm-Sidak's multiple comparisons test	APL unlab, kept 22ºC vs. APL>dTRPA1, kept 22ºC	0.3174	ns
			APL unlab, kept 22ºC vs. APL unlab, kept 31ºC	0.0208	*
			APL>dTRPA1, kept 22ºC vs. APL>dTRPA1, kept 31ºC	<0.0001	****
			APL unlab, kept 31ºC vs. APL>dTRPA1, kept 31ºC	0.0208	*
	gamma, IA	2-way ANOVA	interaction	<0.0001	****
			kept at 22 C vs. kept at 31 C	<0.0001	****
			APL unlabeled vs. APL labeled	<0.0001	****
		Ordinary 1-way ANOVA		<0.0001	****
		Holm-Sidak's multiple comparisons test	APL unlab, kept 22ºC vs. APL>dTRPA1, kept 22ºC	0.8358	ns
			APL unlab, kept 22ºC vs. APL unlab, kept 31ºC	0.6543	ns
			APL>dTRPA1, kept 22ºC vs. APL>dTRPA1, kept 31ºC	<0.0001	****
			APL unlab, kept 31ºC vs. APL>dTRPA1, kept 31ºC	<0.0001	****
	alpha', d-DL	2-way ANOVA	n/a (residuals not normal)		
		Kruskal-Wallis test		<0.0001	****
		Dunn's multiple comparisons test	APL unlab, kept 22ºC vs. APL>dTRPA1, kept 22ºC	>0.9999	ns
			APL unlab, kept 22ºC vs. APL unlab, kept 31ºC	>0.9999	ns
			APL>dTRPA1, kept 22ºC vs. APL>dTRPA1, kept 31ºC	<0.0001	****

Figure	Data	Statistical test	Comparison	P-value	Significance
2C: APL>dTRPA1 adaptation, d-DL			APL unlab, kept 31ºC vs. APL>dTRPA1, kept 31ºC	0.0003	***
	beta', d-DL	2-way ANOVA	interaction	0.0005	***
			kept at 22 C vs. kept at 31 C	0.0008	***
			APL unlabeled vs. APL labeled	0.0046	**
		Welch's ANOVA		0.0019	**
		Dunnett's T3 multiple comparisons test	APL unlab, kept 22ºC vs. APL>dTRPA1, kept 22ºC	0.8689	ns
			APL unlab, kept 22ºC vs. APL unlab, kept 31ºC	0.9998	ns
			APL>dTRPA1, kept 22ºC vs. APL>dTRPA1, kept 31ºC	0.0013	**
			APL unlab, kept 31ºC vs. APL>dTRPA1, kept 31ºC	0.0029	**
	alpha, d-DL	2-way ANOVA	interaction	0.0003	***
			kept at 22 C vs. kept at 31 C	<0.0001	****
			APL unlabeled vs. APL labeled	<0.0001	****
		Welch's ANOVA		<0.0001	****
		Dunnett's T3 multiple comparisons test	APL unlab, kept 22ºC vs. APL>dTRPA1, kept 22ºC	0.9744	ns
			APL unlab, kept 22ºC vs. APL unlab, kept 31ºC	0.3449	ns
			APL>dTRPA1, kept 22ºC vs. APL>dTRPA1, kept 31ºC	<0.0001	****
			APL unlab, kept 31ºC vs. APL>dTRPA1, kept 31ºC	0.0002	***
	beta, d-DL	2-way ANOVA	interaction	0.0013	**
			kept at 22 C vs. kept at 31 C	<0.0001	****
			APL unlabeled vs. APL labeled	0.0005	***
		Welch's ANOVA		0.0002	***
		Dunnett's T3 multiple comparisons test	APL unlab, kept 22ºC vs. APL>dTRPA1, kept 22ºC	0.9796	ns
			APL unlab, kept 22ºC vs. APL unlab, kept 31ºC	0.1068	ns
			APL>dTRPA1, kept 22ºC vs. APL>dTRPA1, kept 31ºC	0.0008	***
			APL unlab, kept 31ºC vs. APL>dTRPA1, kept 31ºC	0.0036	**
	gamma, d-DL	2-way ANOVA	interaction	<0.0001	****
			kept at 22 C vs. kept at 31 C	<0.0001	****
			APL unlabeled vs. APL labeled	<0.0001	****
		Welch's ANOVA		0.0001	***
		Dunnett's T3 multiple comparisons test	APL unlab, kept 22ºC vs. APL>dTRPA1, kept 22ºC	0.9551	ns
			APL unlab, kept 22ºC vs. APL unlab, kept 31ºC	0.9976	ns
			APL>dTRPA1, kept 22ºC vs. APL>dTRPA1, kept 31ºC	0.0002	***
			APL unlab, kept 31ºC vs. APL>dTRPA1, kept 31ºC	0.0003	***
2E: sparseness		Unpaired t-test	APL unlabeled vs. APL>dTRPA1	0.0003	***
S2: KC>GCaMP3, APL>dTRPA1, odor responses after adaptation	alpha', IA	Kruskal-Wallis test		0.0223	*
		Dunn's multiple comparisons test	APL unlab, kept 22ºC vs. APL>dTRPA1, kept 22ºC	0.0088	**
			APL unlab, kept 22ºC vs. APL unlab, kept 31ºC	0.6146	ns
			APL>dTRPA1, kept 22ºC vs. APL>dTRPA1, kept 31ºC	0.1445	ns
			APL unlab, kept 31ºC vs. APL>dTRPA1, kept 31ºC	>0.9999	ns
	beta', IA	Ordinary 1-way ANOVA		0.0022	**
		Holm-Sidak multiple comparisons test	APL unlab, kept 22ºC vs. APL>dTRPA1, kept 22ºC	0.8251	ns
			APL unlab, kept 22ºC vs. APL unlab, kept 31ºC	0.8251	ns
			APL>dTRPA1, kept 22ºC vs. APL>dTRPA1, kept 31ºC	0.0061	**
			APL unlab, kept 31ºC vs. APL>dTRPA1, kept 31ºC	0.0441	*
	alpha, IA	Ordinary 1-way ANOVA		0.0034	**
		Holm-Sidak multiple comparisons test	APL unlab, kept 22ºC vs. APL>dTRPA1, kept 22ºC	0.3967	ns
			APL unlab, kept 22ºC vs. APL unlab, kept 31ºC	0.1209	ns
			APL>dTRPA1, kept 22ºC vs. APL>dTRPA1, kept 31ºC	0.0277	*
			APL unlab, kept 31ºC vs. APL>dTRPA1, kept 31ºC	0.0019	**
	beta, IA	Kruskal-Wallis test		0.0174	*
		Dunn's multiple comparisons test	APL unlab, kept 22ºC vs. APL>dTRPA1, kept 22ºC	>0.9999	ns
			APL unlab, kept 22ºC vs. APL unlab, kept 31ºC	>0.9999	ns
			APL>dTRPA1, kept 22ºC vs. APL>dTRPA1, kept 31ºC	0.0436	*
			APL unlab, kept 31ºC vs. APL>dTRPA1, kept 31ºC	0.2168	ns
	gamma, IA	Ordinary 1-way ANOVA		0.0002	***
		Holm-Sidak multiple comparisons test	APL unlab, kept 22ºC vs. APL>dTRPA1, kept 22ºC	0.3343	ns
			APL unlab, kept 22ºC vs. APL unlab, kept 31ºC	0.3343	ns
			APL>dTRPA1, kept 22ºC vs. APL>dTRPA1, kept 31ºC	0.0023	**
			APL unlab, kept 31ºC vs. APL>dTRPA1, kept 31ºC	0.0239	*
Fig. S5A, sparseness for different odor		Mixed-effects model (matching across odors)	main effect APL unlabeled vs. APL>dTRPA1	0.0004	***
			main effect across odors	<0.0001	****
			interaction odor x (APL unlabeled vs. APL>dTRPA1)	0.0032	**
Fig. S5C, inter-odor correlation		Unpaired t-test	APL unlabeled vs. APL>dTRPA1	0.1457	ns
		Mixed-effects model (matching across odor pairs)	main effect APL unlabeled vs. APL>dTRPA1	0.1808	ns
			main effect across odor pairs	<0.0001	****
			interaction odor pairs x (APL unlabeled vs. APL>dTRPA1)	0.3646	ns
S5D: APL>TNT vs. APL>dTRPA1		Welch's ANOVA		<0.0001	****
			APL unlab, dTRPA1, kept 31ºC vs. APL>dTRPA1, kept 31ºC	<0.0001	****
			APL unlab, dTRPA1, kept 31ºC vs. APL unlab, TNT	0.0769	ns

Figure	Data	Statistical test	Comparison	P-value	Significance
S5D: APL>TNT vs. APL>dTRPA1 adaptation		Dunnett's T3 multiple comparisons test	APL unlab, dTRPA1, kept 31ºC vs. APL>TNT acute	<0.0001	****
			APL>dTRPA1, kept 31ºC vs. APL unlab, TNT	<0.0001	****
			APL>dTRPA1, kept 31ºC vs. APL>TNT acute	<0.0001	****
			APL unlab, TNT vs. APL>TNT acute	<0.0001	****
S7A: APL>dTRPA1 effect of heating during imaging, mean ΔF/F	APL unlabeled, kept at 22 ºC, IA	Mixed-effects model with Geisser-Greenhouse correction (matching across lobes and across temperature at time of measurement)	lobe	0.6803	ns
			temperature	0.4272	ns
			lobe x temperature	0.3621	ns
	APL>dTRPA1, kept at 22 ºC, IA	2-way repeated measures ANOVA with Geisser-Greenhouse correction (matching across lobes and across temperature at time of measurement)	lobe	<0.0001	****
			temperature	0.0017	**
			lobe x temperature	<0.0001	****
		Holm-Sidak multiple comparison test (22 ºC vs. 31 ºC)	alpha'	0.7426	ns
			beta'	0.044	*
			alpha	<0.0001	****
			beta	0.0004	***
			gamma	0.0015	**
	APL unlabeled, kept at 31 ºC, IA	Mixed-effects model with Geisser-Greenhouse correction (matching across lobes and across temperature at time of measurement)	lobe	0.0024	**
			temperature	0.1031	ns
			lobe x temperature	0.4676	ns
	APL>dTRPA1, kept at 31 ºC, IA	Mixed-effects model with Geisser-Greenhouse correction (matching across lobes and across temperature at time of measurement)	lobe	<0.0001	****
			temperature	0.0018	**
			lobe x temperature	<0.0001	****
		Holm-Sidak multiple comparison test (22 ºC vs. 31 ºC)	alpha'	0.2072	ns
			beta'	0.1344	ns
			alpha	0.0033	**
			beta	0.0042	**
			gamma	0.003	**
	APL unlabeled, kept at 22 ºC, dDL	Mixed-effects model with Geisser-Greenhouse correction (matching across lobes and across temperature at time of measurement)	lobe	0.0352	*
			temperature	0.8346	ns
			lobe x temperature	0.3694	ns
	APL>dTRPA1, kept at 22 ºC, dDL	2-way repeated measures ANOVA with Geisser-Greenhouse correction (matching across lobes and across temperature at time of measurement)	lobe	0.0006	***
			temperature	0.0002	***
			lobe x temperature	0.0012	**
		Holm-Sidak multiple comparison test (22 ºC vs. 31 ºC)	alpha'	0.071	ns
			beta'	0.052	ns
			alpha	<0.0001	****
			beta	0.0015	**
			gamma	<0.0001	****
	APL unlabeled, kept at 31 ºC, dDL	Mixed-effects model with Geisser-Greenhouse correction (matching across lobes and across temperature at time of measurement)	lobe	0.0006	***
			temperature	0.561	ns
			lobe x temperature	0.0185	*
	APL>dTRPA1, kept at 31 ºC, IA	Mixed-effects model with Geisser-Greenhouse correction (matching across lobes and across temperature at time of measurement)	lobe	<0.0001	****
			temperature	<0.0001	****
			lobe x temperature	<0.0001	****
		Holm-Sidak multiple comparison test (22 ºC vs. 31 ºC)	alpha'	0.0058	**
			beta'	0.0026	**
			alpha	0.0002	***
			beta	0.0005	***
			gamma	0.0006	***
	APL unlabeled, kept at 22 ºC, IA	Mixed-effects model with Geisser-Greenhouse correction (matching across lobes and across temperature at time of measurement)	lobe	0.5361	ns
			temperature	0.1998	ns
			lobe x temperature	0.3806	ns
	APL>dTRPA1, kept at 22 ºC, IA	2-way repeated measures ANOVA with Geisser-Greenhouse correction (matching across lobes and across temperature at time of measurement)	lobe	0.0011	**
			temperature	0.0103	*
			lobe x temperature	<0.0001	****
		Holm-Sidak multiple comparison test (22 ºC vs. 31 ºC)	alpha'	0.9831	ns
			beta'	0.0032	**
			alpha	<0.0001	****
			beta	0.0003	***
			gamma	0.0082	**
	APL unlabeled, kept at 31 ºC, IA	Mixed-effects model with Geisser-Greenhouse correction (matching across lobes and across temperature at time of measurement)	lobe	0.0001	***
			temperature	0.0464	*
			lobe x temperature	0.2941	ns
		Holm-Sidak multiple comparison test (22 ºC vs. 31 ºC)	alpha'	0.8542	ns
			beta'	0.1352	ns
			alpha	0.0217	*
			beta	0.3134	ns
			gamma	0.6756	ns
		Mixed-effects model with Geisser-Greenhouse correction (matching across lobes and across temperature at time of	lobe	0.0001	***
			temperature	0.0088	**

Figure	Data	Statistical test	Comparison	P-value	Significance
S7B: APL>dTRPA1 effect of heating during imaging - max. ΔF/F	APL>dTRPA1, kept at 31 ºC, IA	[illegible] measurement)	lobe x temperature	<0.0001	****
		Holm-Sidak multiple comparison test (22 ºC vs. 31 ºC)	alpha'	0.4606	ns
			beta'	0.4606	ns
			alpha	0.0228	*
			beta	0.0412	*
			gamma	0.0018	**
	APL unlabeled, kept at 22 ºC, dDL	Mixed-effects model with Geisser-Greenhouse correction (matching across lobes and across temperature at time of measurement)	lobe	0.0034	**
			temperature	0.9247	ns
			lobe x temperature	0.3579	ns
	APL>dTRPA1, kept at 22 ºC, dDL	2-way repeated measures ANOVA with Geisser-Greenhouse correction (matching across lobes and across temperature at time of measurement)	lobe	<0.0001	****
			temperature	0.0002	***
			lobe x temperature	0.0003	***
		Holm-Sidak multiple comparison test (22 ºC vs. 31 ºC)	alpha'	0.533	ns
			beta'	0.533	ns
			alpha	<0.0001	****
			beta	0.0003	***
			gamma	<0.0001	****
	APL unlabeled, kept at 31 ºC, dDL	Mixed-effects model with Geisser-Greenhouse correction (matching across lobes and across temperature at time of measurement)	lobe	<0.0001	****
			temperature	0.6791	ns
			lobe x temperature	0.0006	***
	APL>dTRPA1, kept at 31 ºC, IA	Mixed-effects model with Geisser-Greenhouse correction (matching across lobes and across temperature at time of measurement)	lobe	<0.0001	****
			temperature	0.0001	***
			lobe x temperature	<0.0001	****
		Holm-Sidak multiple comparison test (22 ºC vs. 31 ºC)	alpha'	0.0289	*
			beta'	0.0247	*
			alpha	0.0007	***
			beta	0.0016	**
			gamma	0.0003	***
Fig. S9, APL>dTRPA1 adaptation, IA after 1d and 4d adaptation	alpha', IA	2-way ANOVA	interaction	0.3092	ns
			1d adaptation vs. 4d adaptation	0.8735	ns
			UAS TRPA vs. APL TRPA	0.4222	ns
		Ordinary 1-way ANOVA		0.5952	ns
	beta', IA	2-way ANOVA	interaction	0.0033	**
			1d adaptation vs. 4d adaptation	0.9944	ns
			UAS TRPA vs. APL TRPA	0.0036	**
		Ordinary 1-way ANOVA		0.0006	***
		Holm-Sidak's multiple comparisons test	UAS TRPA 1d vs. APL TRPA 1d	0.9998	ns
			UAS TRPA 4d vs. APL TRPA 4d	<0.0001	****
	alpha, IA	2-way ANOVA	interaction	0.0803	ns
			1d adaptation vs. 4d adaptation	0.0503	ns
			UAS TRPA vs. APL TRPA	0.0665	ns
		Ordinary 1-way ANOVA		0.0185	*
		Holm-Sidak's multiple comparisons test	UAS TRPA 1d vs. APL TRPA 1d	0.9975	ns
			UAS TRPA 4d vs. APL TRPA 4d	0.0185	*
	beta, IA	2-way ANOVA	interaction	0.3323	ns
			1d adaptation vs. 4d adaptation	0.638	ns
			UAS TRPA vs. APL TRPA	0.0031	**
		Ordinary 1-way ANOVA		0.0151	*
		Holm-Sidak's multiple comparisons test	UAS TRPA 1d vs. APL TRPA 1d	0.2767	ns
			UAS TRPA 4d vs. APL TRPA 4d	0.0078	**
	gamma, IA	2-way ANOVA		0.0187	*
			1d adaptation vs. 4d adaptation	0.4415	ns
			UAS TRPA vs. APL TRPA	0.0002	***
		Ordinary 1-way ANOVA		0.0002	***
		Holm-Sidak's multiple comparisons test	UAS TRPA 1d vs. APL TRPA 1d	0.4469	ns
			UAS TRPA 4d vs. APL TRPA 4d	<0.0001	****
Fig. S9, [illegible]	alpha', dDL	2-way ANOVA	interaction	0.3624	ns
			1d adaptation vs. 4d adaptation	0.466	ns
			UAS TRPA vs. APL TRPA	0.1286	ns
		Ordinary 1-way ANOVA		0.3528	ns
	beta', dDL	2-way ANOVA	interaction	0.0011	**
			1d adaptation vs. 4d adaptation	0.2283	ns
			UAS TRPA vs. APL TRPA	0.0207	*
		Ordinary 1-way ANOVA		0.0073	**
		Holm-Sidak's multiple comparisons test	UAS TRPA 1d vs. APL TRPA 1d	0.5612	ns
			UAS TRPA 4d vs. APL TRPA 4d	0.0019	**
	[illegible]	2-way ANOVA	interaction	0.0427	*
			1d adaptation vs. 4d adaptation	0.0304	*
			UAS TRPA vs. APL TRPA	0.0411	*

Figure	Data	Statistical test	Comparison	P-value	Significance
APL>dTRPA1 adaptation, d-DL after 1d and 4d adaptation	alpha, dDL	Ordinary 1-way ANOVA		0.0079	**
		Holm-Sidak's multiple comparisons test	UAS TRPA 1d vs. APL TRPA 1d	>0.9999	ns
			UAS TRPA 4d vs. APL TRPA 4d	0.011	*
	beta, dDL	2-way ANOVA	interaction	0.3142	ns
			1d adaptation vs. 4d adaptation	0.0231	*
			UAS TRPA vs. APL TRPA	0.0049	**
		Ordinary 1-way ANOVA		0.0022	**
		Holm-Sidak's multiple comparisons test	UAS TRPA 1d vs. APL TRPA 1d	0.3058	ns
			UAS TRPA 4d vs. APL TRPA 4d	0.0158	*
	gamma, dDL	2-way ANOVA	interaction	0.281	ns
			1d adaptation vs. 4d adaptation	0.8239	ns
			UAS TRPA vs. APL TRPA	0.0056	**
		Ordinary 1-way ANOVA		0.0284	*
		Holm-Sidak's multiple comparisons test	UAS TRPA 1d vs. APL TRPA 1d	0.3507	ns
			UAS TRPA 4d vs. APL TRPA 4d	0.0151	*
Fig S10, APL>dTRPA1 1d adaptation (imaged at 1 d old)	alpha', IA	Mann-Whitney test	no dTRPA1 vs. APL>dTRPA1	0.4985	ns
	beta', IA	Unpaired t-test	no dTRPA1 vs. APL>dTRPA1	0.7981	ns
	alpha, IA	Mann-Whitney test	no dTRPA1 vs. APL>dTRPA1	0.6788	ns
	beta, IA	Unpaired t-test	no dTRPA1 vs. APL>dTRPA1	0.6934	ns
	gamma, IA	Unpaired t-test	no dTRPA1 vs. APL>dTRPA1	0.7713	ns
	alpha', d-DL	Unpaired t-test	no dTRPA1 vs. APL>dTRPA1	0.5653	ns
	beta', d-DL	Mann-Whitney test	no dTRPA1 vs. APL>dTRPA1	0.5145	ns
	alpha, d-DL	Unpaired t-test	no dTRPA1 vs. APL>dTRPA1	0.3114	ns
	beta, d-DL	Mann-Whitney test	no dTRPA1 vs. APL>dTRPA1	0.9215	ns
	gamma, d-DL	Mann-Whitney test	no dTRPA1 vs. APL>dTRPA1	0.7374	ns
Fig 3, S11, APL>dTRPA1 1,2,3,4 d adaptation	alpha', IA	2-way ANOVA	interaction	0.5387	ns
			main effect of days at 31 ºC	<0.0001	****
			main effect of APL unlabeled vs. APL>dTRPA1	<0.0001	****
		Sidak multiple comparisons test	1 d	0.9266	ns
			2 d	0.0112	*
			3 d	0.046	*
			4 d	0.0608	ns
	beta', IA	2-way ANOVA	interaction	0.4041	ns
			main effect of days at 31 ºC	0.0018	**
			main effect of APL unlabeled vs. APL>dTRPA1	0.0074	**
		Sidak multiple comparisons test	1 d	ns	0.3357
			2 d	ns	0.9997
			3 d	ns	0.6155
			4 d	ns	0.1045
	alpha, IA	2-way ANOVA	interaction	0.8591	ns
			main effect of days at 31 ºC	<0.0001	****
			main effect of APL unlabeled vs. APL>dTRPA1	<0.0001	****
		Sidak multiple comparisons test	1 d	0.4206	ns
			2 d	0.0338	*
			3 d	0.2485	ns
			4 d	0.0162	*
	beta, IA	2-way ANOVA	interaction	0.1678	ns
			main effect of days at 31 ºC	<0.0001	****
			main effect of APL unlabeled vs. APL>dTRPA1	<0.0001	****
		Sidak multiple comparisons test	1 d	0.3706	ns
			2 d	0.2266	ns
			3 d	0.0332	*
			4 d	<0.0001	****
	gamma, IA	2-way ANOVA	interaction	0.3869	ns
			main effect of days at 31 ºC	0.0065	**
			main effect of APL unlabeled vs. APL>dTRPA1	0.0005	***
		Sidak multiple comparisons test	1 d	0.7576	ns
			2 d	0.8093	ns
			3 d	0.0338	*
			4 d	0.041	*
	alpha', IA	2-way ANOVA	interaction	0.8996	ns
			main effect of days at 31 ºC	0.0363	*
			main effect of APL unlabeled vs. APL>dTRPA1	<0.0001	****
		Sidak multiple comparisons test	1 d	0.0459	*
			2 d	0.3131	ns
			3 d	0.0643	ns
			4 d	0.0463	*
		2-way ANOVA	interaction	0.2786	ns
			main effect of days at 31 ºC	0.0106	*

Table S2: Details of statistics

Figure	Data	Statistical test	Comparison	P-value	Significance
Fig 3, S12, APL>dTRPA1 0,1,2,3 d loss of adaptation	beta', IA		main effect of APL unlabeled vs. APL>dTRPA1	0.0016	**
		Sidak multiple comparisons test	1 d	0.1053	ns
			2 d	0.0694	ns
			3 d	>0.9999	ns
			4 d	0.343	ns
	alpha, IA	2-way ANOVA	interaction	0.8594	ns
			main effect of days at 31 ºC	0.0003	***
			main effect of APL unlabeled vs. APL>dTRPA1	<0.0001	****
		Sidak multiple comparisons test	1 d	0.0228	*
			2 d	0.1343	ns
			3 d	0.1595	ns
			4 d	0.3751	ns
	beta, IA	2-way ANOVA	interaction	0.0073	**
			main effect of days at 31 ºC	<0.0001	****
			main effect of APL unlabeled vs. APL>dTRPA1	<0.0001	****
		Sidak multiple comparisons test	1 d	<0.0001	****
			2 d	0.0901	ns
			3 d	0.9886	ns
			4 d	0.154	ns
	gamma, IA	2-way ANOVA	interaction	0.6227	ns
			main effect of days at 31 ºC	0.9096	ns
			main effect of APL unlabeled vs. APL>dTRPA1	<0.0001	****
		Sidak multiple comparisons test	1 d	0.0081	**
			2 d	0.0488	*
			3 d	0.2186	ns
			4 d	0.4802	ns
Fig 4: APL>dTRPA,GCaMP6f	alpha', IA	Mann-Whitney test	no dTRPA1 vs. APL>dTRPA1	0.0205	*
	beta', IA	Unpaired t-test	no dTRPA1 vs. APL>dTRPA1	0.0498	*
	alpha, IA	Unpaired t-test	no dTRPA1 vs. APL>dTRPA1	0.0111	*
	beta, IA	Unpaired t-test	no dTRPA1 vs. APL>dTRPA1	0.0235	*
	gamma, IA	Unpaired t-test	no dTRPA1 vs. APL>dTRPA1	0.0048	**
Fig S13B: APL>dTRPA,GCaMP6f, responses to d-DL	alpha', d-DL	Mann-Whitney test	no dTRPA1 vs. APL>dTRPA1	0.6495	ns
	beta', d-DL	Mann-Whitney test	no dTRPA1 vs. APL>dTRPA1	0.3475	ns
	alpha, d-DL	Unpaired t-test	no dTRPA1 vs. APL>dTRPA1	0.0271	*
	beta, d-DL	Unpaired t-test	no dTRPA1 vs. APL>dTRPA1	0.1355	ns
	gamma, d-DL	Mann-Whitney test	no dTRPA1 vs. APL>dTRPA1	0.0768	ns
Fig S13C: APL>dTRPA1,GCaMP6f, steady state responses	alpha', IA	Mann-Whitney test	no dTRPA1 vs. APL>dTRPA1	0.4776	ns
	beta', IA	Unpaired t-test	no dTRPA1 vs. APL>dTRPA1	0.5483	ns
	alpha, IA	Unpaired t-test	no dTRPA1 vs. APL>dTRPA1	0.4987	ns
	beta, IA	Unpaired t-test	no dTRPA1 vs. APL>dTRPA1	0.6323	ns
	gamma, IA	Unpaired t-test	no dTRPA1 vs. APL>dTRPA1	0.0652	ns
	alpha', d-DL	Mann-Whitney test	no dTRPA1 vs. APL>dTRPA1	0.1366	ns
	beta', d-DL	Unpaired t-test	no dTRPA1 vs. APL>dTRPA1	0.2305	ns
	alpha, d-DL	Unpaired t-test	no dTRPA1 vs. APL>dTRPA1	0.1425	ns
	beta, d-DL	Unpaired t-test	no dTRPA1 vs. APL>dTRPA1	0.9134	ns
	gamma, d-DL	Unpaired t-test	no dTRPA1 vs. APL>dTRPA1	0.5768	ns
Fig 5B, S14: APL>dTRPA,GCaMP6f	alpha', heat	Mann-Whitney test	kept 22°C 4d vs. kept 31°C 4d	0.6009	ns
	alpha', heat + IA	Mann-Whitney test	kept 22°C 4d vs. kept 31°C 4d	0.9623	ns
	dDL	Mann-Whitney test	kept 22°C 4d vs. kept 31°C 4d	0.7396	ns
	alpha, heat	Unpaired t-test	kept 22°C 4d vs. kept 31°C 4d	0.6606	ns
	alpha, heat + IA	Unpaired t-test	kept 22°C 4d vs. kept 31°C 4d	0.5465	ns
	dDL	Unpaired t-test	kept 22°C 4d vs. kept 31°C 4d	0.5223	ns
	beta, heat	Unpaired t-test	kept 22°C 4d vs. kept 31°C 4d	0.7655	ns
	beta, heat + IA	Unpaired t-test	kept 22°C 4d vs. kept 31°C 4d	0.7018	ns
	beta, heat + dDL	Unpaired t-test	kept 22°C 4d vs. kept 31°C 4d	0.9975	ns
	gamma, heat	Unpaired t-test	kept 22°C 4d vs. kept 31°C 4d	0.1617	ns
	gamma, heat + IA	Unpaired t-test	kept 22°C 4d vs. kept 31°C 4d	0.1225	ns
	dDL	Unpaired t-test	kept 22°C 4d vs. kept 31°C 4d	0.0881	ns
	alpha', IA	Welch's ANOVA		0.1045	ns
	beta', IA	Welch's ANOVA	Post hoc tests below with Holm-Bonferroni correction	<0.0001	****
		Paired t-test	Kept at 22 ºC, measured at 22 ºC v. 31 ºC	0.066	ns
		Paired t-test	Kept at 31 ºC, measured at 22 ºC v. 31 ºC	0.0696	ns
		Welch's t-test	Measured at 22 ºC, kept at 22 ºC v. kept at 31 ºC	0.0002	***
		Welch's t-test	Measured at 31 ºC, kept at 22 ºC v. kept at 31 ºC	0.0028	***
		Welch's t-test	Kept @22ºC, meas. @22ºC v. kept @31ºC, meas. @31ºC	0.1348	ns
	alpha, IA	Welch's ANOVA	Post hoc tests below with Holm-Bonferroni correction	<0.0001	****
		Paired t-test	Kept at 22 ºC, measured at 22 ºC v. 31 ºC	<0.0001	****
		Paired t-test	Kept at 31 ºC, measured at 22 ºC v. 31 ºC	0.0024	**
		Welch's t-test	Measured at 22 ºC, kept at 22 ºC v. kept at 31 ºC	0.0028	**

Figure	Data	Statistical test	Comparison	P-value	Significance
Fig 5E, S15A: APL>dTRPA1, KC>GCaMP6f, responses measured at 31c (mean ΔF/F)		Welch's t-test	Measured at 31 ºC, kept at 22 ºC v. kept at 31 ºC	0.0609	ns
		Welch's t-test	Kept @22ºC, meas. @22ºC v. kept @31ºC, meas. @31ºC	0.104	ns
	beta, IA	Welch's ANOVA	Post hoc tests below with Holm-Bonferroni correction	<0.0001	****
		Paired t-test	Kept at 22 ºC, measured at 22 ºC v. 31 ºC	0.0005	***
		Paired t-test	Kept at 31 ºC, measured at 22 ºC v. 31 ºC	0.0042	**
		Welch's t-test	Measured at 22 ºC, kept at 22 ºC v. kept at 31 ºC	<0.0001	****
		Welch's t-test	Measured at 31 ºC, kept at 22 ºC v. kept at 31 ºC	0.04	*
		Welch's t-test	Kept @22ºC, meas. @22ºC v. kept @31ºC, meas. @31ºC	0.5275	ns
	gamma, IA	Welch's ANOVA	Post hoc tests below with Holm-Bonferroni correction	<0.0001	****
		Paired t-test	Kept at 22 ºC, measured at 22 ºC v. 31 ºC	0.002	**
		Paired t-test	Kept at 31 ºC, measured at 22 ºC v. 31 ºC	0.0018	**
		Welch's t-test	Measured at 22 ºC, kept at 22 ºC v. kept at 31 ºC	0.0011	**
		Welch's t-test	Measured at 31 ºC, kept at 22 ºC v. kept at 31 ºC	0.9022	ns
		Welch's t-test	Kept @22ºC, meas. @22ºC v. kept @31ºC, meas. @31ºC	0.0318	*
	alpha', dDL	Welch's ANOVA	Post hoc tests below with Holm-Bonferroni correction	0.0002	***
		Paired t-test	Kept at 22 ºC, measured at 22 ºC v. 31 ºC	0.213	ns
		Paired t-test	Kept at 31 ºC, measured at 22 ºC v. 31 ºC	0.029	*
		Welch's t-test	Measured at 22 ºC, kept at 22 ºC v. kept at 31 ºC	0.034	*
		Welch's t-test	Measured at 31 ºC, kept at 22 ºC v. kept at 31 ºC	0.6808	ns
		Welch's t-test	Kept @22ºC, meas. @22ºC v. kept @31ºC, meas. @31ºC	0.3088	ns
	beta', dDL	Welch's ANOVA	Post hoc tests below with Holm-Bonferroni correction	<0.0001	****
		Paired t-test	Kept at 22 ºC, measured at 22 ºC v. 31 ºC	0.0526	ns
		Paired t-test	Kept at 31 ºC, measured at 22 ºC v. 31 ºC	0.0052	**
		Welch's t-test	Measured at 22 ºC, kept at 22 ºC v. kept at 31 ºC	0.001	**
		Welch's t-test	Measured at 31 ºC, kept at 22 ºC v. kept at 31 ºC	0.072	ns
		Welch's t-test	Kept @22ºC, meas. @22ºC v. kept @31ºC, meas. @31ºC	0.3252	ns
	alpha, dDL	Welch's ANOVA	Post hoc tests below with Holm-Bonferroni correction	<0.0001	****
		Paired t-test	Kept at 22 ºC, measured at 22 ºC v. 31 ºC	<0.0001	****
		Paired t-test	Kept at 31 ºC, measured at 22 ºC v. 31 ºC	0.00012	***
		Welch's t-test	Measured at 22 ºC, kept at 22 ºC v. kept at 31 ºC	<0.0001	****
		Welch's t-test	Measured at 31 ºC, kept at 22 ºC v. kept at 31 ºC	0.0374	*
		Welch's t-test	Kept @22ºC, meas. @22ºC v. kept @31ºC, meas. @31ºC	0.0032	**
	beta, dDL	Welch's ANOVA	Post hoc tests below with Holm-Bonferroni correction	0.0002	***
		Paired t-test	Kept at 22 ºC, measured at 22 ºC v. 31 ºC	0.0015	**
		Paired t-test	Kept at 31 ºC, measured at 22 ºC v. 31 ºC	0.0005	***
		Welch's t-test	Measured at 22 ºC, kept at 22 ºC v. kept at 31 ºC	0.00044	***
		Welch's t-test	Measured at 31 ºC, kept at 22 ºC v. kept at 31 ºC	0.0194	*
		Welch's t-test	Kept @22ºC, meas. @22ºC v. kept @31ºC, meas. @31ºC	0.5368	ns
	gamma, dDL	Welch's ANOVA	Post hoc tests below with Holm-Bonferroni correction	<0.0001	****
		Paired t-test	Kept at 22 ºC, measured at 22 ºC v. 31 ºC	<0.0001	****
		Paired t-test	Kept at 31 ºC, measured at 22 ºC v. 31 ºC	0.0008	***
		Welch's t-test	Measured at 22 ºC, kept at 22 ºC v. kept at 31 ºC	0.0008	***
		Welch's t-test	Measured at 31 ºC, kept at 22 ºC v. kept at 31 ºC	0.1946	ns
		Welch's t-test	Kept @22ºC, meas. @22ºC v. kept @31ºC, meas. @31ºC	0.0084	**
	alpha', IA	Welch's ANOVA		0.0599	ns
	beta', IA	Kruskal-Wallis test	Post hoc tests below with Holm-Bonferroni correction	<0.0001	****
		Paired t-test	Kept at 22 ºC, measured at 22 ºC v. 31 ºC	0.0022	**
		Wilcoxon signed rank test	Kept at 31 ºC, measured at 22 ºC v. 31 ºC	0.2334	ns
		Mann-Whitney test	Measured at 22 ºC, kept at 22 ºC v. kept at 31 ºC	<0.0001	****
		Welch's t-test	Measured at 31 ºC, kept at 22 ºC v. kept at 31 ºC	0.0024	**
		Welch's t-test	Kept @22ºC, meas. @22ºC v. kept @31ºC, meas. @31ºC	<0.0001	****
	alpha, IA	Welch's ANOVA	Post hoc tests below with Holm-Bonferroni correction	<0.0001	****
		Paired t-test	Kept at 22 ºC, measured at 22 ºC v. 31 ºC	<0.0001	****
		Paired t-test	Kept at 31 ºC, measured at 22 ºC v. 31 ºC	0.0174	*
		Welch's t-test	Measured at 22 ºC, kept at 22 ºC v. kept at 31 ºC	0.0032	**
		Welch's t-test	Measured at 31 ºC, kept at 22 ºC v. kept at 31 ºC	0.1724	ns
		Welch's t-test	Kept @22ºC, meas. @22ºC v. kept @31ºC, meas. @31ºC	0.3025	ns
	beta, IA	Welch's ANOVA	Post hoc tests below with Holm-Bonferroni correction	<0.0001	****
		Paired t-test	Kept at 22 ºC, measured at 22 ºC v. 31 ºC	0.0002	***
		Paired t-test	Kept at 31 ºC, measured at 22 ºC v. 31 ºC	0.0278	*
		Welch's t-test	Measured at 22 ºC, kept at 22 ºC v. kept at 31 ºC	0.0002	***
		Welch's t-test	Measured at 31 ºC, kept at 22 ºC v. kept at 31 ºC	0.0015	**
		Welch's t-test	Kept @22ºC, meas. @22ºC v. kept @31ºC, meas. @31ºC	0.1597	ns
	gamma, IA	Welch's ANOVA	Post hoc tests below with Holm-Bonferroni correction	<0.0001	****
		Paired t-test	Kept at 22 ºC, measured at 22 ºC v. 31 ºC	0.0123	*
		Paired t-test	Kept at 31 ºC, measured at 22 ºC v. 31 ºC	0.0016	**
		Welch's t-test	Measured at 22 ºC, kept at 22 ºC v. kept at 31 ºC	<0.0001	****
		Welch's t-test	Measured at 31 ºC, kept at 22 ºC v. kept at 31 ºC	0.4147	ns
		Welch's t-test	Kept @22ºC, meas. @22ºC v. kept @31ºC, meas. @31ºC	0.6607	ns

Figure	Data	Statistical test	Comparison	P-value	Significance
Fig S15B: APL>dTRPA1, KC>GCaMP6f, responses measured at 31c (max ΔF/F)	alpha', dDL	Welch's ANOVA	Post hoc tests below with Holm-Bonferroni correction	0.0027	**
		Paired t-test	Kept at 22 ºC, measured at 22 ºC v. 31 ºC	0.4921	ns
		Paired t-test	Kept at 31 ºC, measured at 22 ºC v. 31 ºC	0.1156	ns
		Welch's t-test	Measured at 22 ºC, kept at 22 ºC v. kept at 31 ºC	0.0035	**
		Welch's t-test	Measured at 31 ºC, kept at 22 ºC v. kept at 31 ºC	0.8121	ns
		Welch's t-test	Kept @22ºC, meas. @22ºC v. kept @31ºC, meas. @31ºC	0.8322	ns
	beta', dDL	Welch's ANOVA	Post hoc tests below with Holm-Bonferroni correction	<0.0001	****
		Paired t-test	Kept at 22 ºC, measured at 22 ºC v. 31 ºC	0.3166	ns
		Paired t-test	Kept at 31 ºC, measured at 22 ºC v. 31 ºC	0.0248	*
		Welch's t-test	Measured at 22 ºC, kept at 22 ºC v. kept at 31 ºC	0.0005	***
		Welch's t-test	Measured at 31 ºC, kept at 22 ºC v. kept at 31 ºC	0.0087	**
		Welch's t-test	Kept @22ºC, meas. @22ºC v. kept @31ºC, meas. @31ºC	0.0072	**
	alpha, dDL	Welch's ANOVA	Post hoc tests below with Holm-Bonferroni correction	<0.0001	****
		Paired t-test	Kept at 22 ºC, measured at 22 ºC v. 31 ºC	<0.0001	****
		Paired t-test	Kept at 31 ºC, measured at 22 ºC v. 31 ºC	0.0006	***
		Welch's t-test	Measured at 22 ºC, kept at 22 ºC v. kept at 31 ºC	0.0002	***
		Welch's t-test	Measured at 31 ºC, kept at 22 ºC v. kept at 31 ºC	0.0126	*
		Welch's t-test	Kept @22ºC, meas. @22ºC v. kept @31ºC, meas. @31ºC	0.0178	*
	beta, dDL	Welch's ANOVA	Post hoc tests below with Holm-Bonferroni correction	<0.0001	****
		Paired t-test	Kept at 22 ºC, measured at 22 ºC v. 31 ºC	0.0005	***
		Paired t-test	Kept at 31 ºC, measured at 22 ºC v. 31 ºC	0.0015	**
		Welch's t-test	Measured at 22 ºC, kept at 22 ºC v. kept at 31 ºC	0.0004	***
		Welch's t-test	Measured at 31 ºC, kept at 22 ºC v. kept at 31 ºC	0.0042	**
		Welch's t-test	Kept @22ºC, meas. @22ºC v. kept @31ºC, meas. @31ºC	0.2224	ns
	gamma, dDL	Welch's ANOVA	Post hoc tests below with Holm-Bonferroni correction	<0.0001	****
		Paired t-test	Kept at 22 ºC, measured at 22 ºC v. 31 ºC	<0.0001	****
		Paired t-test	Kept at 31 ºC, measured at 22 ºC v. 31 ºC	0.0002	***
		Welch's t-test	Measured at 22 ºC, kept at 22 ºC v. kept at 31 ºC	0.0002	***
		Welch's t-test	Measured at 31 ºC, kept at 22 ºC v. kept at 31 ºC	0.51	ns
		Welch's t-test	Kept @22ºC, meas. @22ºC v. kept @31ºC, meas. @31ºC	0.0008	***
Note: for Fig 6/S17, pairwise comparisons were Holm-Bonferroni corrected for the 4 comparisons within each lobe (2 paired, 2 unpaired)					
Fig 6, S17: APL>Ort	alpha', IA	Wilcoxon signed-rank test	no dTRPA1: before vs. +histamine	0.0002	***
		Wilcoxon signed-rank test	APL>dTRPA1: before vs. +histamine	0.0002	***
		Mann-Whitney test	before: no dTRPA1 vs. APL>dTRPA1	0.0974	ns
		Mann-Whitney test	+histamine: no dTRPA1 vs. APL>dTRPA1	0.8173	ns
	beta', IA	paired t-test	no dTRPA1: before vs. +histamine	<0.0001	****
		paired t-test	APL>dTRPA1: before vs. +histamine	<0.0001	****
		unpaired t-test	before: no dTRPA1 vs. APL>dTRPA1	0.3371	ns
		unpaired t-test	+histamine: no dTRPA1 vs. APL>dTRPA1	0.6116	ns
	alpha, IA	paired t-test	no dTRPA1: before vs. +histamine	<0.0001	****
		paired t-test	APL>dTRPA1: before vs. +histamine	<0.0001	****
		unpaired t-test	before: no dTRPA1 vs. APL>dTRPA1	0.0214	*
		unpaired t-test	+histamine: no dTRPA1 vs. APL>dTRPA1	0.042	*
	beta, IA	paired t-test	no dTRPA1: before vs. +histamine	<0.0001	****
		paired t-test	APL>dTRPA1: before vs. +histamine	<0.0001	****
		unpaired t-test	before: no dTRPA1 vs. APL>dTRPA1	0.002	**
		unpaired t-test	+histamine: no dTRPA1 vs. APL>dTRPA1	0.0352	*
	gamma, IA	Wilcoxon signed-rank test	no dTRPA1: before vs. +histamine	0.0006	***
		Wilcoxon signed-rank test	APL>dTRPA1: before vs. +histamine	0.0002	***
		Mann-Whitney test	before: no dTRPA1 vs. APL>dTRPA1	0.0038	**
		unpaired t-test	+histamine: no dTRPA1 vs. APL>dTRPA1	0.4998	ns
	calyx, IA	paired t-test	no dTRPA1: before vs. +histamine	0.0006	***
		paired t-test	APL>dTRPA1: before vs. +histamine	0.0002	***
		unpaired t-test	before: no dTRPA1 vs. APL>dTRPA1	0.0046	**
		unpaired t-test	+histamine: no dTRPA1 vs. APL>dTRPA1	0.3891	ns
	alpha', dDL	Wilcoxon signed-rank test	no dTRPA1: before vs. +histamine	0.0008	***
		paired t-test	APL>dTRPA1: before vs. +histamine	0.0018	**
		Mann-Whitney test	before: no dTRPA1 vs. APL>dTRPA1	0.139	ns
		Mann-Whitney test	+histamine: no dTRPA1 vs. APL>dTRPA1	0.7658	ns
	beta', dDL	paired t-test	no dTRPA1: before vs. +histamine	0.0008	***
		paired t-test	APL>dTRPA1: before vs. +histamine	0.0018	**
		unpaired t-test	before: no dTRPA1 vs. APL>dTRPA1	0.5005	ns
		unpaired t-test	+histamine: no dTRPA1 vs. APL>dTRPA1	0.6698	ns
	alpha, dDL	paired t-test	no dTRPA1: before vs. +histamine	0.0147	*
		paired t-test	APL>dTRPA1: before vs. +histamine	0.0132	*
		unpaired t-test	before: no dTRPA1 vs. APL>dTRPA1	0.0254	*
		unpaired t-test	+histamine: no dTRPA1 vs. APL>dTRPA1	0.4561	ns
	beta, dDL	paired t-test	no dTRPA1: before vs. +histamine	0.0064	**
		paired t-test	APL>dTRPA1: before vs. +histamine	0.0057	**

Figure	Data	Statistical test	Comparison	P-value	Significance
	beta, dDL	unpaired t-test	before: no dTRPA1 vs. APL>dTRPA1	0.002	**
		unpaired t-test	+histamine: no dTRPA1 vs. APL>dTRPA1	0.016	*
	gamma, dDL	Wilcoxon signed-rank test	no dTRPA1: before vs. +histamine	0.033	*
		Wilcoxon signed-rank test	APL>dTRPA1: before vs. +histamine	0.214	ns
		Mann-Whitney test	before: no dTRPA1 vs. APL>dTRPA1	0.0164	*
		unpaired t-test	+histamine: no dTRPA1 vs. APL>dTRPA1	0.2777	ns
	calyx, dDL	paired t-test	no dTRPA1: before vs. +histamine	0.0801	ns
		paired t-test	APL>dTRPA1: before vs. +histamine	0.1358	ns
		unpaired t-test	before: no dTRPA1 vs. APL>dTRPA1	0.0548	ns
		unpaired t-test	+histamine: no dTRPA1 vs. APL>dTRPA1	0.3275	ns
Note: for Fig S18, pairwise comparisons were Holm-Bonferroni corrected for the 4 comparisons within each lobe (2 paired, 2 unpaired)					
Fig S18: APL>TNT vs. APL.Ort	alpha', IA	Welch's t-test	APL unlabeled vs. APL>TNT	<0.0001	****
		Wilcoxon signed rank test	APL>Ort, histamine vs. no histamine	0.0002	***
		Mann-Whitney test	APL unlabeled vs. APL>Ort no histamine	0.102	ns
		Welch's t-test	APL>TNT vs. APL>Ort + histamine	0.8805	ns
	beta', IA	Mann-Whitney test	APL unlabeled vs. APL>TNT	<0.0001	****
		Paired t-test	APL>Ort, histamine vs. no histamine	<0.0001	****
		Welch's t-test	APL unlabeled vs. APL>Ort no histamine	0.2128	ns
		Mann-Whitney test	APL>TNT vs. APL>Ort + histamine	0.6682	ns
	alpha, IA	Welch's t-test	APL unlabeled vs. APL>TNT	<0.0001	****
		Paired t-test	APL>Ort, histamine vs. no histamine	<0.0001	****
		Welch's t-test	APL unlabeled vs. APL>Ort no histamine	0.0016	**
		Welch's t-test	APL>TNT vs. APL>Ort + histamine	0.0008	***
	beta, IA	Welch's t-test	APL unlabeled vs. APL>TNT	<0.0001	****
		Paired t-test	APL>Ort, histamine vs. no histamine	<0.0001	****
		Welch's t-test	APL unlabeled vs. APL>Ort no histamine	0.006	**
		Welch's t-test	APL>TNT vs. APL>Ort + histamine	0.011	*
	gamma, IA	Welch's t-test	APL unlabeled vs. APL>TNT	<0.0001	****
		Wilcoxon signed rank test	APL>Ort, histamine vs. no histamine	0.0006	***
		Mann-Whitney test	APL unlabeled vs. APL>Ort no histamine	0.02	*
		Welch's t-test	APL>TNT vs. APL>Ort + histamine	0.4298	ns
	alpha', dDL	Welch's t-test	APL unlabeled vs. APL>TNT	<0.0001	****
		Wilcoxon signed rank test	APL>Ort, histamine vs. no histamine	0.0006	***
		Mann-Whitney test	APL unlabeled vs. APL>Ort no histamine	>0.99	ns
		Welch's t-test	APL>TNT vs. APL>Ort + histamine	>0.99	ns
	beta', dDL	Welch's t-test	APL unlabeled vs. APL>TNT	<0.0001	****
		Paired t-test	APL>Ort, histamine vs. no histamine	0.0006	***
		Welch's t-test	APL unlabeled vs. APL>Ort no histamine	0.9555	ns
		Welch's t-test	APL>TNT vs. APL>Ort + histamine	0.1324	ns
	alpha, dDL	Welch's t-test	APL unlabeled vs. APL>TNT	<0.0001	****
		Paired t-test	APL>Ort, histamine vs. no histamine	0.0147	*
		Welch's t-test	APL unlabeled vs. APL>Ort no histamine	0.1487	ns
		Welch's t-test	APL>TNT vs. APL>Ort + histamine	0.2208	ns
	beta, dDL	Welch's t-test	APL unlabeled vs. APL>TNT	<0.0001	****
		Paired t-test	APL>Ort, histamine vs. no histamine	0.0038	**
		Welch's t-test	APL unlabeled vs. APL>Ort no histamine	0.03	*
		Welch's t-test	APL>TNT vs. APL>Ort + histamine	0.3994	ns
	gamma, dDL	Welch's t-test	APL unlabeled vs. APL>TNT	<0.0001	****
		Wilcoxon signed rank test	APL>Ort, histamine vs. no histamine	0.033	*
		Mann-Whitney test	APL unlabeled vs. APL>Ort no histamine	0.8266	ns
		Welch's t-test	APL>TNT vs. APL>Ort + histamine	0.2188	ns